Welding of carbide-free bainitic steels for railway applications

Marta Muñiz Mangas

Thesis Submitted for the Degree of Doctor of Engineering

Department of Materials Science and Engineering

The University of Sheffield

September 2020

Abstract

Carbide Free Bainitic (CFB) steels B360 and B320 show an outstanding behaviour in terms of fatigue deformation mechanisms, mainly when analysing its resistance to head checks. This, results in a lower necessity for maintenance and therefore, in a reduction of costs. However, problems have been encountered when welding CFB rails, showing cracks when in track, in both the entry and the exit site of the weld. The mechanisms of failure of these rails is not entirely clear.

Nowadays, with the rise in use of high-speed trains and high loads, Continuously Welded Rails (CWR) are gaining importance; as other joining mechanisms such as fish-plates are becoming obsolete. Almost 90% of the CWR are welded by Flash Butt Welding (FBW); which is known as one of the most reliable welding processes; nevertheless, the welds are a weak link between rails due to mechanical and microstructural variations with the parent rail.

Welding of conventional pearlitic rail steels, has been under investigation on numerous occasions; however, the same has not been made as extensively on CFB rail steels. On this thesis, an extensive examination of the Heat Affected Zone (HAZ) of three FBW rails (B360, B320 and R260) is discussed.

CFB FBWs showed much wider HAZ extension than conventional pearlitic steels, of importance will be the extension of the tempered or Subcritical HAZ (SCHAZ), as CFBs, mainly B360 has shown low resistance to tempering; this, could result on preferential wear and plastic deformation in track applications.

With the purpose of reducing the extension of the tempered SCHAZ, weld trials were carried out on B360 rails using a stationary FBW GAAS 80 / 580 Schlatter welding machine in Scunthorpe, UK. Those, were produced by variations on the number of Pre-Heat (PH) cycles, on the preheating time (s) (ON) and delay period (s) (OFF) and additions of Post Weld Heat Pulses (PWHP) at the end of the welds. Finally, an analysis of the welded rails mechanical properties was made.

1

Acknowledgements

I have encountered many people during these years who had helped me. In particular I would like to acknowledge the following people.

Foremost, I would like thank my advisors Professor Eric J. Palmiere and Dr. Lindsey Smith for the guidance, patience, support and technical knowledge they have provided me during my EngD. Thank you for keeping up my motivation and encouraging me.

I would also like to acknowledge the financial support from the EPSRC and British Steel who provided the funding for this project. I would like to thank everybody in British Steel Rail Technologies, special thanks to Sandra Fretwell-Smith and John Wilkinson, who had been supporting me since the beginning. Also, to Howard Smith for his help and patience.

I am very grateful for the help I received from the CDT and the University staff, for all the trainings, direction and help they provided. I also thank my colleagues at the University; Eduardo Pineda, Luis Romano and Daniel Olguin. Thank you for being an amazing research group.

Thank you to all my friends, in special to Bea and Pablo who have been like a family to me during these years.

I would like to express my gratitude to my parents and brother, this work could not have been completed without their unconditional help and support.

Last but not least, I would like to thank Fernando, thank you for your patience, for always believing in me, encouraging me and for giving me your constant support. This work would have not been possible without you.

Table of contents

List of Abbreviations

CFB   Carbide Free Bainite.

HAZ   Heat Affected Zone.

CWR   Continuously Welded Rail.

FBW   Flash Butt Welding.

ATW   Aluminothermic Welding.

CHAZ   Critical Heat Affected Zone.

CGHAZ   Coarse Grained Heat Affected Zone.

FGHAZ   Fine Grained Heat Affected Zone.

ICHAZ   Intercritical Heat Affected Zone.

SCHAZ   Subcritical Heat Affected Zone.

PH   Pre-Heat.

PWHP   Post Weld Heat Pulses.

FZ   Fusion Zone.

RD   Rolling Direction.

OM   Optical Microscopy.

SEM   Scanning Electron Micrograph.

EBSD   Electron Backscattering Diffraction.

TEM	Transmission Electron Microscopy
XRD	X-Ray Diffraction.
HB	Brinell Hardness.
HV	Vickers Hardness.
TTT	Time Temperature Transformation.
CCT	Continuous Cooling Transformation.
FCC	Face Centred Cubic.
BCC	Body Centred Cubic.
BCT	Body Centred Tetragonal.
IPS	Invariant Plane Strain.
BC	Band Contrast.
RA	Retained Austenite.
MA	Martensite Austenite.
BF	Bainitic Ferrite.
HAGB	High Angle Grain Boundaries.
AF	Acicular Ferrite.
YS	Yield Strength.
UTS	Ultimate Tensile Strength.
EDX	Energy Dispersive X-Ray.
AC	Alternating Electric Current.
P	Parent rail hardness.

Introduction

Railway components are usually designed to last as long as possible. Nevertheless, a small number of fractures occur in practice. Since the October 2000 Hatfield incident with four casualties and more than seventy injured due to a fractured rail produced by fatigue cracks, rail maintenance and quality have become two of the major concerns in the railway industry [1].

Over the last years, it has been demonstrated that failure produced by wheels or axles has decreased and rail failures are becoming less frequent [2]. Another positive trend is that rail damage detection before failure is continuously improving [3].

Recently, with the increase in use of heavier and faster trains, there is an increasing need for harder, strong steels. Currently, the vast majority of rail steels are pearlitic. Pearlite microstructure consist on "soft" ferrite and "hard" cementite, and it confers high resistance to the main degradation mechanism of the railway industry. However, in track preventive grinding has not yet being eliminated.

Carbide free bainitic (CFB) steels were developed in the 20th century and used for rail applications as an improvement from the previously employed rail grades, with the purpose of reducing maintenance cost. To date, those CFB grades have shown excellent properties in service for mitigation against fatigue defects [4].

However, problems were encountered on CFB welds; as cracks were being developed in both the entry and exit side of the welds, nevertheless, the mechanism of deformation of these types of welds is not entirely clear.

This thesis is going to focus in two main aspects; understanding conventional CFB welds and its microstructural evolution after welding and developing an improved welding program for these grades in order to overcome the problems encountered when in track. For this purpose, it was decided to divide this thesis into seven chapters.

Chapter 1. Introduction

A general introduction of the work carried out is discussed.

Chapter 2. Background

In chapter 2 an analysis of the necessary background information needed to have a better understanding of the study can be found.

From rail steel manufacturing, types of rail steels and its use when in track, to the most common rail degradation mechanisms and welding techniques. Also, an analysis of other steel grades utilized for rail applications will be discussed together with the development of CFB steels and phase transformation mechanisms.

Chapter 3. Challenges and objectives

This chapter will be focused on the concerns regarding CFB and the work carried out by British Steel; together with the explained main objectives of the study.

Chapter 4. Experimental procedure

The different techniques used for the development of this work are discussed on this chapter.

Chapter 5. Analysis of a B360 FBW and comparison with other steel grades

An analysis of both a standard B360 CFB steel and a "conventional" B360 Flash Butt Weld (FBW) was performed with the use of advanced characterisation techniques. A comparison of this steel with other steel grades is also discussed on this chapter. All the welded rails utilized were supplied by British Steel.

Chapter 6. Narrower FBW of a B360 CFB rail

Focused on a discussion of the FBW trials performed in the FBW Schlatter machine in British Steel Scunthorpe, UK.

Chapter 7. Summary and future work

A summary of the work carried out together with the necessary future work will be discussed on this chapter.

CHAPTER 1

Background

1.1.   The railway

I.Track formation

A sound foundation, which sustains the strains produced during railway circulation, becomes necessary to obtain proper guidance and rolling of vehicles. A railway line is comprised of two dissimilar structures: The superstructure and the subgrade [5], both represented in Figure 1.
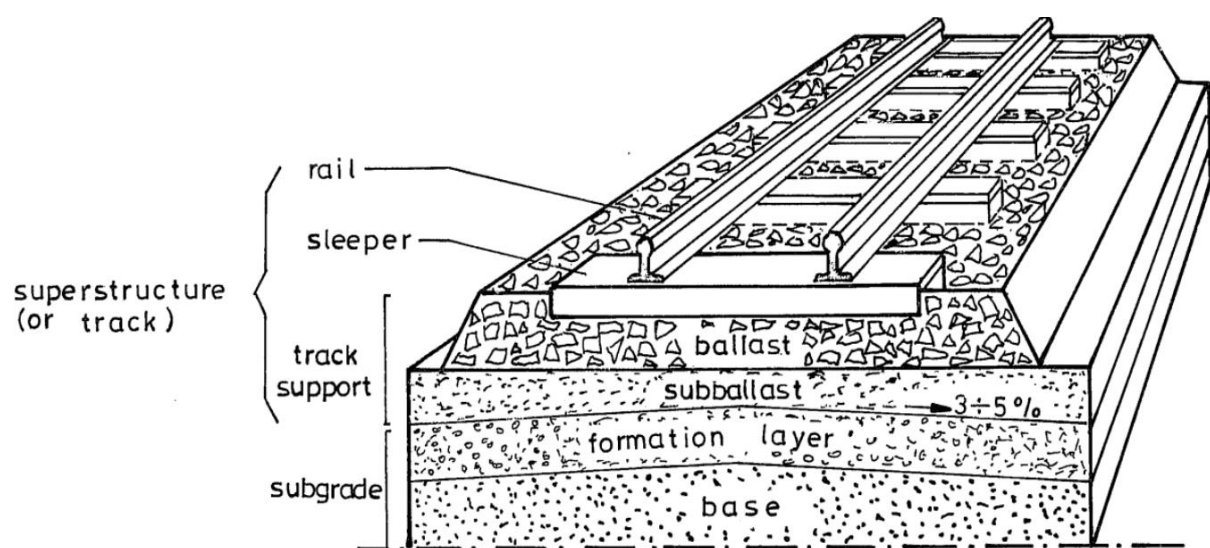
Figure 1. Track formation. Superstructure and subgrade [5]

The main purpose of the whole superstructure system is to improve load distribution within the rail-wheel contact [6]. As represented in Figure 1, the superstructure includes rails, ballast, sub ballast and sleepers [1],[8]. Rails are the most critical railway element, they are fastened to the ballast by sleepers [9] on a rubber pad and placed with a lateral tilt inwards to improve stability.

The track usually sits in one of two support systems: slab or ballast. Ballast is the most common.

Slab track, which is also known as ballastless track, consists of combinations of concrete slab and pavement [10]. It is mainly used for high velocity heavy trains, and for light trains in tunnels and bridges; particularly where maintenance is more challenging. Its construction is around 30% more expensive than conventional ballasted track, nonetheless, they are known to be more durable, decreasing maintenance costs [11],[10].

Conventional ballast track is made up of a granular coarse material, which is usually produced from the crushing of siliceous stones; this type of track is more common not only due to the low production cost but also because of its flexibility which provides dynamic stress absorption. The sub-ballast is a coarse-grained layer situated between superstructure and subgrade, which will help, together with the ballast, to improve load distribution and facilitate the flow of excess water toward the drains. In contrast, the subgrade, consisting of base and formation layers, is made of rock and mainly used to support the superstructure loading and reduce track maintenance.

II. Rail steel manufacture

As previously mentioned, rails are the element of the superstructure or track on which train rolling takes place, therefore, its main purpose is to absorb and transmit stress and strain caused by train rolling into the sleepers.

The first evidence of rails appeared during the 5th century BC. These were made of wood and mainly used for mining transportation. Later, more specifically in 1767, wood was replaced by the development of the first cast-iron rails in Shropshire [12]. But it was not until the development of the Bessemer converter, in 1856, that steel rails were first produced [13].

Trial steel rails were firstly installed on Midland Railway's Derby Station. Although these rails had poorer performance compared to the ones under use nowadays, their behaviour in track applications was undoubtedly advantageous in comparison with the previous cast iron steel rails [14]. Therefore, by 1878, the majority of in-service rail on the UK was made of steel [15].

Nowadays, rail steels are expected to not only have high toughness and resistance to abrasion, but also, to be cost effective and weldable. That is why, elements such as manganese and silicon are used during fabrication, improving toughness and wear resistance; on the contrary; sulphur and phosphorus must be reduced, increasing the steel purity and decreasing the probability of embrittlement.

Rail steels are continuously cast into hot rolled blooms. During the hot rolling process, the bloom passes through a series of rollers which, by the pressure exerted, will reduce the cross-sectional area of the product. Subsequently, an identification number is branded on the rails web and they are cut to the lengths corresponding to the customer's orders, usually 108 meters long for UK railways [16].

Following rolling, rails are usually air cooled to ambient temperature or heat treated and, once cold, straightening by rollers is carried out. Finally, rails are inspected both visually and by non-destructive methods, e.g., ultrasonic and eddy current testing, laser profiling.

III. Rail profiles

The selection of an ideal material for rail production and its position in track, are not the only factors to take into account when studying its performance, but its cross-sectional shape is also of interest.

Nowadays, most rail steels are produced according to standardisation, and the choice of its cross sectional shape depends on factors such as its application and traffic load [7].

The dissimilar rail cross sectional shapes are achieved in the middle of a specific rolling program, by controlling the grooves of the rolling stands. The rail profiles that are currently being used were developed within the 20th century and can be divided

into two main groups: Bullhead and Flat bottom rails [16]. Figure 2, shows a schematic representation of those. All the profiles consist of head, web and foot.

a.

b.

c.
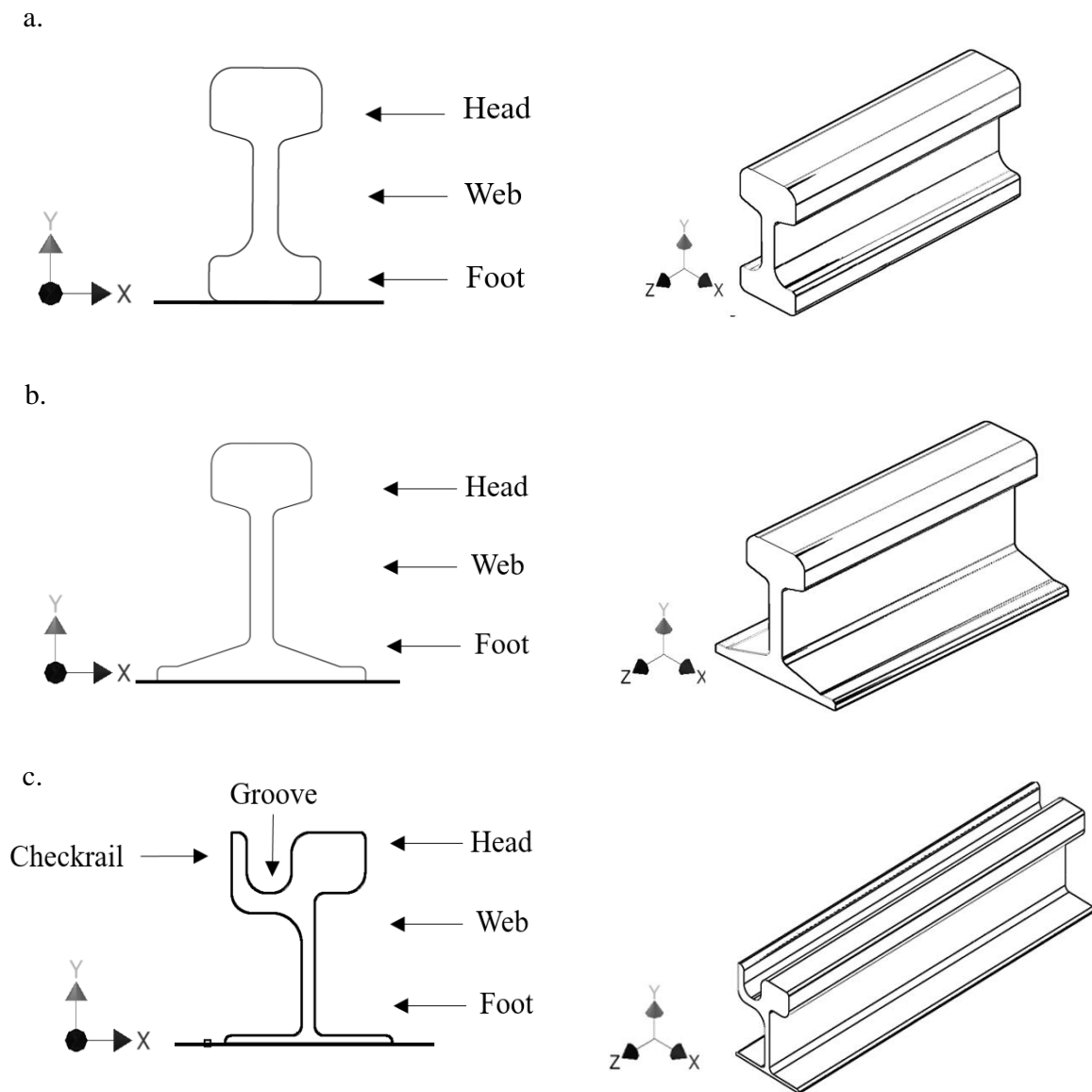
Figure 2. Schematic representation of dissimilar rail profiles used in the railway industry, a. Bullhead, b. Flat Bottomed Vignole, c. Flat Bottomed Grooved

Bullhead rails were developed with the aim of using the foot of the rail once the head had worn severely, however, this envisioned use was never achieved as the underside was also found to wear where the rail was secured to the sleeper [17]. Nevertheless, this rail profile is still being used within the UK.

Currently, almost all rail profiles in the world are Flat Bottomed. There are two types of Flat-bottomed rails used depending on the application, Vignole and Grooved rails.

Flat Bottomed Grooved rails are mainly used in tramlines; its head shape, consisting of groove and checkrail, helps this application. This is because tramways have sharper curves than conventional railways, therefore, when the wheel flange sits on the railhead, the groove and checkrail will act as a restraint for the wheel on curves to prevent derailment, Vignole rails are currently widely used in conventional railway tracks.

As an example, one of the most common flat bottom vignole rails used in Europe are 60E1 whose dimensions are represented in Figure 3. The number 60 indicates the rail has a section weight of 60 kg/m and the E1 is the profile rolled on the rail head.

EN 13674-1:2003 (E)

Dimensions in millimetres

Key

1   Centre line of branding

Cross-sectional area	:	76,70	cm^2
Mass per metre	:	60,21	kg/m
Moment of inertia x-x axis	:	3038,3	cm^4
Section modulus - Head	:	333,6	cm^3
Section modulus - Base	:	375,5	cm^3
Moment of inertia y-y axis	:	512,3	cm^4
Section modulus y-y axis	:	68,3	cm^3

Indicative dimensions : A = 20,456 mm
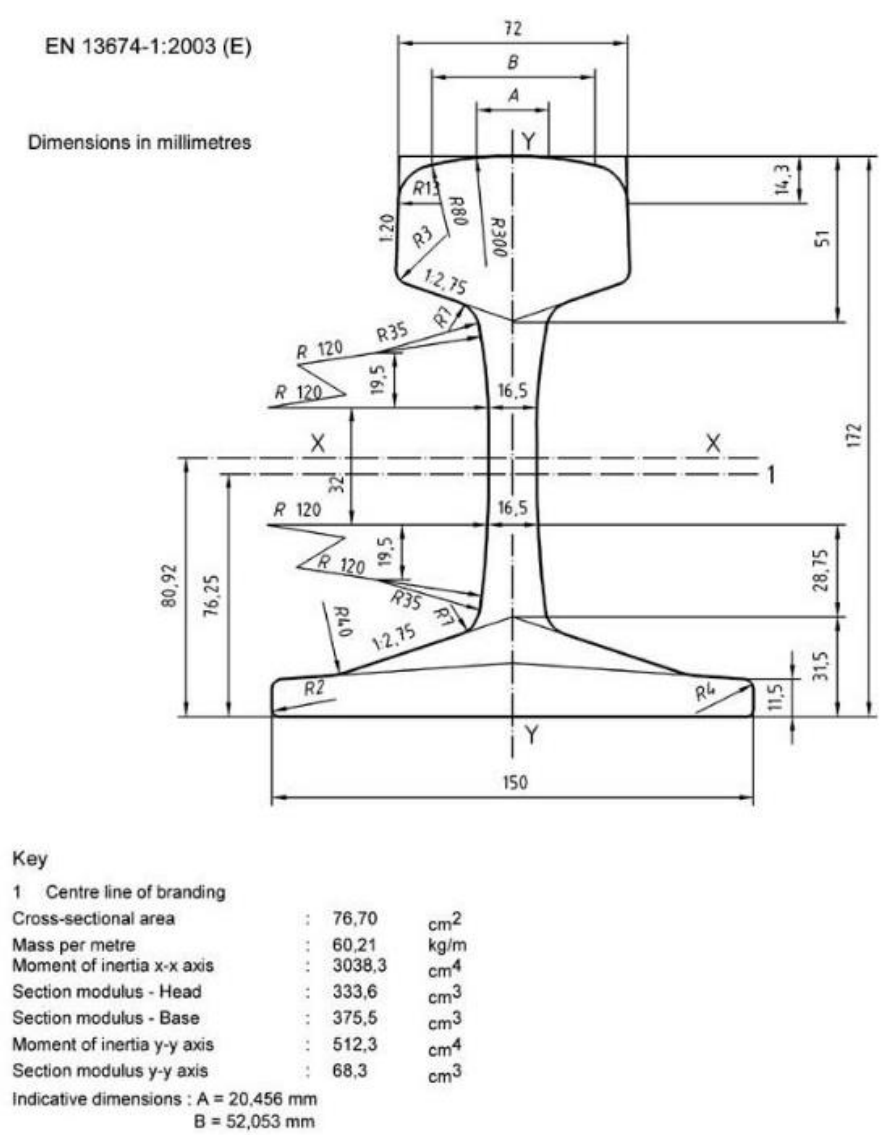   B = 52,053 mm

Figure 3. Flat Bottomed Vignole rail profile, 60E1 according to the European standard [18].

1.2.   Rail defects

As previously stated, the rail and wheel meet in the wheel-rail contact area. The vehicle body transfers the load between the bogies and wheelsets. Therefore, the stresses produced in the rails running surface are the highest that can be found in a railway, where loads of 25 tonnes can produce forces of circa 1500 MPa [6].

Some factors that could limit rail life are wear, plastic deformation, Rolling Contact Fatigue (RCF), traffic type and frequency of rail grinding. This thesis is going to focus on two of the most common degradation mechanisms: Wear and RCF [19].

I. Wear

Wear can be defined as the loss of material from a contact surface. In terms of the wheel-rail contact, wear is generally developed on the rail head. There are two distinguishable types of wear deformation. One produced on the top running surface of the head of high and low rails, also called "vertical wear", and the other formed down the edge of the rail head of high rails and called "lateral or side wear" [20]; a representation of both can be observed in Figure 4.
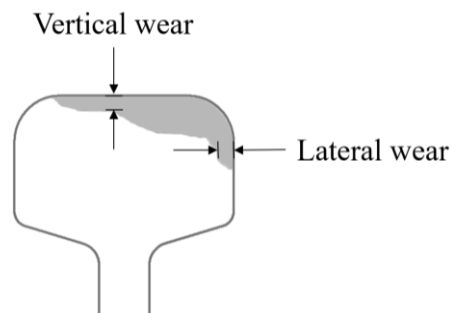
Figure 4. Schematic representation of wear deformation on a low Vignole flat bottom rail head.

The aforementioned, is activated due to repeating loading above the elastic limit which leads to plastic deformation [21]. As the depth of the plastic flow plays an important role in the development of wear, harder steels are commonly used to combat this problem [22].

Taking only conventional pearlitic rail grades into account, it has been shown that to achieve a higher wear resistance, the rail hardness should be higher than 350HB [2].

Wear is frequently generated on heavy axle loads [14]. It is known to be produced mainly because of poorly lubricated conditions on the running surface of both high and low rails[1]. Nevertheless, intentional grinding would be also detrimental [21]. As stated, in order to avoid wear deformation, lubrication is commonly used. However, the use of lubrication will promote other types of fractures such as Rolling Contact Fatigue (RCF) [23], which is discussed in the section below.

II. Rolling Contact Fatigue (RCF)

RCF consists of damage accumulation due to the nucleation and growth of cracks subjected to variable loads. On the wheel-rail contact, these cracks are generally initiated at the rail running surface or just under it [23]. RCF cracks are known to be more common on high velocity tracks, in high rails.

During the formation of a RCF crack, these grow at a very shallow angle of approximately 15-30°. The crack growth takes place at the maximum shear stress region at a very slow pace. However, once it has propagated enough, crack growth is much easier and rapid, having a steep angle of 60°, and failing by brittle failure [2]. It is known that harder steels will impede the premature initiation of these micro-cracks [22], as its maximum shear stress is higher, therefore, it takes longer for the rails to go through this layer before the crack starts propagating rapidly.

There is a rough connection between the surface length of an individual crack and its depth of penetration into the rail. There is a classification of RCF into four categories as a function of the crack length: light (< 10 mm surface length of the crack), moderate (10-19 mm), heavy (20-29 mm) and severe (30 mm or longer). Therefore, as represented in Figure 5 [24], if an individual RCF crack length is more than 20 mm there is higher probability of rail fracture.

---

[1] *In curved tracks, high rail (the outside rail) and low rail (the inside rail).*
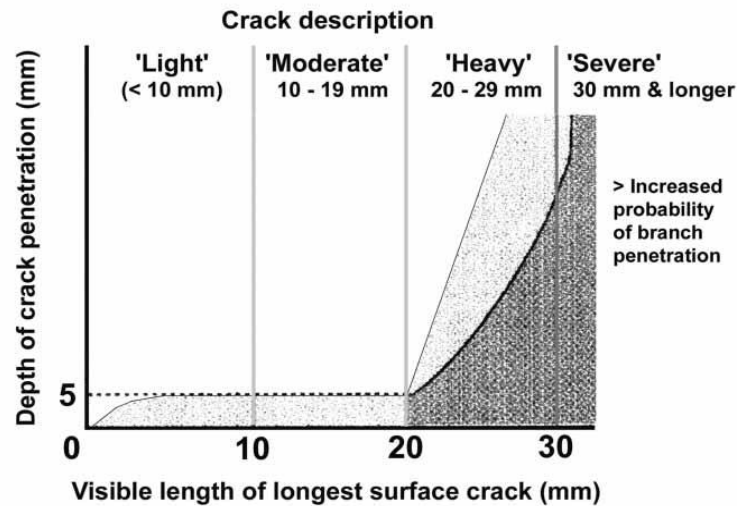
Figure 5. Relationship between crack penetration and surface crack length [24].

Micro-crack growth is dependent on factors such as the rail steel composition, mechanical properties, profile, residual stresses or the presence or not of lubrication. Lubricants can penetrate inside cracks leading to a faster development of the fissure due to hydraulic pressurisation. To impede the formation of these micro-cracks, periodic rail grinding is necessary which can have a negative effect on rail life due to additional metal loss from the rail head in the grinding process.

Head checks and squats are known to be two of the major issues of RCF. Those are fine surface cracks with a separation between them of 1 to 7 mm on the gauge corner of the rail head [22]. They are mainly produced on high rails of curves with radii below that of 1500 m and on switch and crossings. When head checking is in its early stages, as represented in Figure 6, grinding is necessary.
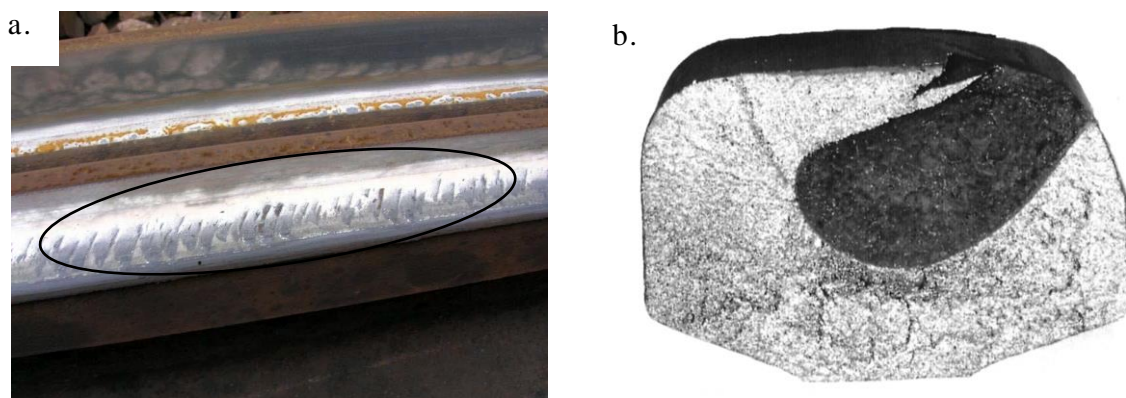

Figure 6. Representation of head checking on a rail head [25]. a. Early initiation of head checking on a rail head; b. Representation of a broken rail due to head checking.

If the aforementioned is not fully removed by the grinding process, then sudden failure of the rail may ultimately occur. Therefore, track inspection methods such as manual, eddy current, optical or ultrasonic are constantly needed.

Otherwise, squats are generally developed on gradients, acceleration areas and tracks with modern locomotives with anti-slip control systems. Those are nowadays a growing cause of increased track maintenance. Figure 7, represents the appearance of a squat, these are characterised for having a depression on the rail running surface, nevertheless, the cause of squat formation is currently under debate [26].

Figure 7. Photograph of a squat [26].

III.RCF and Wear relationship

As previously stated, wear and RCF are two types of deformation mechanisms which occur on the rail head of high and low rails. Wear and RCF are believed to act as opposites, this is because wear removes material from the rail head contact surface in which RCF surface cracks could be developed. Therefore, if there is a high amount of wear degradation on the material, RCF could be eliminated [14]. A summary of its previously mentioned properties can be observed in Table 1.

Table 1. Summary of Wear and RCF properties.

	Wear	Rolling Contact Fatigue (RCF)
Affects	Rail head.	Rail head or just under the head.
Type of rail	High and Low rails.	High and Low rails.
Material	Harder steels.	Harder steels.
Maintenance	Lubrication.	Grinding.
Detrimental	Grinding.	Lubrication.

1.3.   Rail residual stresses

Another aspect to consider when studying rails in-track performance are its residual stresses. These can be defined as the internal stresses within a material that is not subjected to any kind of load. Residual stresses could be compressive or tensile, both could be beneficial or detrimental depending on the material's main application.

On rail steels, tensile residual stresses will help propagation of cracks, increasing the risk of fatigue deformation. In contrast, compressive residual stresses will improve fatigue resistance [27]. As studied by Xiao el al. [28] compressive residual stresses could be added to the rail surface by shot peening.

Residual stresses could also be influenced by the wheel-rail contact in service, welding or straightening processes. Therefore, the residual stresses of a rail after hot rolling and air cooling, will differ to the ones after in-service performance or welding.

Two of the most common welding mechanisms for rails, Flash Butt Welding (FBW) and Aluminothermic Welding (AT), which will be discussed later in the report; will change the residual stress pattern at the location of the weld compared to that of the parent rail and this will influence the RCF susceptibility

Residual stresses on the rail foot have the strongest influence on in-service performance of rail steels [29]. Figure 8 represents the measurement of a rail residual stress after cooling, roller straightened, as welded and after in-service performance.

Different techniques are used to determine the residual stresses within a material; those can be divided into destructive or non-destructive. Some destructive ways to measure residual stresses are by hole drilling and web saw opening. Otherwise, non-destructive methods such as ultrasound and X-ray are also commonly used [16],[27].
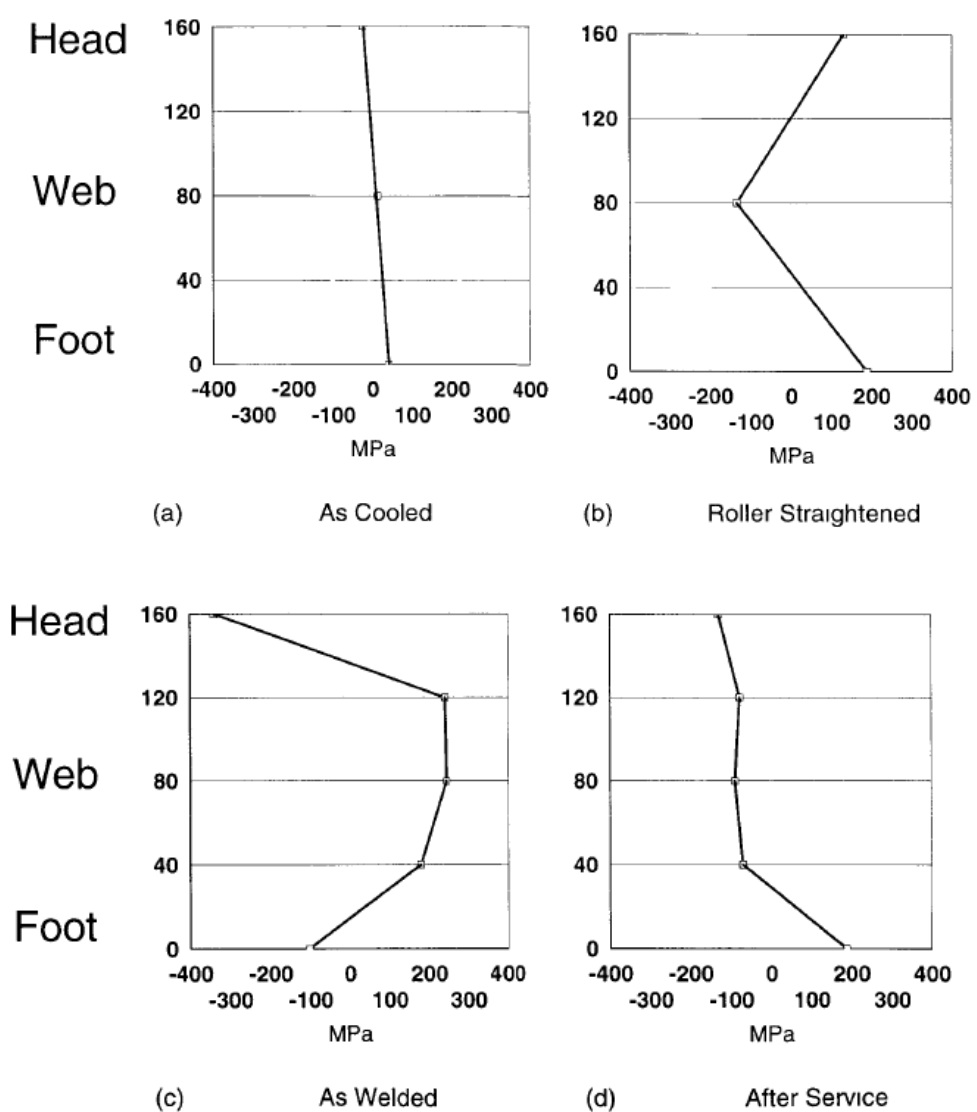
Figure 8. Variation of residual stresses on a rail. [54]

1.4. Rail steels

Currently, the vast majority of rail steels are pearlitic. A pearlitic microstructure consisting of soft ferrite (α) and hard cementite (Fe_3C), confers high resistance to the previously named main degradation mechanisms of the railway industry wear and RCF.

Table 2, represents the chemical analyses and hardness measurements of the most common rail steels that are currently manufactured by British Steel, both as-rolled and Heat-Treated rails (HT).

With the continuous implementation of heavier and faster trains, there is a rise in need for harder, strong steels, as it was demonstrated that harder rails will have a direct effect on both wear and RCF resistance of rail steels.

Increasing the number of alloying elements in pearlitic grades has been widely used to improve its resistance to RCF and wear, even increasing the carbon content up to hypereutectoid levels as in the HP335 rail (manufactured by British Steel).

Wear and RCF resistance of HP335 rail were compared with "standard" pearlitic grades within British Steel using a twin disc machine [30], observing an outstanding behaviour when compared with "standard" pearlitic rail steels, even with the same hardness levels. Nevertheless, increasing the amount of carbon has a detrimental effect on other properties, lowering its weldability, and ductility.

Therefore, rail manufacturers have been trying to increase rail performance by reducing the interlamellar spacing of pearlitic grades using heat hardening procedures instead. As an example of this, MHH is a low alloyed heat-treated steel, in which accelerated cooling of the rail head and controlled cooling of the remainder of the rail section is carried out after the full rail section is heated. MHH is characterised for having fine grain size, fine pearlitic microstructure and much lower residual stresses in the rail head and foot than conventional pearlitic steels. British Steel MHH grades confer the highest wear resistance of all pearlitic grades including the hypereutectic one, and an excellent resistance to RCF crack initiation and propagation.

This type of steel grade is used mainly in locations in which high wear is expected such as on heavy haul lines [30].

Figure 9, represents a Scanning Electron Microscopy (SEM) examination of an as rolled R260 and a MHH rail, observing the differences between their pearlite interlamellar spacing.
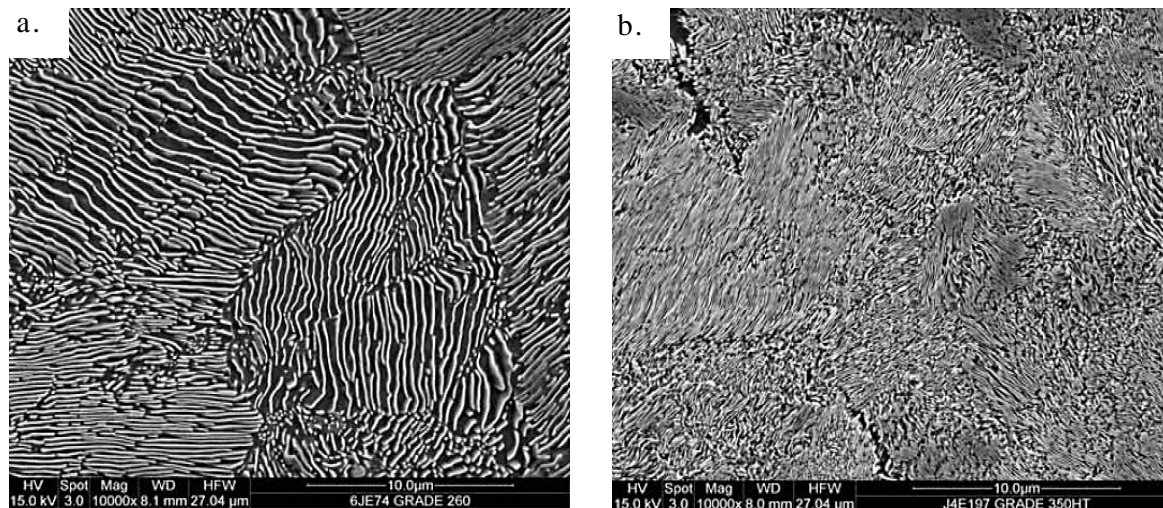

Figure 9. Scanning Electron Microscopy (SEM) of a. R260 and b. MHH [22].

Nevertheless, some problems can also be encountered on heat treated rails, due to the fact that they may exhibit a non-uniform hardness distribution through the rail section because of manufacturing variations and heat treatment procedures [31]. This non-uniform hardness distribution can lead to a fracture or damage of the rail head and, rail life could be dramatically reduced. This effect can be observed when studying differences in hardness across the cross section of the MHH heat treated steel. Hardness may reduce as depth increases, producing variations of the material properties.

Even though these rails have excellent properties in terms of wear and RCF resistance, the use of preventive grinding has not been eliminated in both cases, which leads to high maintenance cost, and even replacement of rails. Therefore, the development of new rail steels seems necessary in order to cope with the continuously high implementation of heavier loads and faster trains.

Consequently, as it was believed that pearlitic steels were approaching their limit in terms of development for in track applications, bainitic steels are starting to be used to replace them [32] .

Those were firstly used in track in the late 70s for switch and crossings, which had excellent properties in terms of RCF resistance at the same hardness of pearlitic but, they were not as good when studying its wear rate [33]. As an example of this, a laboratory study by Clayton et al [34] with the use of a pin ring test, led to the conclusion that for the same and lower hardness levels, low carbon bainitic grades have lower wear resistance than pearlitics, as in Figure 10. This was believed to be a cause of the high presence of inter and interlath carbides in the microstructure making them often brittle [35].
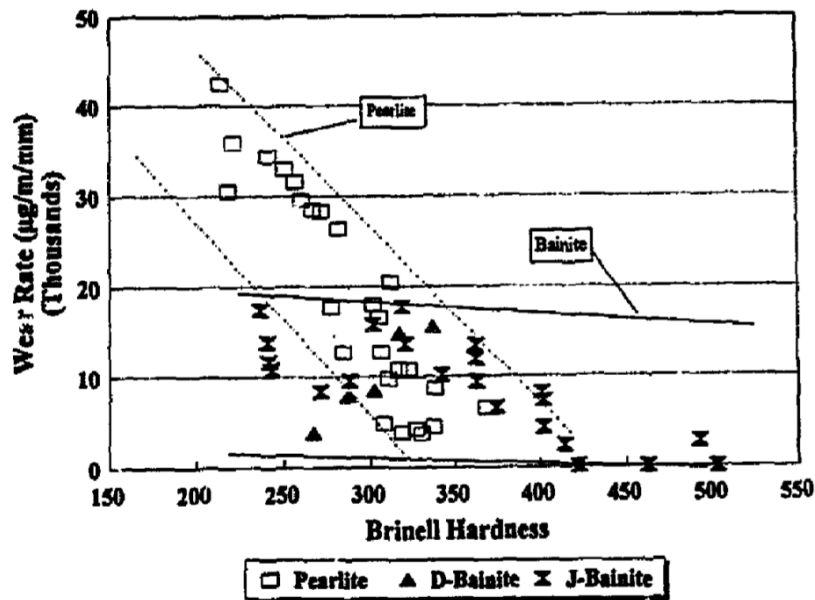

Figure 10. Bainite and pearlite wear rate vs hardness [34].

Therefore, bainitic steels are now marketed as being a development for combating RCF resistance instead of an increased wear resistance.

Table 2. Chemical analysis and hardness values of pearlitic steel grades.

Composition (wt. %)	Rail grade					Heat Treated (HT)
	As rolled					
	R220	R260	260Mn	ML330	HP335	MHH
C	0.5-0.6	0.6-0.82	0.53-0.77	0.73-0.78	0.87-0.97	0.72-0.82
Mn	1.00-1.25	1.00-1.25	1.25/1.75	1.10/1.40	0.75/1.00	0.80-1.10
Si	0.13-0.6	0.13-0.6	0.15-0.6	0.65-1.00	0.75-1.00	0.40-0.82
P	0.03 max	0.03 max	0.03 max	< 0.025	< 0.020	0.020 max
S	0.008/0.03	0.008/0.03	< 0.025	0.008-0.03	0.008-0.03	0.020 max
Cr	< 0.15	< 0.15	0.10 max	0.10 max	< 0.10	0.40-0.60
Al	0.04 max	0.004 max	0.004 max	0.004 max	0.004 max	0.004 max
V	0.03 max	0.03 max	0.03 max	0.03 max	0.03 max	0.03 max
N	0.009 max	0.01 max	0.01 max	0.006 max	0.006 max	0.009 max
Hardness (HV1)	258.2 ± 2.7	273.8 ± 1.9	294.1 ± 4.9	349.9 ± 2.9	353.5 ± 4.6	380.5 ± 3.6

1.5. The bainite transformation

I.Phase transformation mechanisms

Time Temperature Transformation (TTT) and Continuous Cooling Transformation (CCT) diagrams represent transformation percentage as a function of time and temperature for a given composition of steel. The phases present in both TTT and CTT diagrams are ferrite, pearlite, widmanstätten ferrite, bainite and martensite, as a function of the cooling rate.

As observed in Figure 11, in a TTT diagram there are two 'C' curves representing the way in which atoms move during the transformation of dissimilar phases from austenite: reconstructive and displacive.
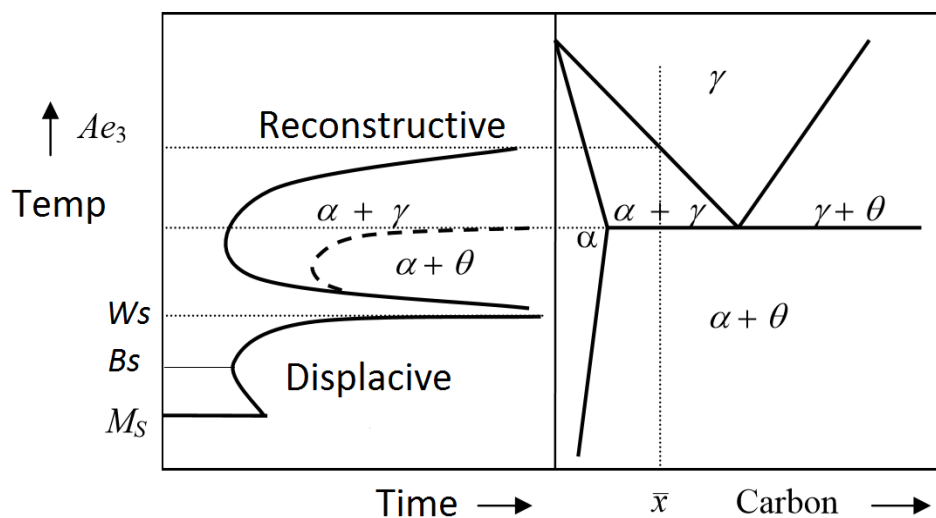

Figure 11. TTT diagram of an hypoeutectoid steel [32].

At high temperatures, diffusion of atoms takes place easily, leading to reconstructive transformations. Ferrite (idiomorphic or allotriomorphic) and pearlite are formed through this mechanism.

For low transformation temperatures, atoms take too long to diffuse, and displacive transformations take place by a shape change of an invariant plane strain (IPS) deformation which takes into account two main components shear (s) and dilation (δ),

26

both values will vary as a function of the transformation product. Widmanstätten ferrite, acicular ferrite, bainite and martensite are formed by displacive transformation. Figure 12, represents a schematic representation of these two transformation mechanisms.
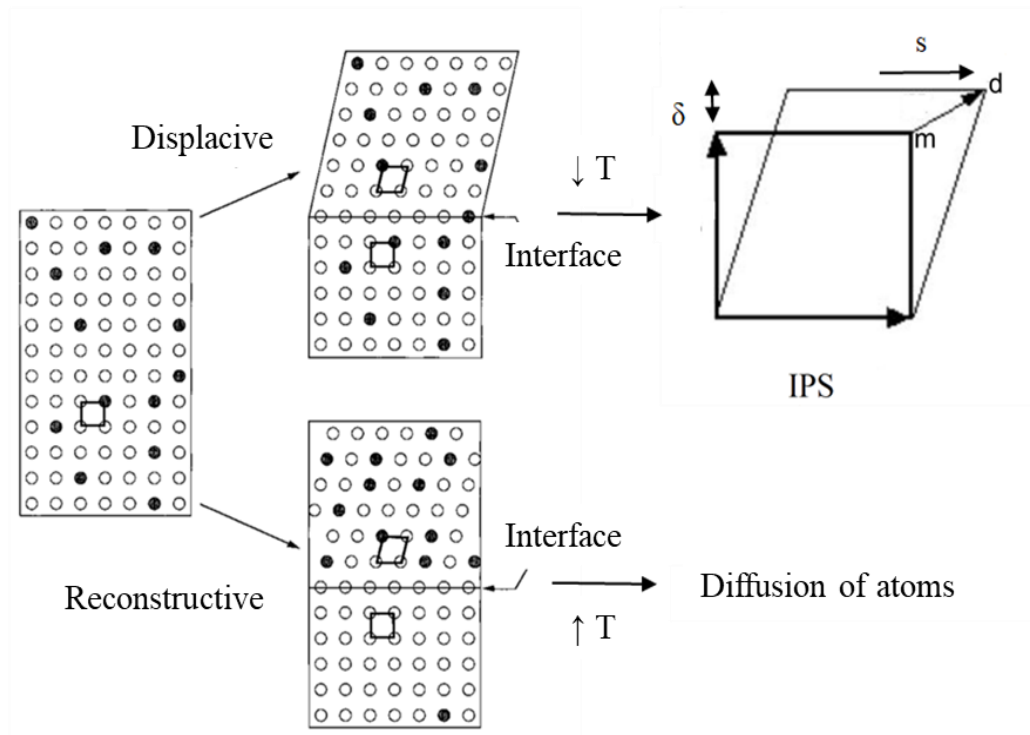

Figure 12. Schematic representation of displacive and reconstructive transformations [32],[36].

Reconstructive transformations such as allotriomorphic and idiomorphic ferrite can be distinguished by their nucleation site and shape, whilst allotriomorphic ferrite nucleates at the prior austenite grain boundary, idiomorphic ferrite does at non-metallic inclusions or carbides and has a more equiaxed shape [37], Figure 13 represents the two types of ferrite.
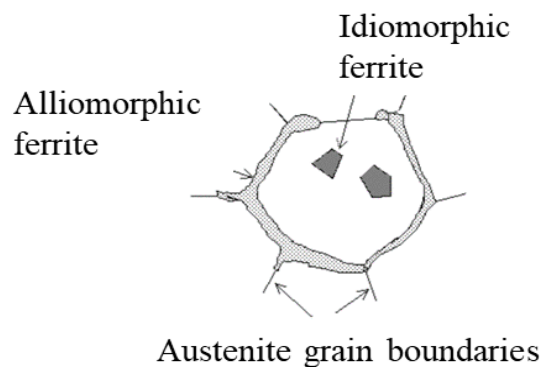

Figure 13. Nucleation of alliomorphic and idiomorphic ferrite [38].

Another reconstructive transformation is pearlite. A lamella of cementite grows in a cooperative way on an austenite crystal defect, such as the grain boundary [6],[7].

As previously mentioned, widmanstätten ferrite, bainite and martensite are **displacive transformations**.

There are two types of widmanstätten ferrite (α_w) primary and secondary. Primary α_w nucleates at the austenite grain boundaries, on the other hand, secondary α_w nucleates in an alliomorphic ferrite previously formed. Figure 14, represents a schematic representation of these two.
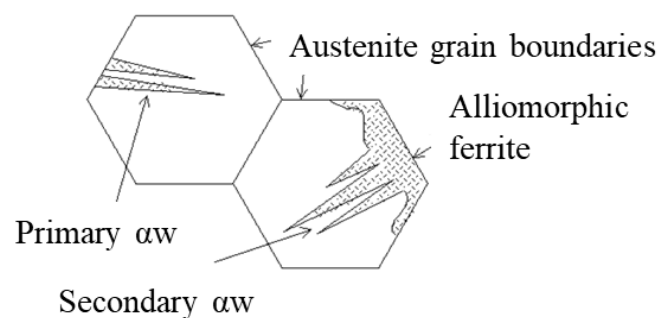

Figure 14. α_w, primary and secondary [39].

From the aforementioned, martensite is the only one that doesn't involve any diffusion of atoms, therefore, is the only pure displacive transformation.

During the transformation of martensite, temperatures are so low that carbon diffusion cannot take place. Austenite, which has a Face Centred Cubic (FCC) crystal structure, is transformed into a very hard, low dense and distorted version of a BCC crystal, which is a Body Centred Tetragonal (BCT) [36]. This is because the BCC crystal structure cannot accommodate the high carbon concentration produced during the martensitic transformation, thus, carbon will occupy more interstitial sites increasing the tetragonality of the BCC, as in Figure 15.
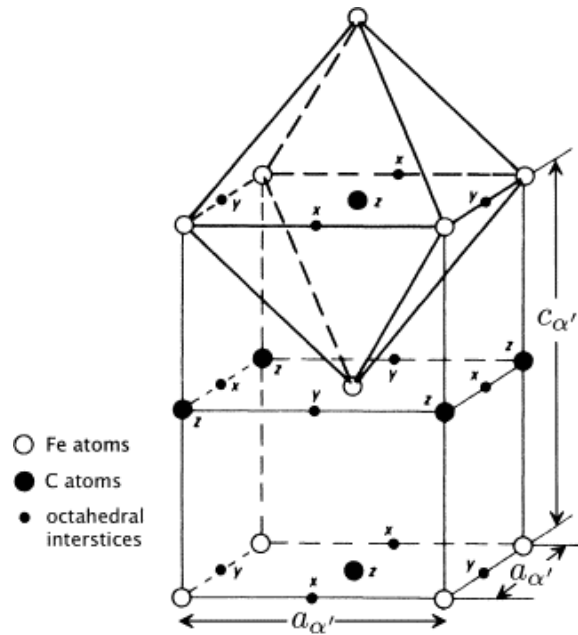
Figure 15. Body Centred Tetragonal (BCT) Martensite crystal structure [40].

As bainite is the main interest for this thesis, a more detailed discussion is made in the section below.

II. Bainite

Bainite was first described by E.S. Davenport and Edgar Bain in 1939 as an 'acicular dark etching aggregate', named "Martensite - Troostite" and usually confused with tempered martensite. Bainite microstructure consists of bainitic ferrite plates (α_b) or subunits and a second phase that can be martensite, cementite or retained austenite (RA). The aggregates of these subunits are called sheaves of bainite [32], Figure 16, represents a schematic representation of a bainite sheaf.
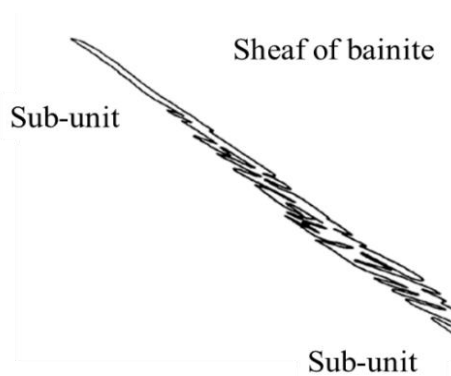

Figure 16. Schematic representation of a sheaf of bainite [32].

Each of the bainitic sheaves will nucleate at an austenite grain boundary as widmanstätten ferrite does [41]. Like other displacive transformations, the mechanism of growth of bainite takes place in an IPS.

From the thermodynamical point of view, the subunits of bainite nucleate involving carbon partitioning processes and grow in a displacive way with carbon oversaturation, immediately after, partitioning of carbon to the residual austenite is produced, leading to cementite precipitation. The next bainitic subunits nucleate and grow from the high carbon austenitic regions. This process is repeated up until the austenite is stabilized due to its increased carbon concentration and it reaches T_o, as observed in Figure 17. Therefore, the phenomenon of bainitic transformation is incomplete, as austenite never reaches its equilibrium composition (A_{e3}) [32],[41],[42].
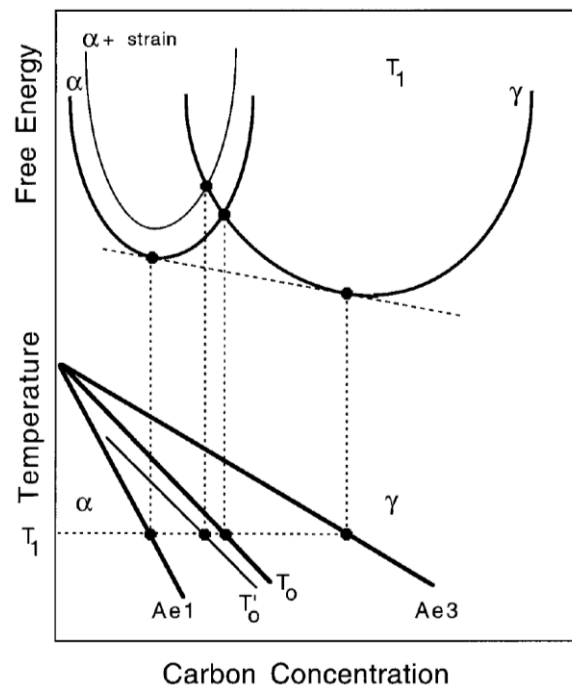

Figure 17. Representation of T_o on the phase diagram [32].

However, the growth mechanism of bainite is still under debate as a "pure" displacive mechanism will mean that no diffusion of atoms will be produced

Within the classification of the dissimilar types of bainite there are two main types as a function of the temperature of transformation and the steel carbon content, as described by Mehl in 1939 [43]: Upper and Lower bainite. Upper bainite occurs at higher temperatures of transformation than lower bainite, this leads to a bainitic ferrite

30

microstructure free of cementite particles within its laths. Lower bainite is produced at lower temperatures at which there is a slow mechanism of carbon partitioning, therefore cementite will precipitate inside the plates and between the plates of bainitic ferrite, having much thinner carbides than upper bainite.

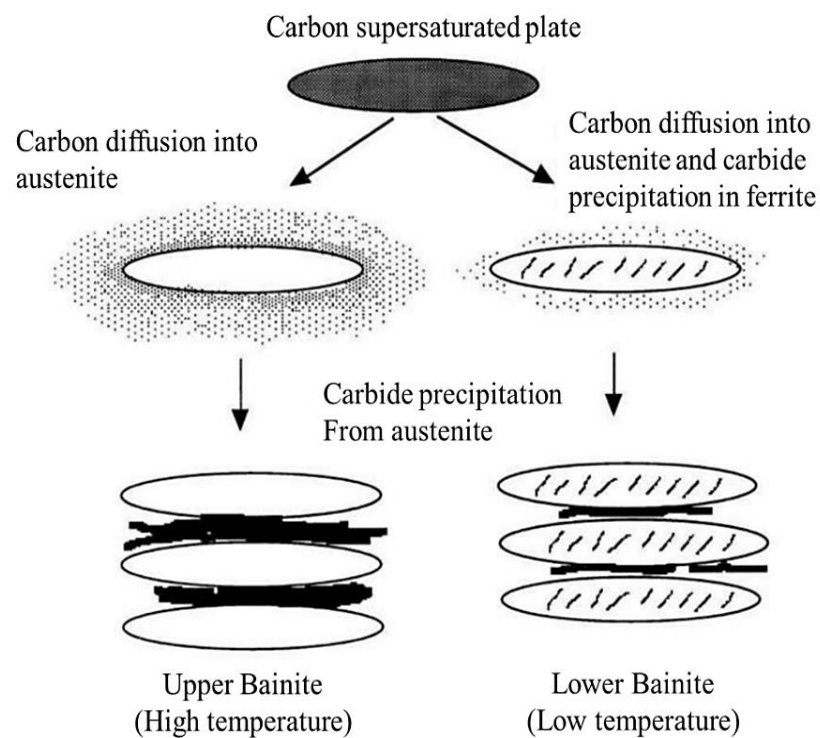Figure 18, shows a schematic representation of both upper and lower bainite.

Figure 18. Schematic representation of upper and lower bainite [32].

1.6. Carbide free bainitic (CFB) steels

As previously discussed, bainitic steels with high hardness levels will have equivalent or slightly reduced in track wear performance than pearlitic steel. This was believed to be a cause of the high presence of inter and interlath carbides in the microstructure making them often brittle; the removal of these carbides in the bainite microstructure was first developed in the late 90s [35].

Bhadeshia et al. [44],[35] studied the addition of large quantities of silicon to low alloy steels (1-2wt%) as this alleviates the presence of deleterious carbides, inhibiting cementite precipitation between the subunits of bainitic ferrite. Silicon becomes trapped in the ferrite during its growth, reducing the free energy for cementite to precipitate.

In silicon rich bainitic steels, bainitic transformation stops before cementite precipitation in the residual austenite. Therefore, carbon enriches austenite, lowering its corresponding Ms temperature, resulting in a stable residual austenite at ambient temperature, or RA. RA will have a beneficial effect in bainitics performance.

Figure 19, represents a Transmission Electron Microscopy (TEM) image of a CFB steel with RA regions in form of films.

Figure 19. TEM image of carbide free bainite, α: bainitic ferrite laths and γ: Retained austenitic regions in form of films [45]

RA is present in both films or blocks, between the bainitic ferrite laths. The carbon content of RA reaches higher contents when in the form of laths rather than in blocks, making blocky regions of RA more susceptible to transform into martensite after a tempering procedure or small stresses.

A collaboration between British Steel, and The University of Cambridge, developed CFB steels for rail applications in order to create a "high wear and RCF resistance steel"[46]. To improve its toughness, the elimination of RA blocks was studied by compositional changes [47],[48].; as blocky RA may play an important role for the initiation of voids and cracks.

CFB steels can achieve high levels of hardness and ductility without the need of any additional thermomechanical procedure, making the fabrication process cheaper [48].

To understand the performance of these rail steels in comparison with pearlitic grades different studies were taken through Europe, which will be discussed below. They were mainly used for switch and crossings, mixed traffic and rail points.

I. First CFB developed for rail applications in British Steel

The study of CFB steels for rail applications started in British steel in 1987. Bainitic 400-440HB rails were the first CFB steels developed and installed at various locations for testing [49], the chemical composition of these grades is represented in Table 3.

Table 3. Chemical composition of 400 and 440 CFB steels.

Grade	Composition (wt.%)							
	C	Mn	Si	P	S	Cr	B	Hardness (HV1)
440	0.24	1.99	1.97	< 0.025	0.013	1.98	~0.0025	432
400	0.26	1.95	1.95	< 0.020	0.011	0.49	~0.0025	395

The 440HB rail was the favoured choice of composition, based on laboratory evaluation and on track performance when tested in British Steel Scunthorpe works, leading to the best performance in terms of wear and RCF resistance [50]. As an example of this, 440HB has shown four times greater fatigue resistance than 400HB.

Unfortunately, both 400 and 440HB bainitic steels, have shown degradation in fracture toughness when tested in Hydrogen Embrittlement (HE) environment, being susceptible to stress corrosion cracking (SCC). After this, commercial application of these grades was not recommended [50],[51]. Grades 320 and 360HB were later developed, as softer grades were believed to have higher resistance to the SCC degradation mechanism.

II. B320 and B360

Both B320 and B360 grades were observed to have similar SCC resistance as other steel grades used within the rail industry. The chemical composition and hardness measurements can be observed in Table 4.

Table 4. Chemical composition of CFB B320 and B360.

Grade	Composition (wt.%)								
	C	Si	Mn	Cr	Mo	B	V	N	Hardness (HV1)
B360	0.32	1.11	1.51	0.58	0.16	0.003	0.02	0.009	360/390
B320	0.23	1.13	1.47	0.51	0.17	0.003	0.19	0.009	320/340

As previously mentioned, more than 1wt.% of silicon will inhibit formation of carbides, leading to bainitic ferritic laths surrounded by RA regions[44]. Other elements such as manganese, in combination with molybdenum and boron help to ensure bainite formation in all the rail section. The synergy of the Mo and B additions are key to the formation of bainite in low C steels as they delay the pearlite transformation. Otherwise, vanadium is used in the B320 grade in order to compensate for the lower carbon content [52]

Both microstructures consist of bainitic ferritic laths without any carbides, and RA regions surrounding the bainite laths, those can be observed in Figure 20; the white regions will represent de bainitic ferrite laths, whilst RA will be presented in black surrounding the laths.
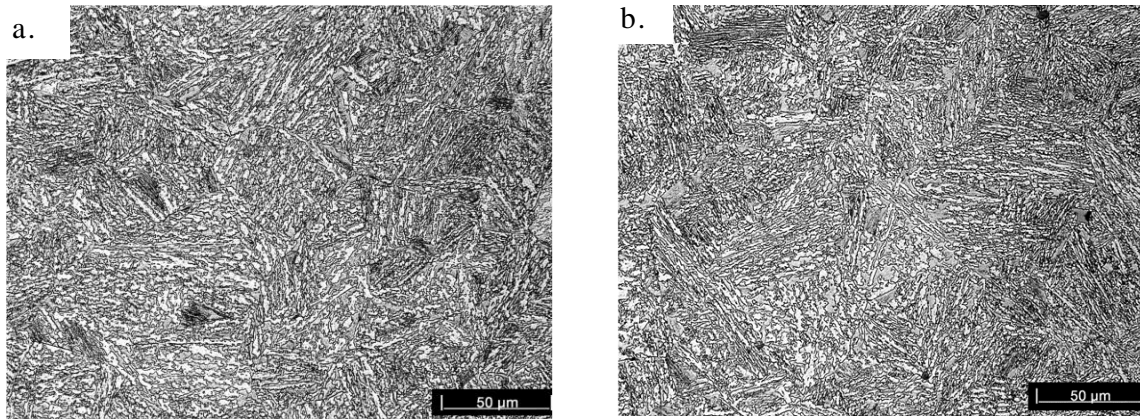
Figure 20. Light micrograph of a. B320 and b. B360 CFB grades [53].

During the cooling of both B320 and B360 rails on the cooling banks during manufacture, the transformation of the austenitic structure takes place between 500 and 300°C and its cooling rate is of 0.15°C/second. Thus, leading to a carbide free upper bainitic microstructure. Figure 21 and Figure 22 represent the CCT diagrams of both B320 and B360, with its corresponding A_{c1} and A_{c3} temperatures, both supplied by British Steel.
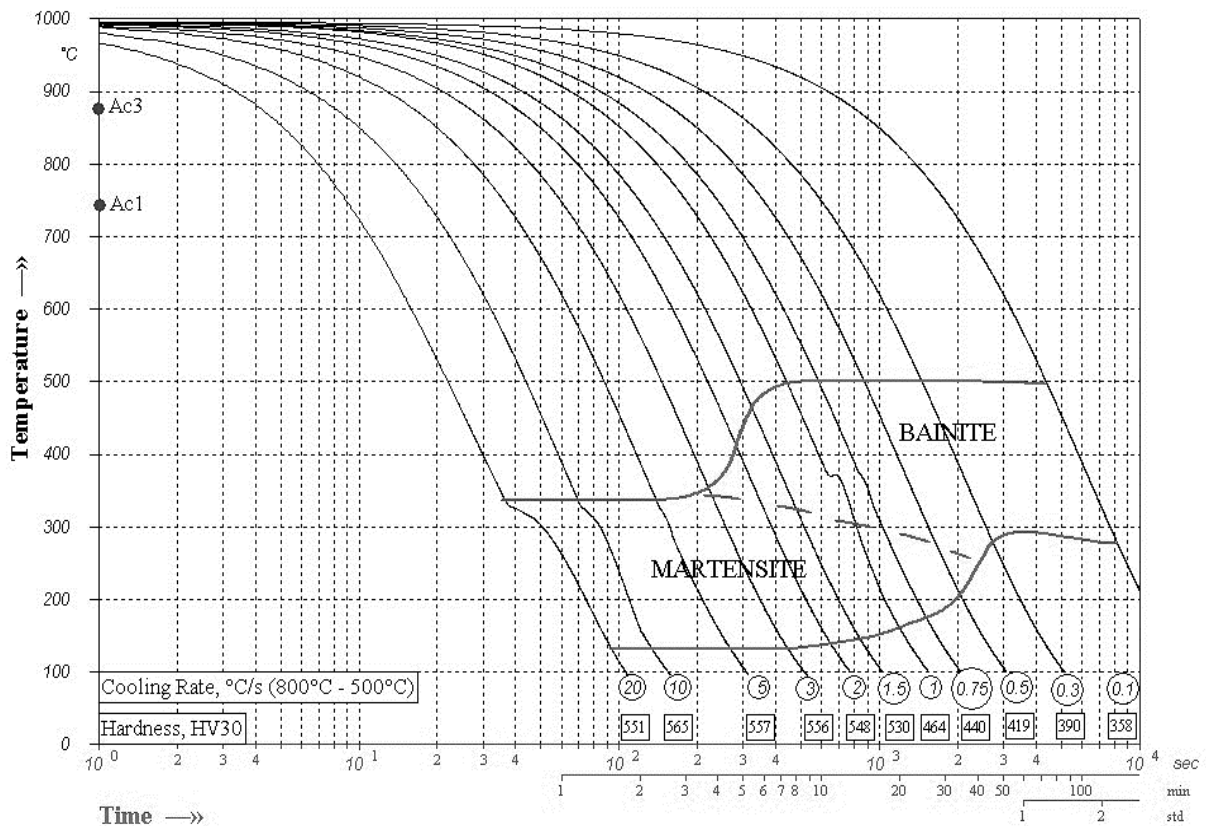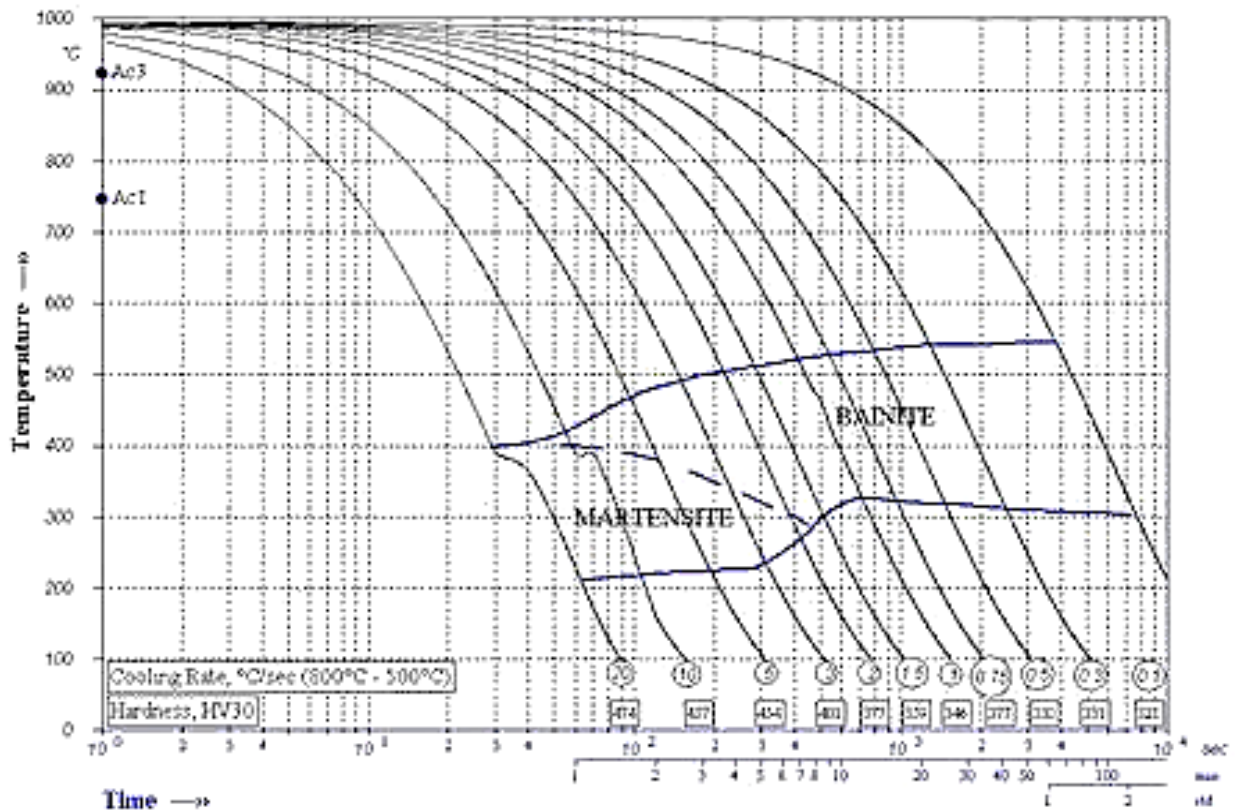

Figure 21. CCT diagram of CFB B360
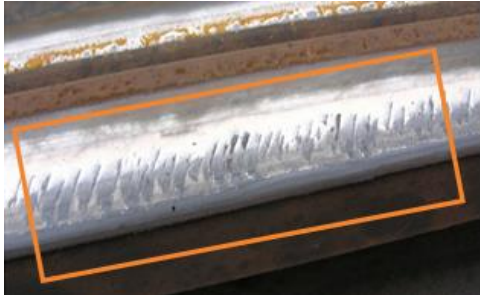
Figure 22. CCT diagram of CFB B320

III.In track performance of as rolled B320 and B360 versus pearlitic rails.

In 1998, both bainitic rails, B320 and B360, were highly recommended for tracks where RCF was the major issue; RCF is considered nowadays as the main criteria limiting rails life in track.

CFB steels B360 and B320 have shown a considerably higher number of cycles to crack initiation than standard pearlitic grades, showing an improvement between 20 and 50%, and having twice more cycles to crack initiation than MHH [29]. Outstanding performance was observed especially when analysing its head checking resistance. Some examples of this are shown in Table 5 [49].

Table 5. Example of in-service head check resistance. Comparison between bainitic and pearlitic grades [49].

After 420 Million Gross Tons (MGT): Rails placed in the Eurotunnel

B320

R260

No grinding required

Grinding required every 6 months

After 30 MGT: Line Paris, Mulhouse, rail placed in Switch blades

B360

R260

No head check

Visible head check

As represented above, for the same track conditions, R260 pearlitic grades are developing many head checks in comparison with the bainitic B360 and B320 grades, in which no head checking was observed. The same behaviour was found even when comparing CFBs with a 350HT rail.

Differently, in terms of its wear performance, B320 has demonstrated to have the same wear rate as pearlitic 260HB. B360 has as much wear resistance as pearlitic 260HB grades, and even hypereutectoid HP335 grades [49]. A summary of in track performance of CFB grades versus pearlitic can be observed in Table 6 and Table 7.

Table 6. In track performance of CFB B320 and B360 versus R260 and 350HT pearlitic grades [54]

Area	Company	SNCF	SBB
	Test area	Dieupentale	Frick
	Line	Bordeaux - Sète	Niederfeld - Frick
	Position	Track 1	
		km 223,385 to 224,075	km 52.689 to 52.362
		High rails	High and low rails
	Lubrication	Locomotives, light	Locomotives, good
	Curve radius	1140 m	449 m
	Cant	124 mm	120 mm
Test rails	Profile	60E1	60E1
	Grade	B320	B360
	Laying	17/12/1998	01/11/1999
	Grinding	No	5/11/00 & 30/10/01
Traffic	Passenger trains	160 kph	95 kph
	Freight trains	140 kph	95 kph
	Axle load	Up to 22.5 t	Up to 22.5 t
	Daily tonnage	40800 t	81000 t
	Total tonnage (21/10/08)	146 MGT	265 MGT

rail	Grade	R260	R350LHT
	Usual type of defect	Head checking	Head checking
	Preventive grinding	Within 6 months	
	Currative grinding	vs. RCF growth	vs. RCF growth

Test rails	Current results	RCF on all the R260 rails No RCF on the bainitic rails	RCF on the R350LHT rails No RCF on the bainitic rails Corrugation on low rails
	Current situation	End of the test on 02/09/08	launching of test phase 2 : 450 t radius 650 to 1200 m : high and low rails radius 500 to 650 m : only high rail

Table 7. In track performance of CFB B320 and B360 versus R260 grades [54]

	SNCF	Eurotunnel	SNCF
Area	Vaux en Pré	Tunnel	Pantin
	LN1 Paris - Lyon	Calais - Folkestone	Paris - Mulhouse
	Track 2	RTN 2	Track 1 Eole
	km 292.123 et 292.995	km 34.651 to 36.098	km 5.600
	point	High and low rails	switch blade
	Locomotives, good	No (forbidden)	locomotives, light
	1/65 60E1A4 Left and right hand V2 Cex 4000	6000 m	tg 0.0372
		35 mm	
Test rails	60E1A4 machined and forged to 60E1	60E1	60E1T2
	B360	B320	B360
	07/06/2005	29/01/2007	14/03/2008
	No	No	No
Traffic	270 kph	160 kph	120 km/h
	No	140 kph	No
	17 t	Up to 22.5 t	up to 20 t
	70000 t	300000 t	42000 t
	85 MGT	189 MGT	9 MGT

rail	R260	R260	R260
	Head checking	Head checking and squats	Head checking
	No	Within 6 months	No
	vs. RCF growth	Once a year	vs. RCF growth

Test rails	No RCF	No RCF on the R260 rails No RCF on bainitic rails	No RCF
	Qualifying process under progress for high speed switches mobile points	Continuation of the test for 3 years	Continuation of the test. A second bainitic switch blade will be installed in the Pantin area.

Therefore, the benefits of CFB rails versus pearlitic are: Enhanced RCF resistance, improved wear resistance in the case of B360 and improved toughness and ductility. Less frequent rail grinding is required, therefore, less maintenance costs are expected, and lower probability of rail fractures [16].

1.7.   Rail joining

In the UK, rails are usually cut during the manufacturing process to a length as requested by the customer. The end of those is connected with the use of fishplates, as in

Figure 23. This is commonly made leaving a gap between the two rails connected, called "expansion joints", as rails could vary its length due to temperature fluctuations [17][16].

Figure 23. Rails connected by fishplates [16].

However, fishplates are not ideal for rail connections as its presence will have a detrimental effect on rails wear; also, they are noisier, decreasing passengers comfort; and, finally, maintenance is required when in use [7],[2]. This, makes fishplates a non-suitable joining mechanism for high-speed trains and high loads. That is why the use of fishplates is becoming obsolete and ,nowadays, many rail steels are continuously welded [2], extending service life of rail steels [55],[56]. Around 900000 t/year of rails are being continuously welded in Europe during recent years[16],[57].

Two of the most common welding mechanisms that are being used nowadays are Alumino Thermic Welding (ATW), Flash Butt Welding (FBW); whilst FBW is commonly used for welding in plant, ATW procedures are used in track.

---

[2] *As previously mentioned, expansion joints are used in jointed track in order to accommodate expansion or contraction of the rails. On continuously welded tracks, anchors are usually being used to prevent rails movement.*

I.Aluminothermic welding (ATW)

Thermic welding (T.W.) is produced due to an exothermic chemical reaction, which involves the reduction of a metal oxide; usually iron oxide; by a metal reducing agent such as aluminium, as shown in the reactions below[5],[16].

$$Fe_2O_3 + 2\ Al \longrightarrow Al_2O_3 + 2\ Fe + Heat$$

$$3FeO + 2\ Al \longrightarrow Al_2O_3 + 3\ Fe + Heat$$

This reaction generates enough heat, with temperatures up to 2500°C, in order to make molten iron. This type of welding mechanism is generally used for in-situ welding of rails, for repair or replace a defective rail [40]. An example of an aluminothermic welding procedure is shown in Figure 24.

Figure 24. ATW of two rails

The first step for the ATW process will be the preparation of the welding joints. For this purpose, the rail ends will be separated at a distance between 18 and 20 mm, this must also be cleaned to remove any oxide, slag or impurity. After that, the horizontal and vertical alignment of the rails is also produced. Then, refractory moulds are placed between the rails gap. The moulds are preheated and the crucible is prepared with the metal to fill the gaps. An ignitor such as barium peroxide starts the Aluminothermic reaction, achieving temperatures up to 2500°C. When the reaction is finished, the crucible is tapped and the molten steel fills the moulds and the gap between the two rails. Once the weld has cooled to 1100-1200°C, the moulds and crucible are removed and the weld is left to cool to an appropriate grinding temperature.

This thesis is going to focus more in detail on the FBW procedure, which will be discussed below.

II.Flash Butt Welding (FBW)

FBW is used nowadays in British Steel facilities as a fully automated method for joining rails. A conventional FBW program takes between 1.5 to 4 minutes per weld [58]. Nowadays, almost 90% of the continuously welded rails are FBW [59]. Figure 25 represents both a fixed FBW for primary in site welding and a mobile FBW.
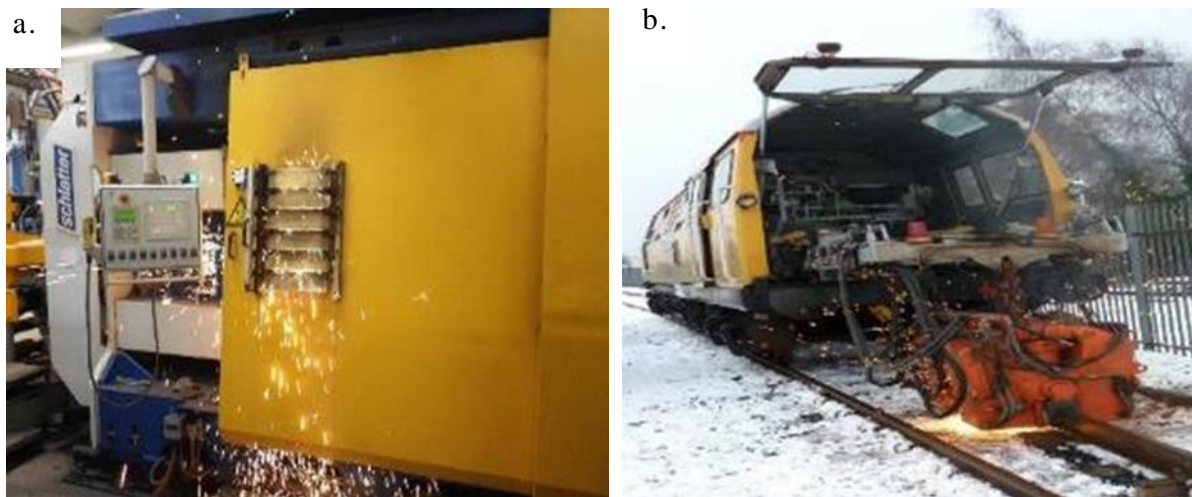

Figure 25. Mobile(b) and Fixed(a) FBW equipment's [60]

During a FBW procedure, no filler material is necessary, as unlike other welding procedures such as ATW this type of welding procedure takes place by melting the rail ends with the use of an electric current. Figure 26, shows a schematic representation of a FBW procedure.

Before starting the welding procedure, grinding of the rails is crucial in order to remove excessive rust and mill scale from the electrode contact areas [58]. Once the rails are in the welder, it is necessary to check if they are aligned together before starting the procedure.

The first stage of the FBW procedure requires between five and ten seconds and it is called burn-off stage. During this stage, in order to square up the rail ends, arcing or flashing while the rail ends are separated is produced. [58]
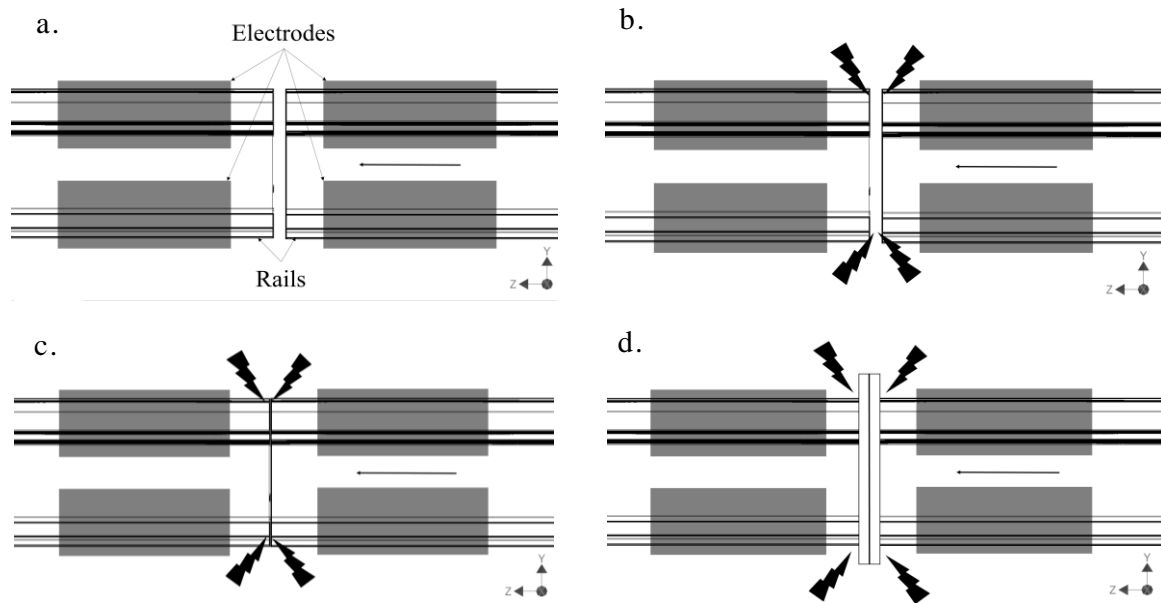
Figure 26. Schematic representation of the FBW procedure of rails. a. Check rails alignment, b. Burn-off, c. Preheating and d. Flashing.

The second stage is called preheating stage; whose main purpose is to achieve sufficient temperature in order to promote easier flashing with a lower secondary voltage. During the preheating stage the rails are brought together at low pressure and high current, this is usually produced between five and ten times and each preheating cycle has a duration between one and ten seconds. This stage also allows the temperature gradient to be less aggressive and therefore, improve the heat distribution.

After the rail ends achieve an appropriate temperature, the next and final flashing is produced, during this stage the rail ends are brought in contact resulting in flash, oxides could be formed, and will be later on removed [59]. The rail interfaces are molten and the conditions for the final upset are achieved. This process takes between 5 and 10 seconds.

Flashing speed is usually accelerating and may be servo controlled for best results. If flashing voltage is too high or forward speed too low, deep craters can be formed on the flashed surfaces which increase the risk of weld interface flaws. Finally, the rail ends are pressed together, this is produced either under a constant platen speed or, an impact loading of up to 1000kN. In order to avoid oxidation in the weld interface, current is usually applied during the final part of the forging process. All the different stages carried out during a FBW process are represented on a weld chart, which shows the force (kN) and current (kA) applied, together with the rails travel or displacement (mm); an example of a weld chart is show in Figure 27.
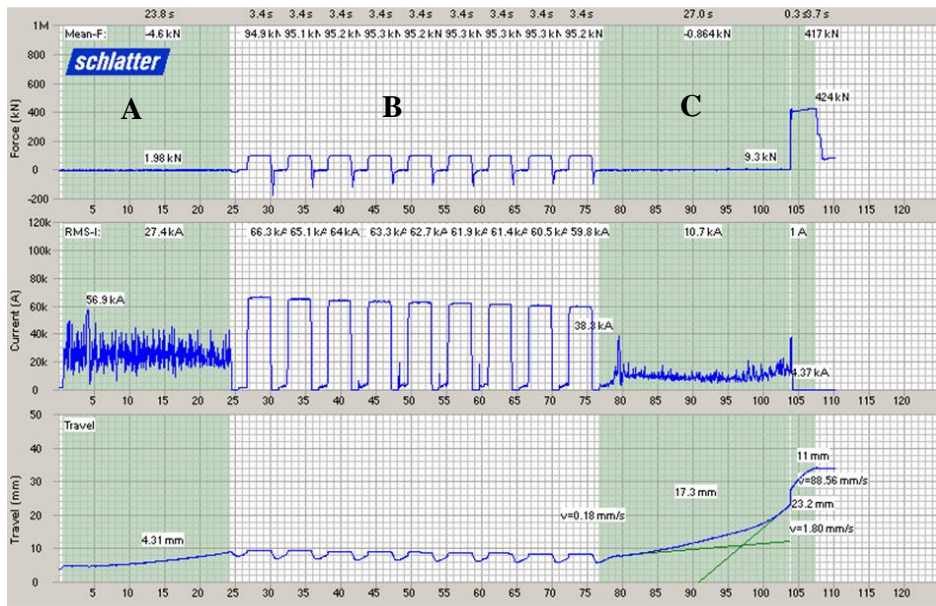
43

Figure 27. Weld Chart of a FBW procedure with 9 preheat cycles. Representing the different stages A. Burn off, B. Pre-heating and C. Flashing [60].

At the end of the welding any excess of material is automatically chipped off, usually by an automatic hydraulic stripper in the welding plant, as observed in Figure 28. Both the welding current and the upset force have a direct influence on this process.
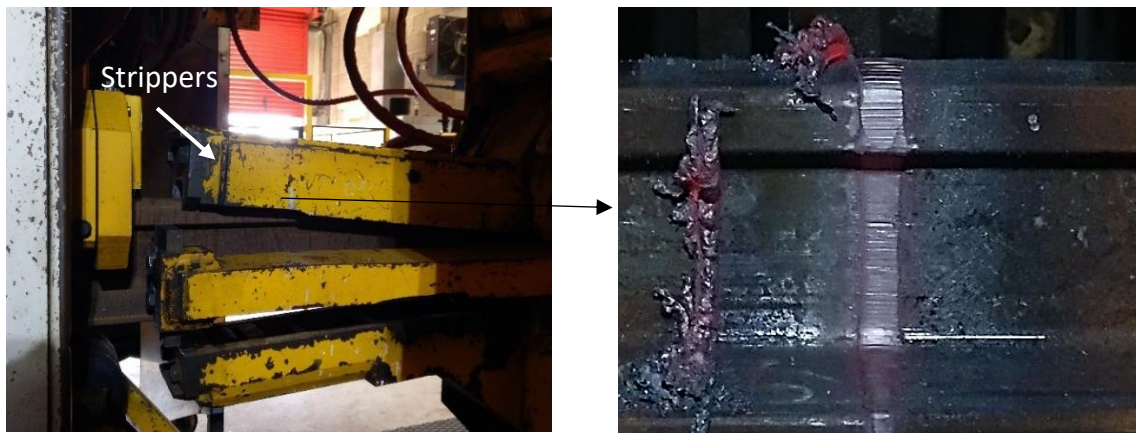

Figure 28. Stripping process. Excess of material is removed from the Flash Butt Welds.

The welding current, which dictates the temperature of the process, has to be high enough to ensure the deformation of the rails.

The quantity of material removed from the weld interface is dictated by the amount of upset force, this has to be high enough to remove any oxide or porosity and ensure weld consolidation. If this is low, oxide inclusions could get trapped within the

44

material, as in Figure 29, being detrimental for the initiation and propagation of fatigue cracks.[59]
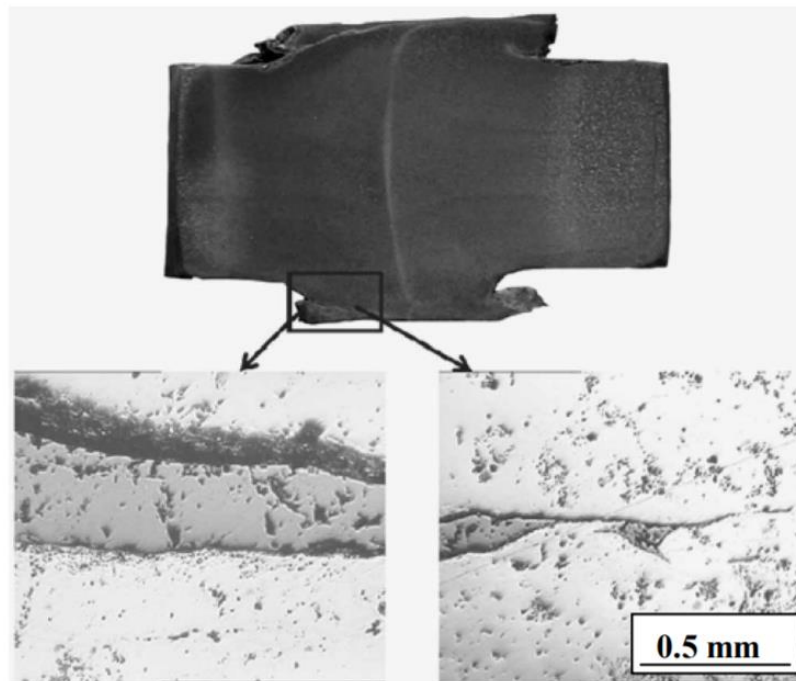
Figure 29. Inclusions trapped during the stripping process [59]

Later on, the weld proceeds to naturally air cool down to <400°C and water quench. Finally, the welds are straightened and ground with the use of a semiautomatic profile grinding system. To determine the weld quality, the FBW procedure is followed by a micrographic and macrographic examination of the welds, a magnetic particle inspection (MPI) test in order to detect surface discontinuities and a three-point bending test.

1.8.   The Heat Affected Zone (HAZ)

During fusion welding procedures such as FBW, the regions that will be of interest are: the fusion zone (FZ), the heat affected zone (HAZ) and the unaffected base material [42]. Our main interest is focused in the HAZ, which is a portion of the material that has not been melted but its mechanical and microstructural properties are affected due to the temperature gradient and cooling rates achieved adjacent to the weld FZ.

In order to understand the aforementioned altered microstructural properties during welding, it is important to consider the dissimilar heating and cooling rates. Figure 30, represents the microstructural evolution of the HAZ during welding. When heating, at temperatures above A_{c1}, austenitic transformation starts to take place, being complete at A_{c3} temperatures; above A_{c3}, austenitic grain growth starts. When cooling, the austenite decomposition starts below Ar3.
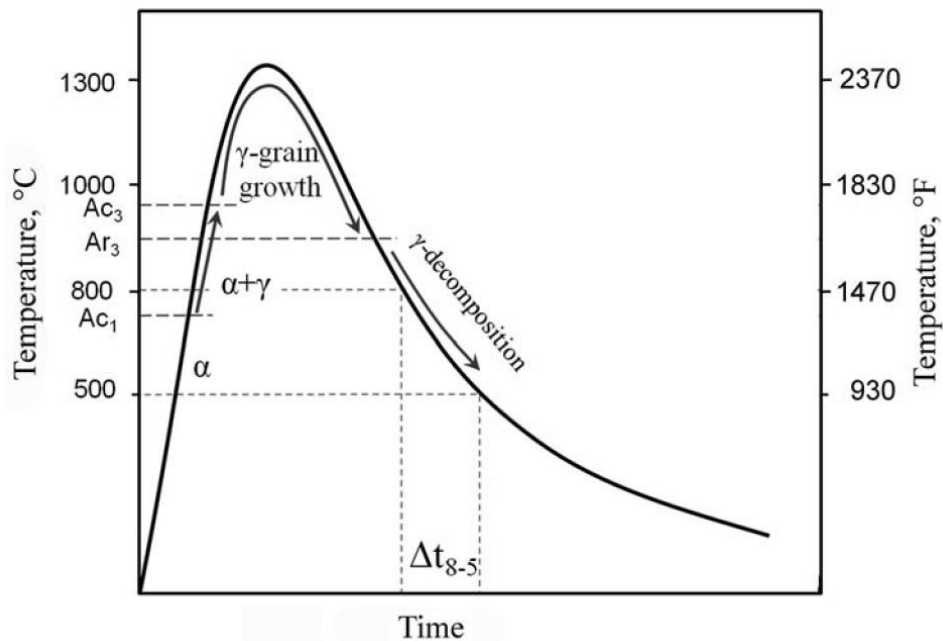
Figure 30. Schematic representation of the microstructural evolution during heating and cooling [61]

Therefore, the HAZ region of a steel its widely considered as a weak link in mechanical testing [62], sometimes leading to fracture mainly due to fatigue in tracks.

When looking at a Fe-Fe3C phase diagram, the different regions present in the microstructure of a steel HAZ can be observed; as represented in Figure 31. The HAZ of a steel can be divided in three main regions: Critical, intercritical and subcritical.
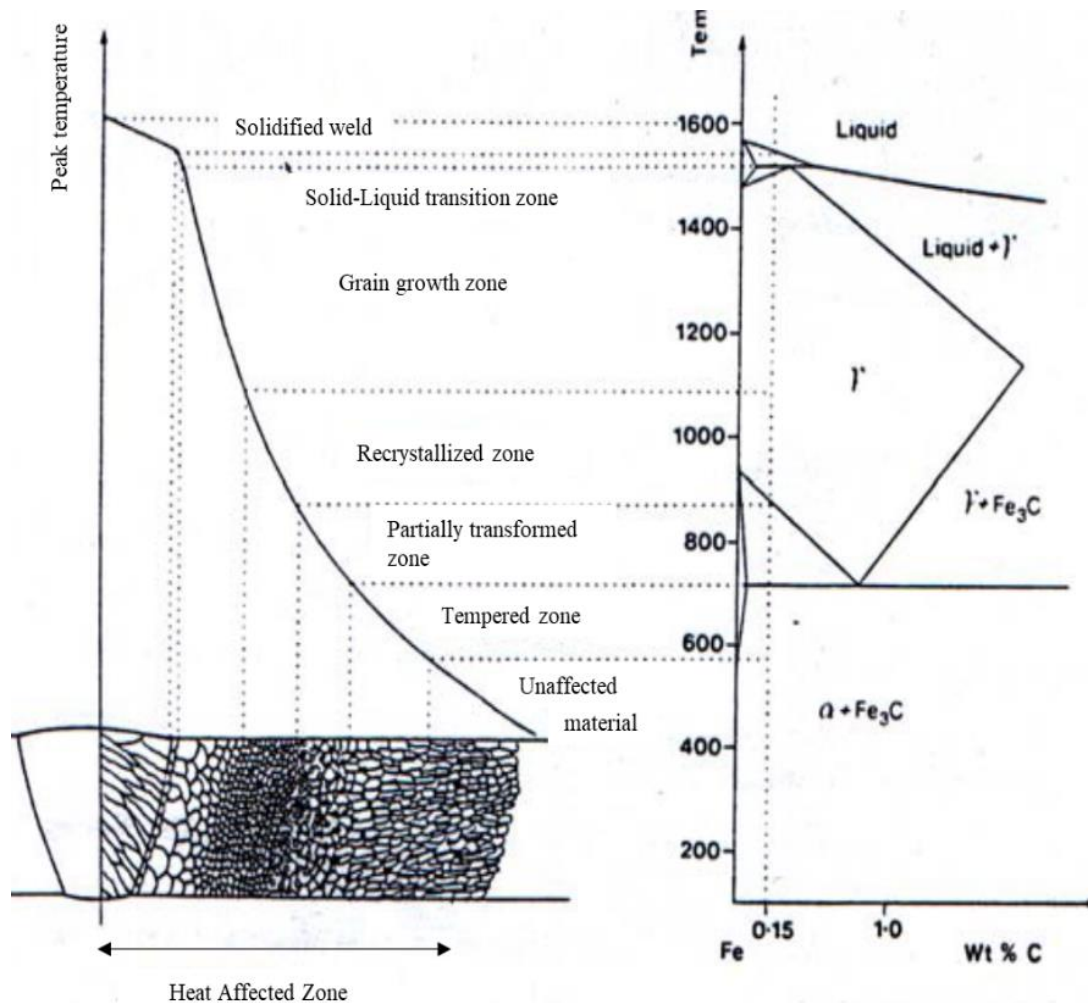

Figure 31. Fe-Fe3C phase diagram and HAZ microstructures [63]

In the **critical** region of the HAZ (CHAZ) temperatures above Ac_3 are achieved, a complete reaustenitisation of the steel is produced leading to a coarse grained region, in which the temperatures reached are between 1500-1200°C [61]; when the temperatures are between 1200 °C-Ac_3 grain growth is limited, leading to a fine grain zone [63]

In the **intercritical** HAZ region (ICHAZ), temperatures between Ac_3 and Ac_1 are achieved [61], leading to a partial reaustenitisation of the steel, the low peak temperatures together with the presence of particles will produce limited grain growth of austenitic regions.

47

At temperatures below Ac_1, heavily tempered microstructures are produced within the **subcritical** HAZ (SCHAZ), leading to a softened region.

These microstructural variations will also cause changes in hardness. Measurements of the welded rail hardness are believed to be the best first approach to determine its quality [64]. Numerous examinations have been made on the HAZ microstructural and hardness variation of conventional rail steels. This is normally carried out on the rail head, as it is the region where higher contact stresses are produced. As an example of this, Figure 32 , represents the hardness distribution on the rail running surface of a compressed air cooled pearlitic 60E1 350HT weld after a FBW procedure [58].
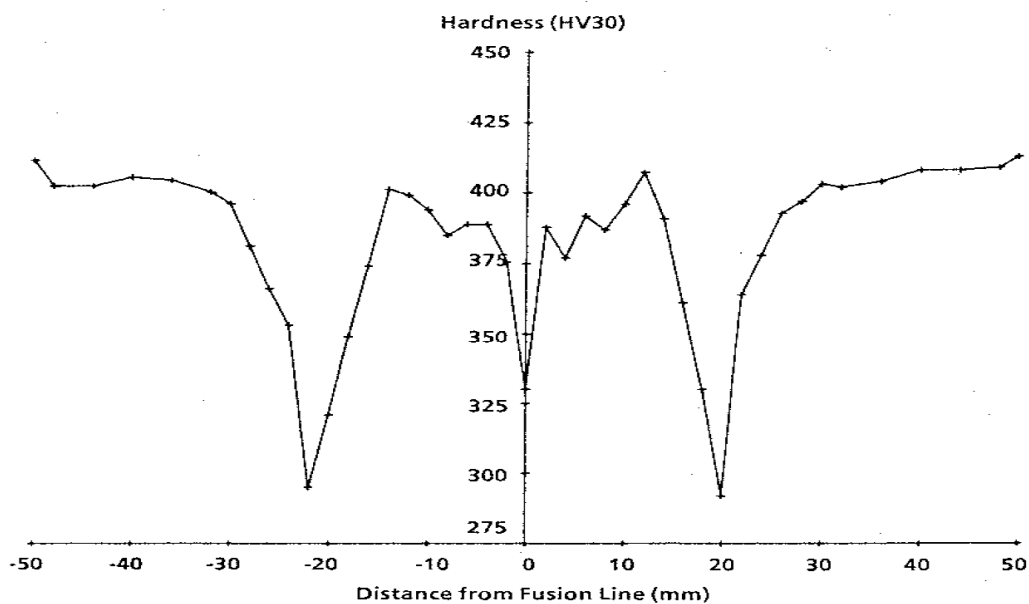
Figure 32. Hardness distribution of a 350HT weld after a FBW procedure [58]

Parameters of the FBW procedure such as the number of preheats and the upset force have a direct influence on the width of the HAZ[16]. Wider HAZs can be detrimental for rail in track performance, leading to formation of preferential wear or "weld batter". Successful attempts have been previously made to reduce the HAZ of FBW procedures by limiting the number of Preheat cycles[16],[65].

1.9.   Summary

To summarize what has been discussed in the literature review;

1. Rails are the element of the track in which higher contact stresses are produced, constant maintenance of rails is required in order to avoid the main degradation mechanisms when in track, such as wear and RCF.

2. As faster and heavier trains are becoming more common, it is believed that "conventional" pearlitic rail steels are reaching the limits of their development and there is a need for a new steel grades to target higher wear and RCF resistance.

3. Carbide-free bainitic steels B360 and B320 were developed during the late 90s; when tested in track they showed an outstanding behaviour in comparison with pearlitic rails, mainly when analysing one type of RCF defect: Head Checks.

4. Two of the main welding mechanisms used nowadays are FBW and ATW, this thesis is going to focus on the FBW. FBW is a type of resistance welding in which melting of the rail ends is produced due to an electrical current, and no filler material is needed

Chapter 2

Challenges and objectives

On this chapter, a review of the problems encountered when welding CFB B320 and B360 will be discussed, together with a summary of previous work performed by British Steel in order to tackle this concern.

2.1.   Welding challenges of CFB rail steels

As previously mentioned, in track performance of CFB rail steels, more specifically B360, has shown to be outstanding in comparison with as rolled pearlitic steels when comparing RCF. However, concerns were raised after cracks were found on B360 FBW and ATW after 6 to 24 months of in track trials [66].

Even after applying grinding procedures, severe RCF was found in CFB welds B360 in track [46], which led to cracking, removal and replacements of the welds [47].

Although the mechanisms of failure are still not entirely clear, for both FBW and ATW the formation of RCF cracks is generally produced in the sub-critical HAZ and severe cracking is mainly developed within the critical region of the HAZ [66]. However, the main cause of propagation and initiation of these cracks has not yet been confirmed, Figure 33 represents a more in detail examination of cracks produced within a FBW of CFB B360.
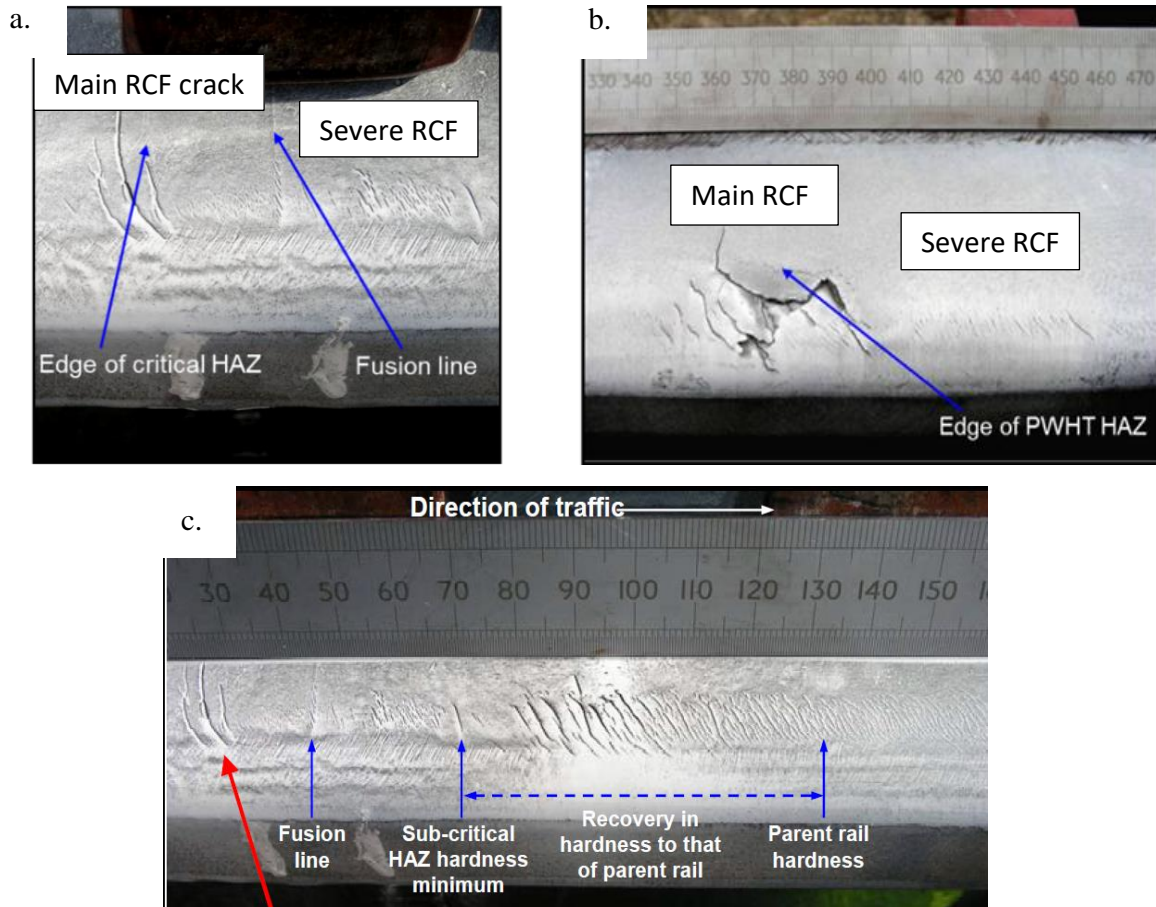
Figure 33. (a)FBW and (b)ATW failures of CFB B360 in track. (c) More in detail examination of cracks produced on a B360 FBW [66].

Welding related problems are not found in B320 grades. An analysis of in-track performance of B320 CFB grades has been done on several occasions by British Steel, showing no cracks. It is believed that the cause of a better in-track performance of the B320 CFB could be [53]:

- The presence of vanadium in the B320 grade could reduce softening in the tempered HAZ.

- The lower carbon content, 0.23wt%, will limit the maximum hardness obtained in the fine-grained HAZ.

2.2. Examination of the HAZ of B360 vs R260

Generally, pearlitic grades are well understood and its HAZ microstructural evolution can be identified by an examination of the iron-iron carbide phase diagram. The austenite to pearlite reaction is the essentially the same as the pearlite to austenite reaction. Nevertheless, studying bainitic steels microstructural evolution is more complicated.

Macrographic comparisons of the HAZ of bainitics and pearlitics were made within British Steel by H M Smith [43]. Figure 34, represents a macrographic examination of a longitudinal-axial section of a FBW, the rails welded were a pearlitic R260 and a CFB B360.

Pearlitic   Bainitic
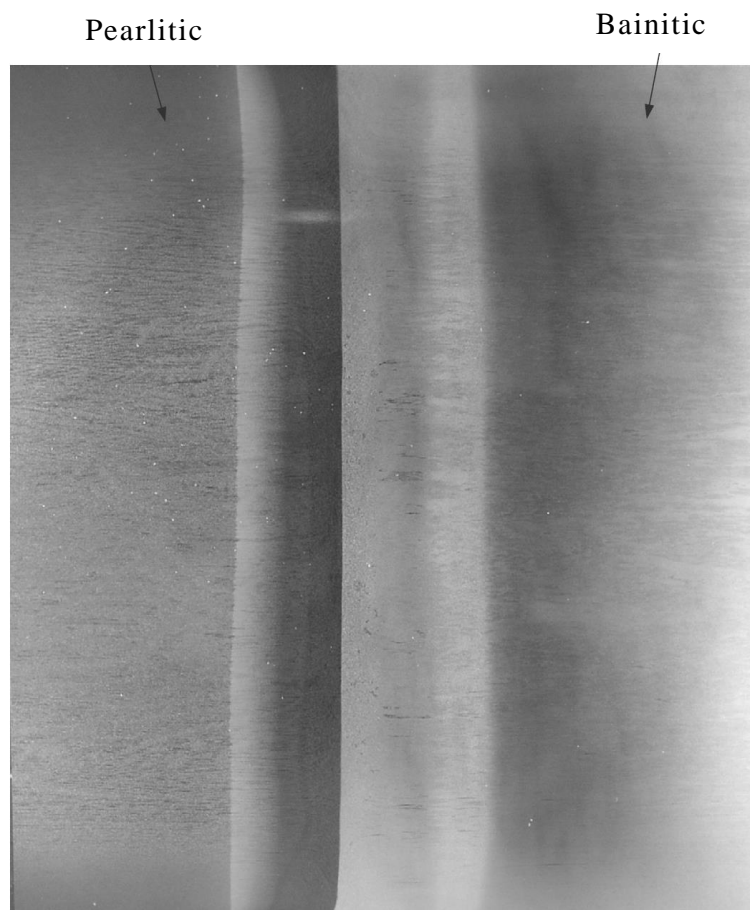
Figure 34. Macrographic examination of a longitudinal-axial section of a pearlitic and bainitic B360 flash butt weld [43].

Measurements of the FBW widths were made 5mm below the running surface, mid height and foot regions of the HAZ as represented in Table 8.

Table 8. HAZ width measurements of FBW pearlitic and bainitic.

Measurement location	HAZ width (mm)	
	Pearlitic	Bainitic
5 mm below running surface	19	26
Mid height of rail	21	28
Base foot	21	28

As observed, FBW CFB B360 has a much wider HAZ than the pearlitic weld, using the sample FBW program. Although the HAZ width variation across the weld satisfied the variation between maximum and minimum value of 10 mm, the measured HAZ width failed to satisfy the limit of 45 mm maximum as specified in EN 14587-1 [67].

The wider HAZ of CFB steels in comparison with pearlitic is believed to be produced because no further microstructural evolution will be developed in pearlitic steels once the temperature of the weld is below ~ 650 °C. Nevertheless, this is not the case for CFB steels, as bainite will be tempered even at 450 °C [66]. A wider HAZ could have a detrimental effect in the rail behaviour, which could be an explanation of its poor in-track performance. Hardness measurements across the HAZ of a pearlitic-bainitic weld were also made, as in Figure 35 confirming the wider HAZ of bainitic rails.
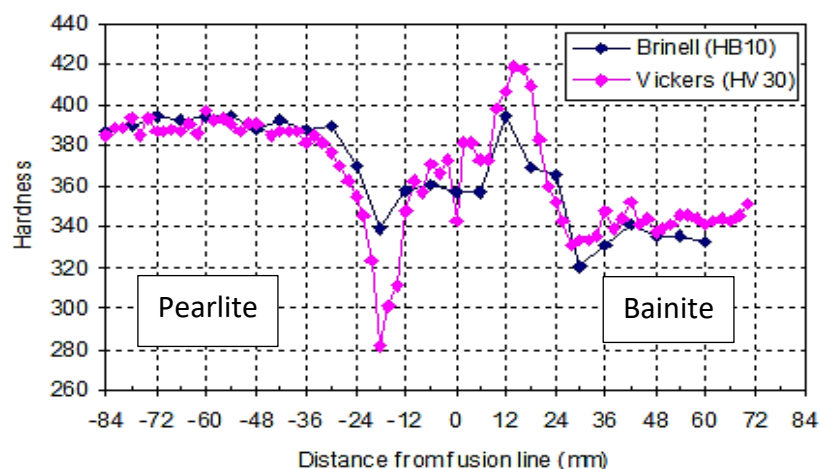

Figure 35. Differences in hardness on the HAZ. Pearlitic - bainitic weld.

As observed above, the sub-critical HAZ minima in the bainitic grade was located at ~27 mm from the weld fusion line, in pearlitic rails this hardness minima were located at ~19 mm. Therefore, the HAZ produced in CFB rail steels is wider than in pearlitics, also high hardness variations were observed across the weld, which may be a cause of deterioration.

Microstructural analysis of the HAZ was made on several occasions, using optical microscopy (OM) techniques. Complex microstructures were observed in the HAZ of CFB B360, those together with the hardness measurements helped to identify phases such as martensite in the critical HAZ region, followed by martensite and bainite microstructures on the IC HAZ and tempered bainite in the SC HAZ. However, very complex microstructures have been encountered.

This thesis is going to focus on the B360 grade, due to the aforementioned problems when in track. An in-depth examination of the dissimilar regions of the HAZ on B360 grades will be performed by the author, in order to achieve a better understanding of its microstructural evolution during welding and its in track performance.

2.3. Developing a narrow HAZ for B360 FBWs

As previously stated, it is believed that one of the causes of the worse in-track performance of B360 FBWs when comparing with pearlitics is its wider HAZ. Therefore, several attempts were made within British Steel to reduce the HAZ in B360 welds. This was made in both ATW and FBW procedures; however, this thesis is going to focus more on the FBW, even though further work is also necessary to determine how to improve B360 ATWs.

Reducing the number of preheat cycles during FBW procedures has proven to reduce the width of the HAZ [16]. As expected and observed in Figure 36, reducing the number and the time between preheats has led to narrower weld HAZ's, with a HAZ less than half that achieved in the standard weld procedures[66].

Narrower HAZ B360

Wider HAZ B360
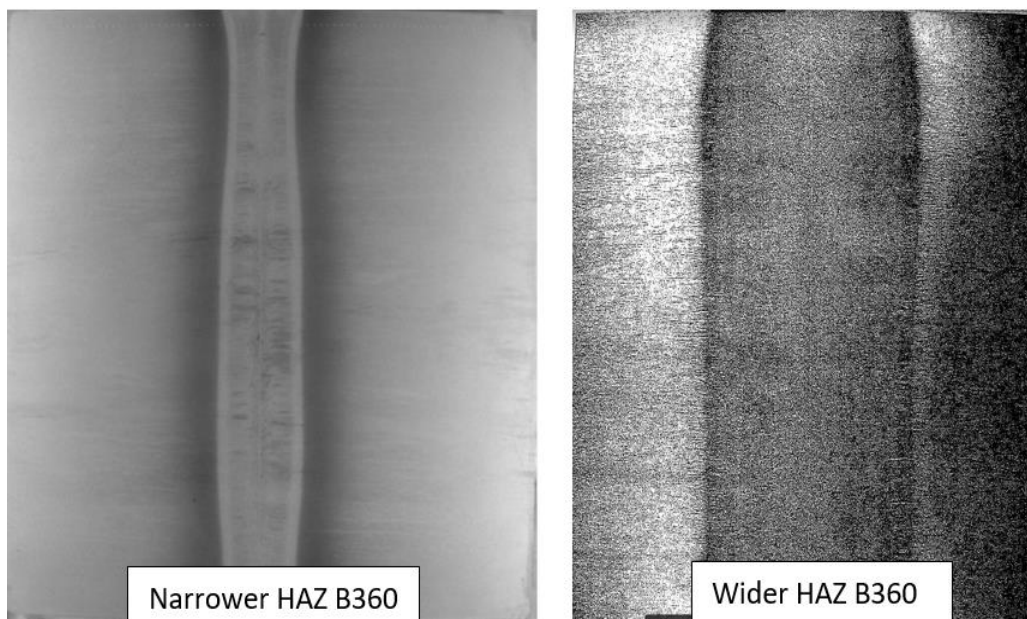
Figure 36. Comparison between wider and narrow bainitic HAZs [66]

The recovery of hardness in wider HAZ seems to be produced in a shorter distance (~50 mm) when applying less PH cycles during the FBW procedure, Figure 37, represents the hardness variation difference between the standard and narrow welds.
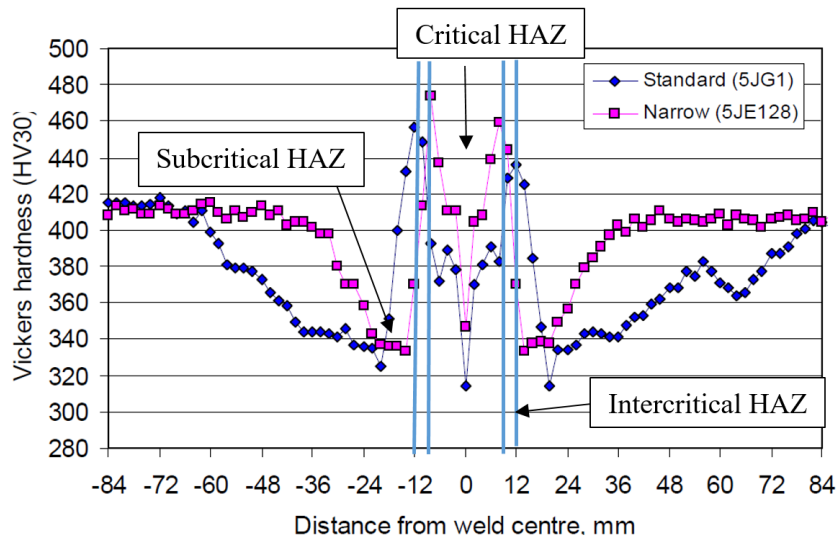
Figure 37. Hardness profile comparison of the narrow and a standard FBW B360 [68].

As stated, a number of FBW procedures with the narrow HAZ program were developed, for FBW of B360-B360 and for B360-R350HT [53],[52].

For B360-B360 FBW, hardness variation and HAZ width measurements were made 5 mm below the rail running surface. The values obtained are represented in Table 9.

Table 9. Hardness data from previously made FBW trials within British Steel [53].

Number of PH cycles	Max Hardness (HV1)	Min Hardness (HV1)	Variation in the IC HAZ	Width of the SCHAZ (mm)
10PH	450	320	130	55
8PH	470	310	160	45
3PH	470	330	140	25

Problems were encountered with the rails using 3PH cycles during the stripping process, as the rails were too cold and, hence, the stripping tool tended to ride over the rail weld rather than cut through it

Other trials were made by welding B360 with 350HT rails, the hardness variation obtained in these weld trials measured in the rail head can be observed in Figure 38.
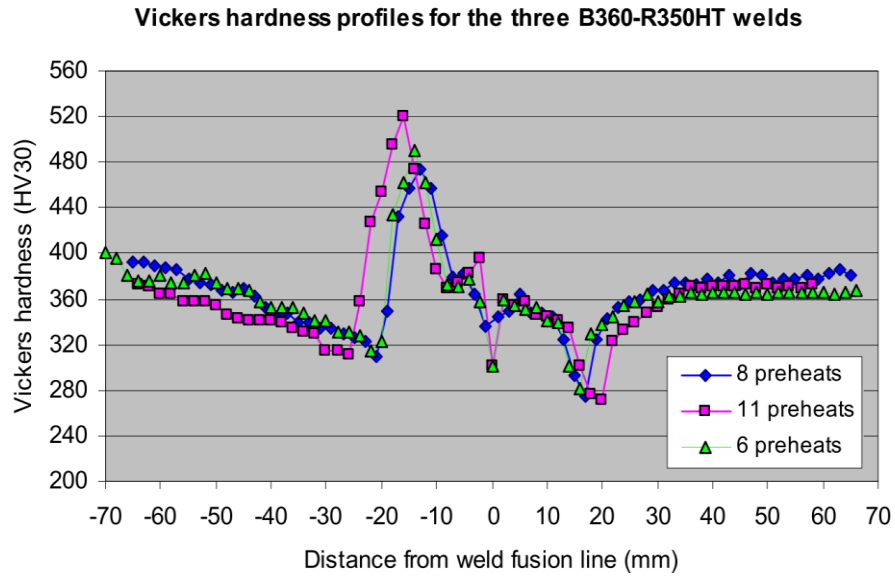
Figure 38. Hardness variation of the rail head from the FBW rail B360-350HT [68].

Problems were encountered in these trials when tested in the three-point bend test, as they did not satisfy the minimum deflection of 20 mm, according to the European specification [67], however, it is important to take into account that this standard is specific for pearlitic grades, as there is not a standard for CFB B320 and B360 [68].

2.4. Summary

On this chapter, a review of the challenges found on B360 grades and the work carried out to date by British Steel was discussed, leading to two main conclusions:

1. Problems were encountered when using welded B360 steels, as RCF cracks were developed within the rail running surface.

2. Bainite tempers at a wider range of temperature than pearlite, leading to a much wider HAZ than pearlitic steels, this is believed to be one of the causes of the rail degradation, however the mechanism of the degradation is still not entirely clear. A further analysis into the HAZ of B360 grades seems necessary and it's going to be performed by the authors.

3. Trials of a narrow weld program were produced within British Steel. Continuation of this work will be carried out using the Schlatter FBW machine in Scunthorpe, UK.

Chapter 3

Experimental procedure

3.1.   Introduction

The experimental procedure of this thesis is divided into five sections in order to achieve the previously described aims of the project.

1. Hardness, OM techniques and HAZ width measurements were used for comparison of "standard" width HAZ, FBWs B320, B360 and pearlitic R260.

2. Further characterisation was made on the B360 FBW, as this was the steel with less favourable in track performance, as stated in the literature review no problems were found during in track performance of B320 or R260 FBW grades.

3. Scanning Electron Microscopy (SEM), Transmission Electron Microscopy (TEM), Electron Backscattering Diffraction (EBSD), were performed in order to understand the complex microstructural evolution and the mechanical properties of CFB grades.

4. Production of a new FBW procedure in order to develop a narrow HAZ weld for B360 CFB in the Schlatter FBW machine situated in Scunthorpe, UK. Analysis of its hardness, microstructural evolution, HAZ width and mechanical testing of the new welds

3.2. Materials

The materials used on this research were three 60E2 grades B320, R260 and B360. From which R260 is a standard pearlitic rail steel, and B320, B360 are CFB grades [53]. Table 10 shows the chemical composition and mechanical properties in terms of hardness, tensile strength and elongation.

Table 10. Chemical composition and mechanical properties of the two CFB grades used, B360 and B320. [1] TS: Tensile Strength, E: Elongation, H: Hardness.

Steel	Chemical composition % by mass						TS (MPa)	E (%)	H* (HBW)
	C	Si	Mn	Cr	V	Mo			
B320	0.15-0.25	1.00-1.50	1.40-1.70	0.30-0.70	0.10-0.20	0.10-0.20	1100	14	320-360
B360	0.25-0.35	1.00-1.50	1.40-1.70	0.30-0.70	-	0.10-0.20	1200	13	350-390
R260	0.6-0.82	0.13-0.60	1.00-1.25	<0.15	0.03 max	-	800	10	260-280

Hardness measurements from the rail running surface.

All the materials were supplied by British Steel, the received material can be divided into as rolled and as welded as described in Table 11.

Table 11. Information of as received material

Rail	General information
As welded	Two FBW were received from British Steel Hayange: B320-R260; B360-350HT
	These were produced using a conventional FBW procedure for pearlitic R260 grades with 8PH cycles.
	The sections of the B320, R260 and B360 rail welds were analysed for comparative purposes.
As rolled	Two sections of 20 m each of an 60E1 B360 grade.
	Those were used on the Schlatter FBW in Scunthorpe, UK.

3.3.   As welded rails.

I.Sample preparation.

The main region of interest regarding CFB welds is the rail head, as the highest contact stresses are produced there.

Longitudinal-vertical sections from the rail head starting in the weld centreline were cut. These had a length of 100 mm each in the rail Rolling Direction (RD). Also, at 200 mm from the weld centre line, a region was cut for analysis of the parent rail. Figure 39, represents a schematic representation of the as welded rails cutting diagram.
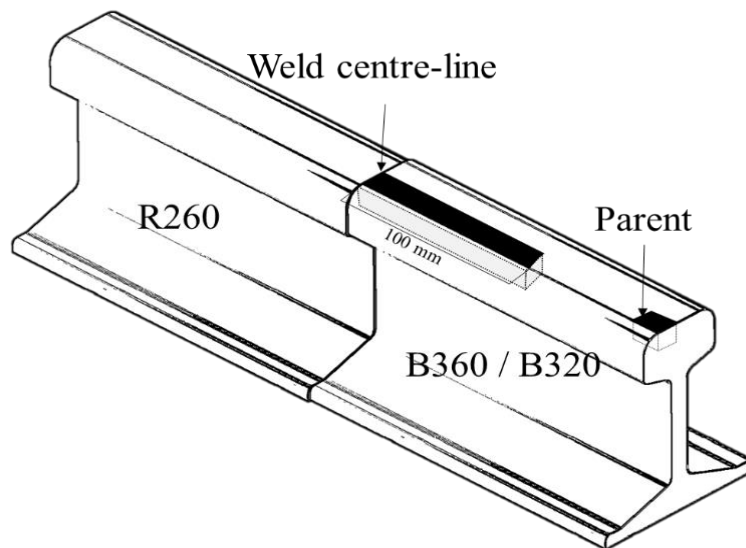
Figure 39. Schematic representation of a cutting diagram for as welded CFBs B320 and B360.

After cutting the longitudinal-vertical sections, they were manually ground from 400 to 2400 grade with silicon carbide papers and then polished down to 1μm with monocrystalline diamond suspensions until a mirror-like finish was observed. The parent rail regions were mounted before grinding and polishing to a mirror finish.

II. Analysis of hardness variation

To investigate the effect of the welding procedure on the rail mechanical properties, micro-indentation techniques were used.

The equipment used was a Durascan 70 micro-hardness tester. In which a diamond indenter with a load of 1kg and a dwell time of 15 seconds was applied.

Indentations were performed towards the welds RD, as represented in Figure 40, analysis of the vertical HAZ sections with 4 rows of 1 mm of distance between indents were used, the distance between arrays was of 5 mm.
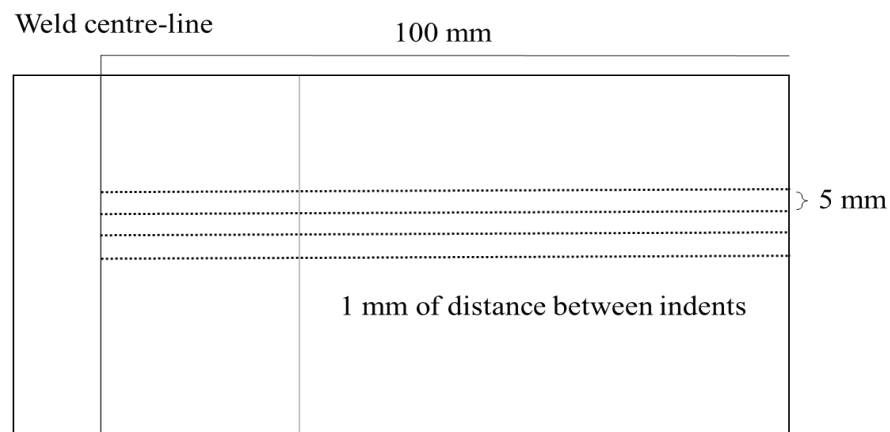
Figure 40. Representation of hardness measurements

The indentation distance of 1 mm was selected as even 1 mm of distance can produce very high variations in terms of hardness and microstructural evolution during the welding of CFB rails. Otherwise, in each of the parent rails five indentations were performed.

The hardness variation of the rail welds was represented by both a hardness map and a gradient map as per Figure 41.
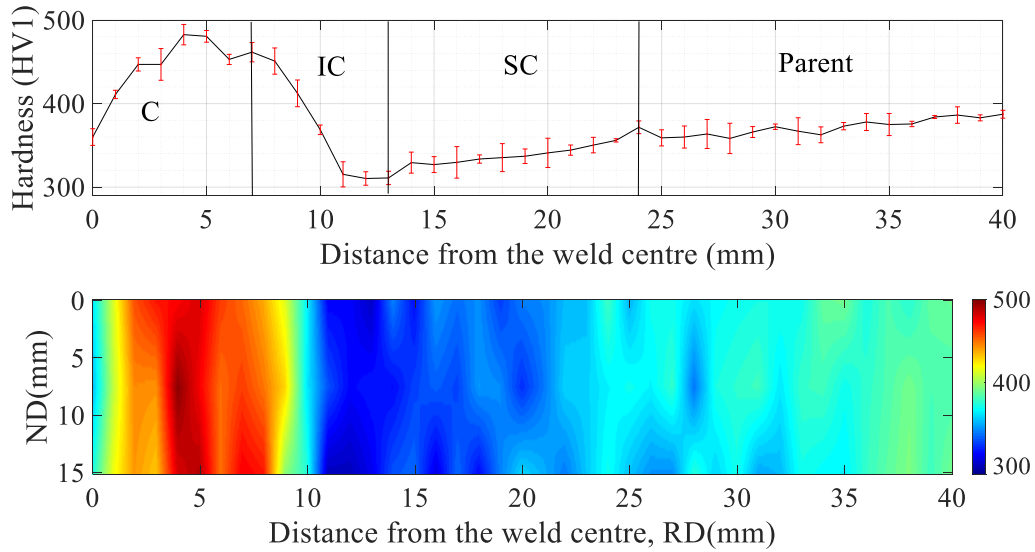
Figure 41. Hardness variation and gradient map of a FBW under analysis

III.HAZ width and microstructural variation

After grinding and polishing, the specimens were etched with a solution of 2% nitric acid for around 20 seconds.

After etching, HAZ width measurements were made by measuring the distance between the weld FZ up to the edge of the HAZ. This usually represents the distance between the FZ up to the beginning of the SCHAZ.

OM images were taken at both the parent rails and at the HAZ regions of interest, which were identified after the hardness measurements.

3.4.   B360

Further analysis of the B360 grade was made, in order to achieve a better understanding of, not only, its complex microstructural evolution, but its mechanical properties in dissimilar regions of the HAZ. The microstructural variation of B360 FBWs has never been analysed extensively as in R260 FBWs [16].

I.Scanning Electron Microscopy (SEM)

Scanning Electron Microscopy (SEM) was used in order to observe micrometric phases in the dissimilar microstructures of both the HAZ and the parent material. Also, an analysis with Energy Dispersive X-Ray Spectroscopy (EDX) of precipitates was made. The microscopes utilized were an Inspect F and Inspect F50, with a voltage of 20kV.

II.Electron Backscattering diffraction mapping (EBSD)

EBSD was used to help distinguish the dissimilar phases found in the HAZ. After establishing the dissimilar HAZ regions with both hardness and OM, the weld sample was cut in four sections which will represent the more characteristic hardness variations produced: Critical, Intercritical, Subcritical and parent. A schematic diagram of this is represented in Figure 42.

Each of those samples were mounted in Bakelite and ground from 600 to 2400 grade with silicon carbide papers. The surface was polished with 3μm and 1μm monocrystalline diamond suspensions and a final polish with colloidal silica was made until mirror like finish was achieved.
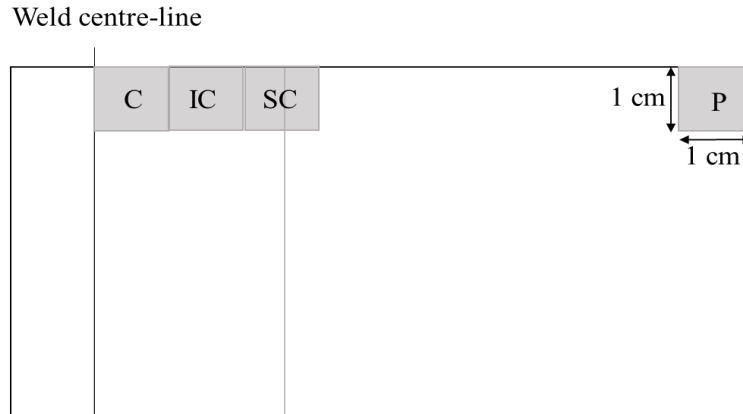
Figure 42. Representation of cutting diagram for EBSD specimens of the Critical (C). intercritical (IC), Subcritical (SC) and parent (P).

The EBSD equipment was used on a FEI inspect F50 with 20 kV of accelerating voltage. The tests were performed towards the rail RD with an inclination of 70º, and a walking distance of 152.4 mm. The phases body centred cubic (BCC) and face centred cubic (FCC) were selected as the matching units during the acquisition of the mapping. A step size of 0.2 µm was selected in all the samples analysed [69]. This was decided to be 0.2 in order for the EBSD to read the fine bainitic ferrite laths.

After acquiring the EBSD patterns, they were corrected and analysed with the use of an HKL Chanel 5 Flamenco software package, which includes Tango, Mambo and Salsa. The indexing rate of all the samples analysed was between 82-89%.

III. Transmission Electron Microscopy (TEM)

The determination of upper, lower bainitic phases, together with the presence of martensite and acicular ferrite was determined with TEM; also, an analysis of the composition of precipitates found in the intercritical and subcritical regions of the HAZ was made.

Two 200 kV TEMs were used for this characterisation, FE1 Tecnai T20 and JEOL F200. The chemical analysis was performed in the JEOL with an Energy Dispersive X-Ray spectroscopy (EDX) detector.

Preparation of both thin foils and carbon replica was necessary. Samples were obtained from the rail running surface after determination of the dissimilar HAZ regions with both hardness and micrographic analysis, as per Figure 43.
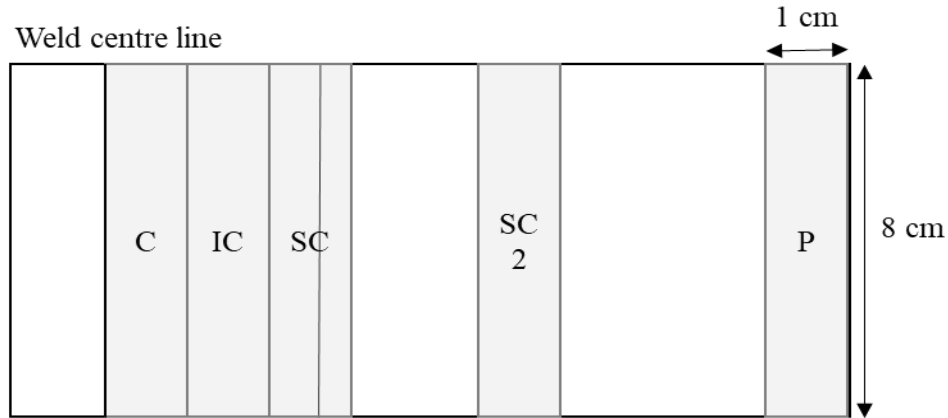
Figure 43. Schematic representation of the sections obtained for further TEM characterisation

a. Carbon replica

Carbon replica were used for chemical analysis of precipitates. Samples were first mounted in Bakelite, ground from 600 to 2400 grade with silicon carbide papers, and polished with 3µm and 1µm monocrystalline diamond suspensions. After polishing, the samples were etched with a 2% Nital solution for a short period of time of 5 seconds in order to expose the precipitates on the steel surface. Later on, a high vacuum carbon coating device was utilised to deposit the carbon in the steel surface. After this, the specimens were etched with Nital 10% up until the removal of the carbon film with the precipitates attached was possible. A schematic diagram of this process can be observed in Figure 44.
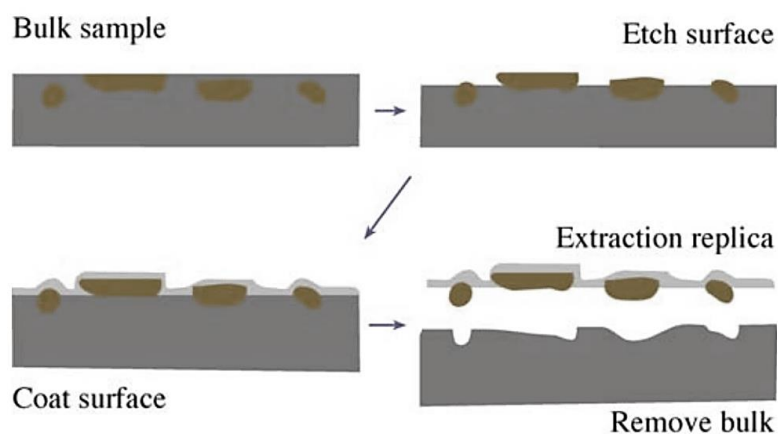
Figure 44. Carbon replica extraction process [70]

b.   Thin foils

Five samples (C, IC, SC, SC2 and P), were first cut from the aforementioned locations with a Struers Secotom 50 up until its thickness was of ~0.70 mm. Beeswax was used to paste those specimens on a flat piece of metal to enable grinding from 120 to 600 silicon carbide paper, down to a thickness of 250-400 µm. Once this thickness was achieved, a disc punch was used to create a disc with a diameter of 3 mm. This disc was ground from 600 to 1200 silicon carbide papers up a thickness of 80 µm.

The final thinning of the discs was made with a Tenupol-5 electropolisher, the solution used was of 5% perchloric acid, 35% butoxyethanol and 60% methanol [71]. The parameters for electropolishing were -40º C and 30-32 mA. This, generates a tiny hole with a thinning area around it, making it easier to observe under TEM.

Figure 45 shows a schematic representation of the dissimilar stages for thin foils preparation.
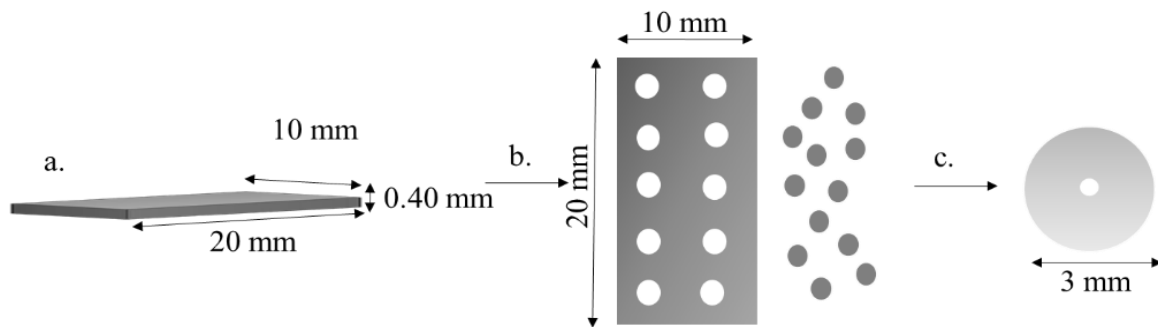
Figure 45. Representation of the stages for TEM sample preparation, a. First thinning obtaining a sample of 0.40 mm of thickness, b. Disc punch creating a 3 mm diameter discs, c. Final thinning with Tenupol-5 electropolisher.

3.5. As rolled rails.

As previously observed in Table 11, two rails of 20 meters each were received from British Steel Scunthorpe, UK. These were used in order to develop a new welding program in the Schlatter machine for narrow HAZ welds.

I.Flash Butt Weld trials.

A stationary GAAS 80/580 Schlatter machine in Scunthorpe, UK was used for these trials. Figure 46, represents an image of the Schlatter machine used.

Figure 46. GAAS 80/580 Schlatter machine [58]**.**

Before starting the welding procedure, auto-clean and manually grinding of the rails was made. Later on, the rail ends were clamped and aligned together with copper electrodes, as in Figure 47.

After the rails are properly ground and aligned together, the FBW procedure can start. As described in the literature review; the procedure can be divided in four stages: Burn off, preheating, flashing and upsetting.
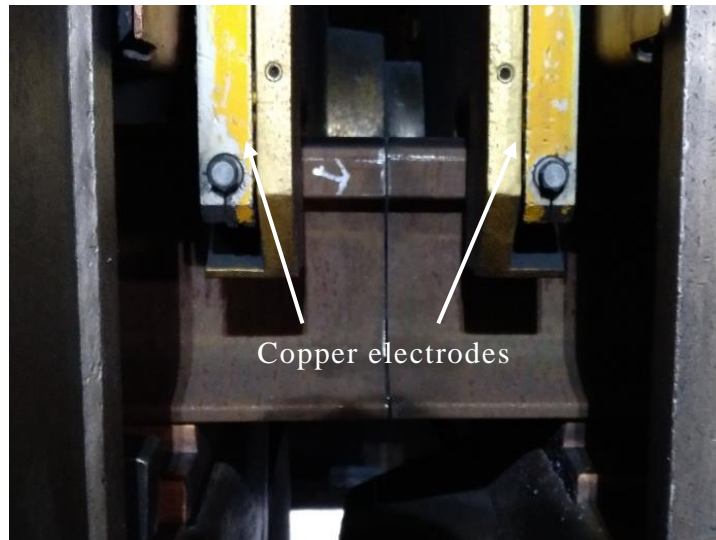
Figure 47. Adjusting the rail ends to be weld.

The main objective of the weld trials was to produce a narrow HAZ and reduce the subcritical HAZ softening extension. For this purpose, modifications were made on a standard program for CFB FBWs developed by British Steel [72]. These changes were made by varying the number of preheat cycles (PH) and ON', 'OFF' times also called pre-contact and separation diffusion time (s) [16].

A reduction of the number of preheat cycles had previously demonstrated to produce a narrow HAZ on both pearlitic and CFB rails [16],[73]. Similar trials were previously made on CFB within British Steel, showcasing a narrower HAZ than the standard FBW procedures.

Another weld was made using post-weld heat pulses (PWHP) after the welding procedures with the purpose of obtaining a more uniform hardness variation.

The 'ON' and 'OFF' times, were selected as 2.0s and 0.5s respectively. As short times will also help to limit the extent of tempering [16].

Figure 48, represents the welding program used for one of the weld trials, in which 3 PH cycles were selected.
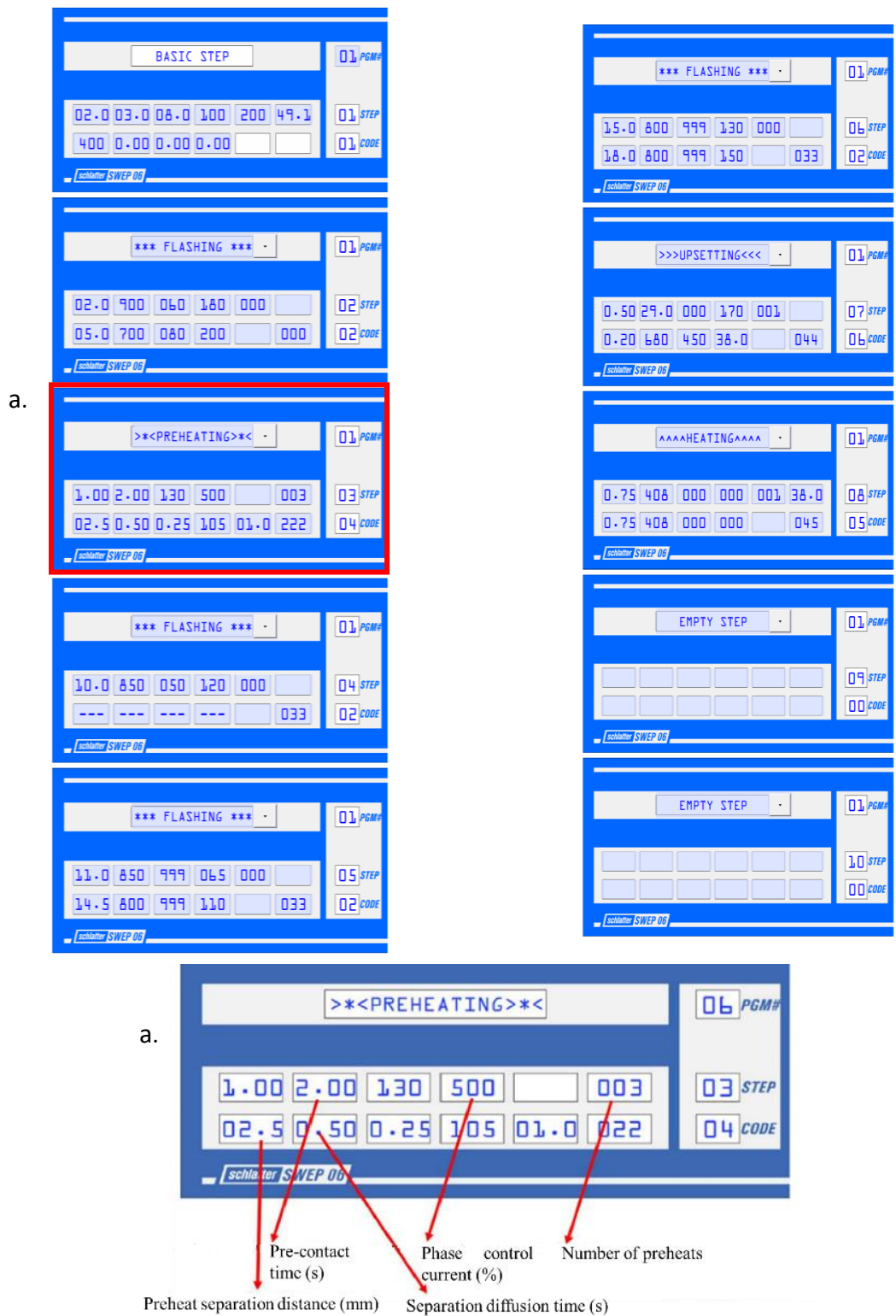
Figure 48. General weld program used for welds in which only variations of PH cycles was produced. a. Representation of the preheating stage.

Figure 49 represents the welding program used for the application of PWHP after the welding procedure. In this case, a stage was added at the end of the welding program.

Figure 49. Weld program used for weld with post-weld heat treatments. a. New stage added for 3 preheating cycles.

More detailed weld programs can be found in the appendix.

Table 12, represents a summary of the parameters selected for the FBW procedures.

Table 12. Parameters selected for FBW trials in the Scatter machine, Scunthorpe, UK.

Trial	Number of preheat cycles	Pre-contact time (s)	Separation diffusion time (s)	Phase control current	Problems encountered
1*[1]	3	2.0	0.5	500	Stripping*
2*[1]	4	2.0	0.5	500	_
3*[2]	4	2.0	0.5	500	_
4*[3]	4	2.0	0.5	500	_
5*[1]	5	2.0	0.5	500	_
6*[2]	5	2.0	0.5	500	_
7*[3]	5	2.0	0.5	500	_
8*[1]	6	2.0	0.5	500	_
9*[2]	6	2.0	0.5	500	_
10*[3]	6	2.0	0.5	500	_
11*[1]	6 + 3 PWHP	2.0	0.5	500	Stripping*

Problems were encountered during the stripping process in two of the welds.
[1] Used for macro, metallographic examination and micro-indentations.
[2] Used for three-point bend test.
[3] Used for analysis of residual stresses.

As can be observed above, problems were encountered in two of the welds (3PH and 6+3PWP) with stripping. This is why these welds could not be repeated.

After the stripping process, it was decided to cool down the welds naturally down to 300 and 200°C and later on, water quench.

If used for metallographic characterisation and hardness measurements, the rails were cut to a length of 400 mm each. After sectioning, its running surface was manually ground towards the rail longitudinal direction and etched with a solution of 2% Nital. Later on, the width of the HAZ was measured as the distance between the visible ends in the top, middle and bottom of the rail head. Brinell hardness measurements were made near the weld FZ of the rails with an Equotip Proceq device. Figure 50 represents the aforementioned.
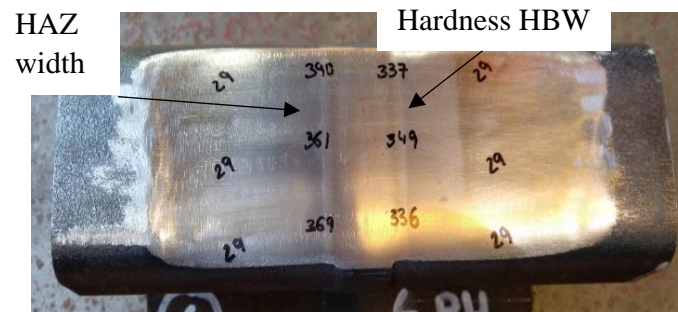
Figure 50. Rail after welding, 6PH, with hardness measurements and HAZ width.

If used for three-point bend testing, the rails were cut to a length of 1150 mm. If used for further characterisation of residual stresses, the rails were cut up to a length of 1200 mm.

II. Characterisation of narrow HAZ FBWs

The FBW sections of 400 mm were used for further characterisation. The same cutting diagram as the one described in section 3.3 was used in order to analyse the rail running surface.

The sections were manually ground with the use of 400-2400 silicon carbide papers and polished with 1-3μm diamond suspension until mirror like finish. Micro-indentations were performed using the Durascan device, with the same procedure as previously described. The samples were etched with a solution of 2% Nital; both OM and measurement of the visual HAZ width were made. A longitudinal-axial section of three welded rails (3PH, 6 PH and 6PH+3PWP) was also cut for further examination, Figure 51 represents a cutting diagram of the longitudinal-axial section.
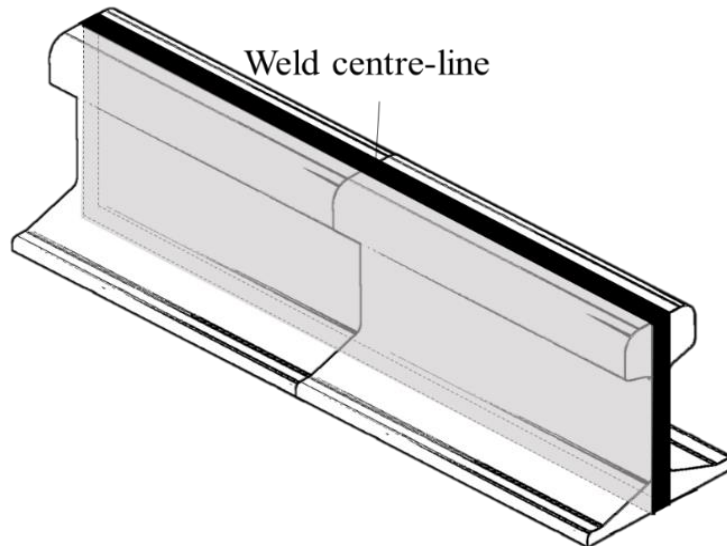
Figure 51. Cutting diagram of longitudinal-axial section.

Firstly, a macrographic examination of the longitudinal-axial section was made, in order to observe any evidence of shrinkage, lack of fusion, porosity or inclusions. Later on, it was polished up to mirror finish and etched with a solution of 2% Nital in order to measure the visible HAZ width variations of the head, web and foot. This variation was measured every 5 mm from the head of the rail.

Also, hardness measurements were made in the Advanced Manufacturing Research Centre (AMRC) in the head, web and foot of the rail. A total of 15 rows of indents were performed, five rows in the head, five in the web and five in the foot region. A diamond indenter with 1 kg load was used, the separation between indents was of 1 mm, and 5 mm of distance was used between rows of five.

III.Residual stresses

Due to time constrains, only three welds were selected for measurement of residual stress after welding, those were cut to a length of 1200 mm.

The location of the residual stress measurement was determined as per standard [18]; in the head, web and foot of the rail as in Figure 52.
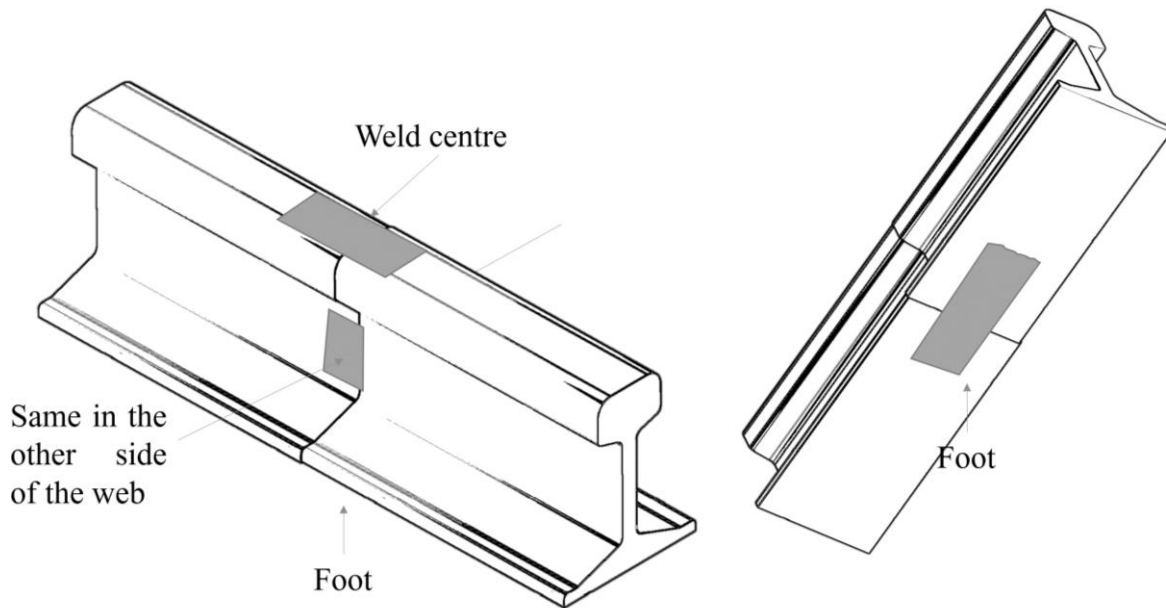
Figure 52. Location of the regions of the head, web and foot in which residual stress measurements took place.

The previous represented regions were ground and polished prior to the attachment of strain gauges as in Figure 53.

Figure 53. Attachment of strain gauges.

Those were cabled to the measurement device as in Figure 54. Afterwards, strain was measured before the beginning of the test. Later on, two slides were cut at a distance of 20mm from the weld centre line, and finally, strain measurements were calculated at the end of the test.

Figure 54. Attachment of strain gauges by cabling to the measurement device.

The calculation of the residual stresses was obtained by transforming the realised strain; multiplying by the young modulus: 207GPa.

IV. Three-point bend testing

As aforementioned, after welding, rails used for three-point bend testing were cut at a length of 1150 mm; 575 mm from each side of the weld centreline. These were performed in British Steel, Scunthorpe. A schematic representation of a three-point bend tester can be observed in Figure 55.
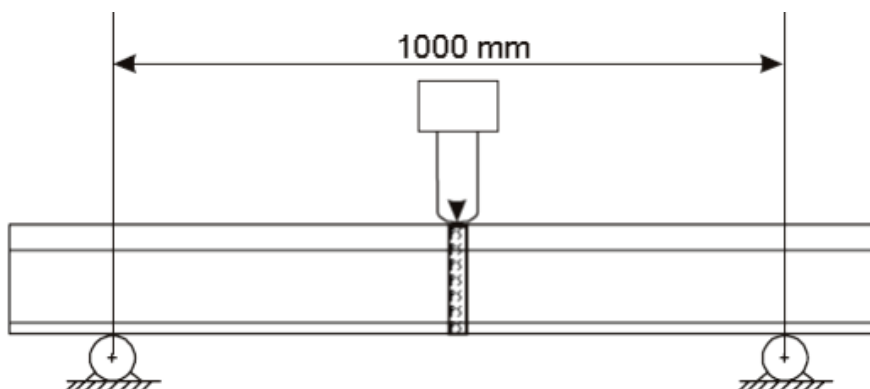
Figure 55. Schematic representation of a three-point bend tester [64].

The weld centre line is situated below the bending load as in Figure 56. During the performance of the test, two parameters are measured; the load (kN) and the deflection (mm).
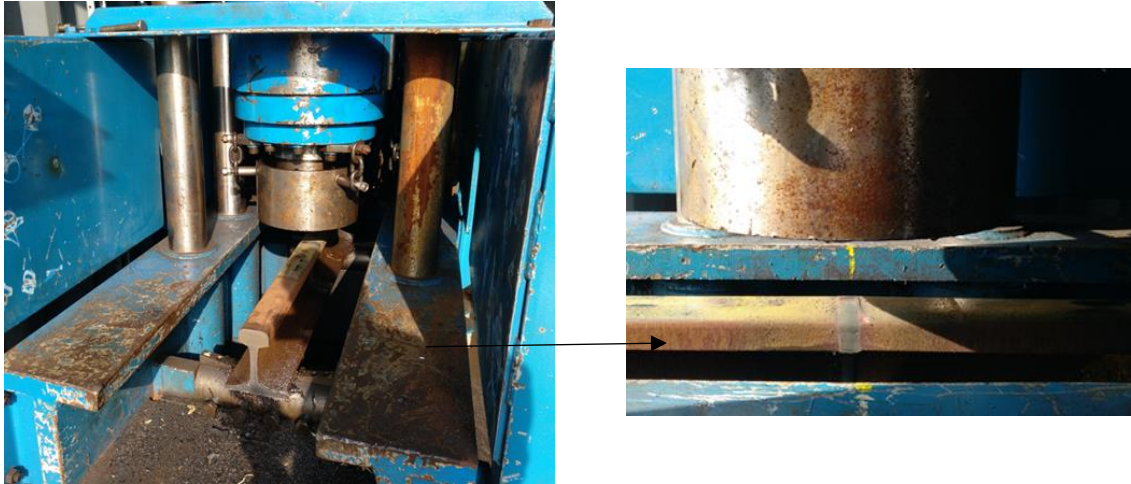
Figure 56. Three-point bend tester, with weld FZ below the bending load.

It was decided to test the rails until complete breakage, however during rail production these are tested just until the minimum load of 1600 kN is reached [18]. Once the rails broke, they were cut to a length of 80 mm on the RD for further macro examination of the fracture surface. Figure 57 represents a rail broken after three-point bend testing.

Figure 57. Rail broken after three-point bend testing.

Chapter 4

Analysis of a B360 FBW and comparison with other steel grades

4.1.   Introduction

In recent years, there has been limited scope for the future development of pearlitic grades on railway applications, which is necessary due to railway continuous advancement. Nowadays, heavier loads and high velocity trains are becoming much more frequent. This, leads to higher maintenance costs and, in some cases, even failure of rails.

CFB steels were first developed during the late 90s, showing greater performance in fatigue deformation mechanisms such as head checks, and high rates of wear resistance.

However, problems have been encountered in track applications of CFB welds, more specifically on B360 steels. B360 CFB rail steels are of great importance due to its higher performance during in track applications, mainly as an inhibitor for head checking and the more expensive manufacturing process of the other CFB manufactured by British Steel, B320, as per addition of alloying elements such as Vanadium.

The HAZ of pearlitic rail steels is well understood, and its microstructural evolution has been studied in multiple occasions[16],[74]. Nevertheless, this characterisation has not been made as extensively on bainitic steels, whose evolution is much more

79

challenging. It is also important to bear in mind that during welding of CFBs, a wider HAZ is generally developed, and this is believed to be a cause of bainite tempering over a wider temperature range and also down to lower temperatures than those at which pearlite spheroidises.

This thesis is mainly focused in one of the two most common welding mechanisms of the railway industry; Flash Butt Welding (FBW), whose basics were discussed in the literature review.

All the rails analysed on this chapter had a 60E2 profile and were supplied by British Steel. Those were received "as welded"; the weld program used was a conventional FBW procedure using 8 PH cycles, 1.1.s of delay period "OFF" and 4.6s of preheating time "ON".

Firstly, an in-depth analysis was made in both the "as rolled" B360 grade and an "standard" FBW B360 grade. Techniques such as micro-indentation, Scanning Electron Microscopy (SEM), Transmission Electron Microscopy (TEM) and Electron Backscatter Diffraction (EBSD) were used in order to obtain a better understanding of the HAZ microstructural evolution and its in track performance.

Later on, an examination of two rails; a carbide-free bainite B320, and a pearlitic R260 was made for comparison with the previously analysed B360. Hardness and micrographic examination were performed at 5 mm below the rails running surface.

The work carried out on this chapter aimed to help achieve a better understanding on B360 "standard" FBW, its microstructural evolution after welding and, therefore, it's in track performance.

4.2. Materials

As described in the experimental procedure, the materials used in this research were supplied by British Steel. Three "as welded" rails were utilised; B360, B320 and R260.

Table 13 represents the chemical composition of the two CFB used B360 and B320; and the pearlitic R260. These rail steels had a 60E2 profile, being flat bottomed.

Table 13. Chemical composition wt.% of an as-rolled B360 grade.[53]

Grade	Chemical composition range % by mass						
	C	Si	Mn	Cr	V	Mo	B
B320	0.15-0.25	1.00-1.50	1.40-1.70	0.30-0.70	0.10-0.20	0.10-0.20	0.003
B360	0.25-0.35	1.00-1.50	1.40-1.70	0.30-0.70	-	0.10-0.20	0.003
R260	0.6-0.82	0.13-0.60	1.00-1.25	≥0.15	0.03 max	-	-

4.3.   Analysis of "as rolled" B360

The B360 60E2 rail was welded with a pearlitic HP335 rail, using a standard FBW procedure: 8 PH cycles, 4.6 s of preheating time "ON" and 1.1 s of delay period "OFF". Only the B360 region was analysed. An initial analysis was made on the "as rolled" B360 steel, whose section was obtained from the welded B360 rail at 200 mm from the weld FZ, in which no variation from the "as rolled" material is expected. Both a light micrograph and a SEM were obtained at 5 mm below the rail running surface towards the rail RD; as in Figure 58.
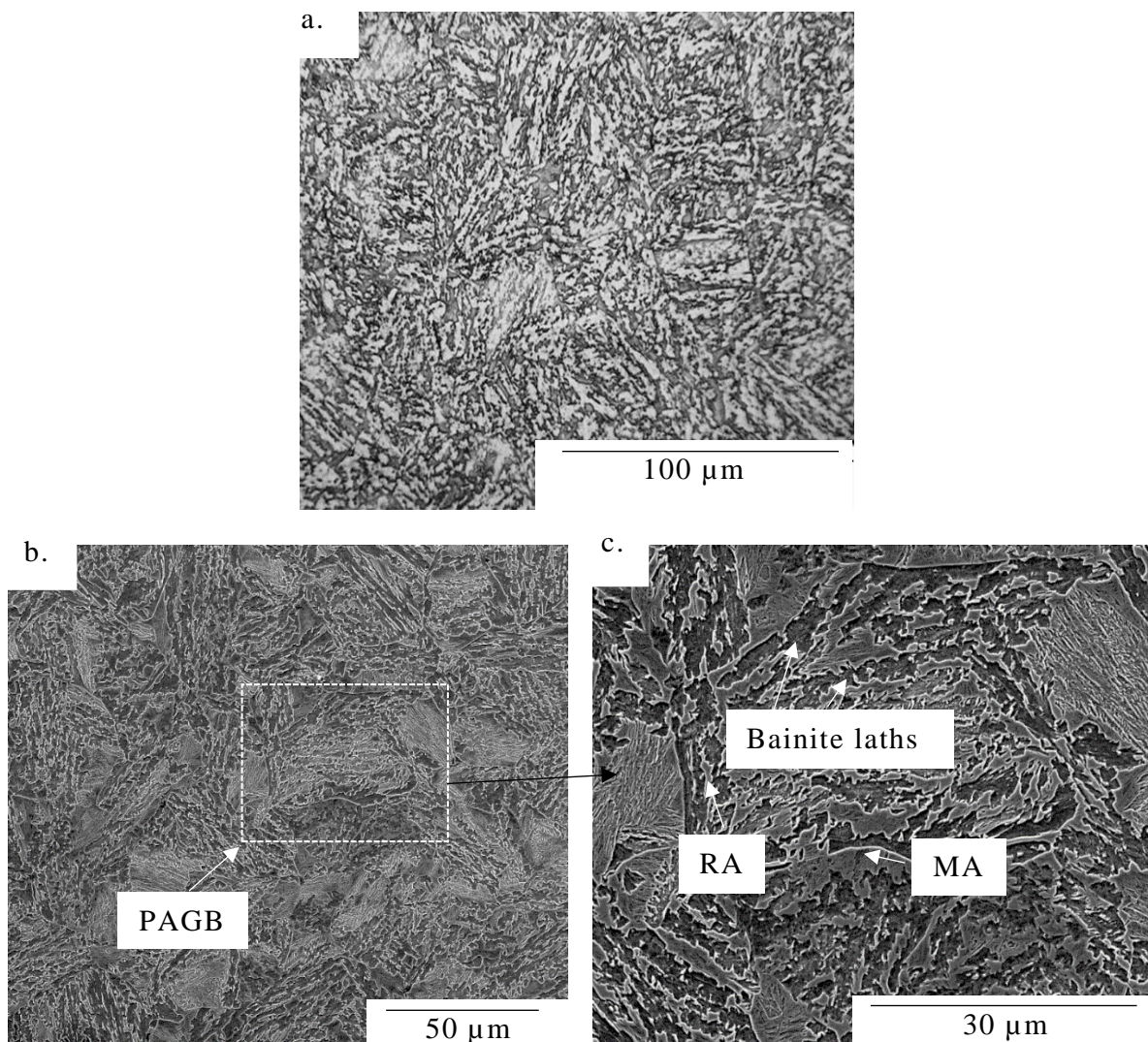
Figure 58. Optical micrograph (a) and Scanning Electron Micrograph (SEM) (b), (c) of an as rolled B360 grade. Images from the rail running surface, etched with 2% Nital.

The images represented above show the expected B360 microstructure, consisting on fine bainitic ferrite laths, together with RA regions. RA is presented in the form of films between ferritic laths or as Martensite Austenite (MA) constituents. The presence of MA constituents is known to reduce steel toughness [75].

As described by British Steel [53]; during the cooling of the rails in the cooling bed the transformation of bainite from the parent austenite structure takes place between 550 and 300°C, leading to the formation of ferrite laths with low carbon content. Carbon migrates into the untransformed austenite which surrounds the ferrite laths. The high silicon content of these steels (≥1wt%), prevents the formation of cementite from the carbon rich austenite, which is stabilized at ambient temperature. Therefore, the microstructure present should consist mainly on upper bainitic ferritic laths, due to the high temperatures of transformation, surrounded by retained austenitic regions (RA).

A series of indentations were performed at 5 mm below the rail running surface, obtaining a hardness value of 386.5 ± 4.6 HV1. This in accordance with previous measurements made on this grade [4].

MnS non-metallic inclusions were present through the entire rail running surface, in the rails RD. Figure 59, represents an EDX analysis of and MnS inclusion situated towards the rail RD.
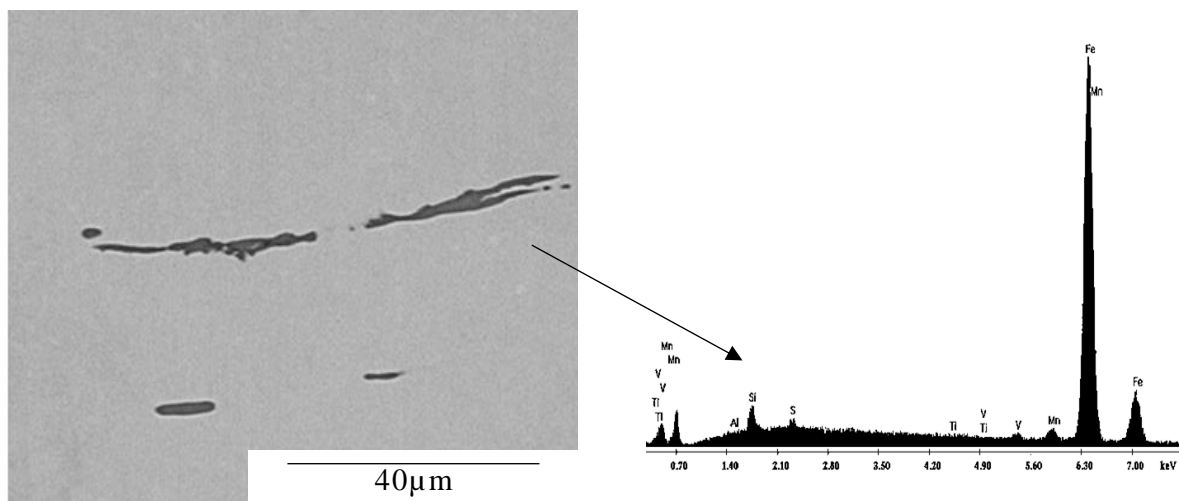
Figure 59. EDS analysis of an MnS inclusion towards the rail Rolling Direction (RD).

A more in-depth analysis of the B360 steel was performed with the use of a TEM as in Figure 60.

Thin foils were obtained from the rail running surface, showing upper bainite laths with no visible carbides within them. The width of the bainitic ferrite laths was measured with the help of TEM bright field images, obtaining a width of 0.24 ± 0.06 µm.

The narrow width of the laths, together with the absence of carbides in the majority of the microstructure; are expected to confer high levels of toughness, increasing rail resistance during in track performance.
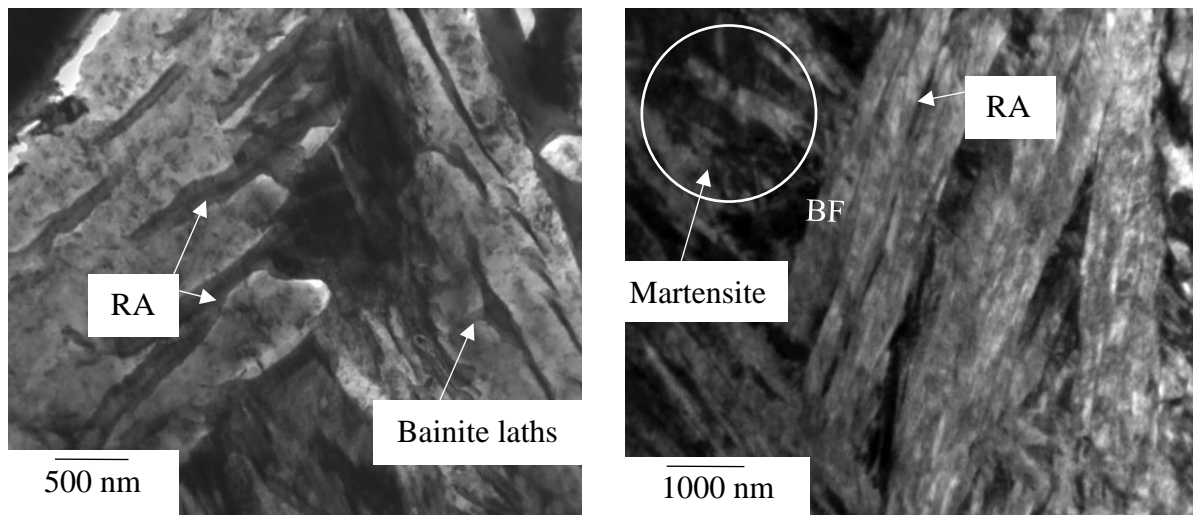
Figure 60. Transmission Electron Micrograph (TEM) showcasing a standard CFB B360 (Thin foil), Bright field image. RA (Retained Austenite), BF (Bainitic Ferrite), Martensite.

The presence of martensite can be easily recognised on the bright field TEM images due to the high density of dislocations, which is generated because of the higher carbon content present in martensite [76].

I.Phase distribution; XRD

Figure 61, shows the XRD spectra of a conventional B360 steel. According to previous works [53] the RA present in the B360 grade is more than 10%. XRD analysis shows 82.95% of ferrite (α-Fe) and 17.05% of austenite (γ-Fe).

The RA content is known to have a direct influence on the steel mechanical properties. Whilst strength is mainly controlled by the fine ferrite plate thickness, ductility is controlled by the amount of RA; a higher amount of RA is known to increase the strain hardening of the steel.

[110], [200], [211] Body Centred Cubic (BCC) α-Fe, and [111], [200], [220] Face Centred Cubic (FCC) γ-Fe, are present in the XRD spectra.
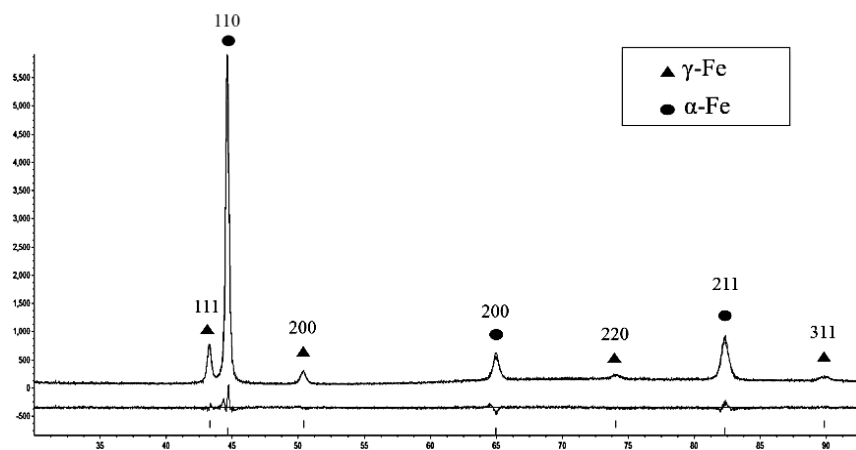
Figure 61. XRD Spectra, showcasing the presence of γ-Fe and α-Fe.

The XRD analysis also helped to determine the lattice parameters for further EBSD characterisation. Those were of 3.62 for γ-Fe and 2.87 for α-Fe.

Due to the dissimilar crystal structure of ferrite and austenite, BCC and FCC respectively, those can be easily separated by phase discrimination during Electron Backscatter Diffraction (EBSD), thanks to the introduction of the aforementioned lattice parameters.

4.4. Analysis of a B360 "standard" FBW

I. Macrographic examination

As previously mentioned, the B360 rail was welded to a pearlitic HP335 rail. A section was cut at 5 mm below the rail running surface, starting at the rail FZ in the rail RD.

The visible HAZ width was measured after etching with 2% Nital. Figure 62, represents the B360 rail with its visible HAZ width.
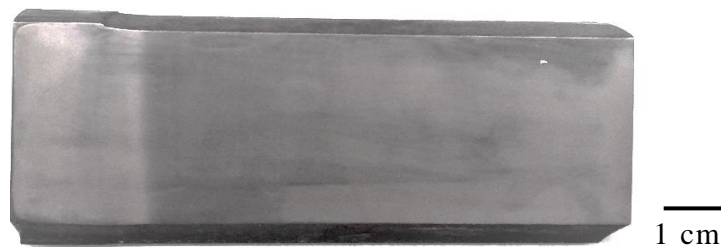

1 cm

Figure 62. Representation of the visible HAZ width from the weld FZ of a B360 FBW.

The visible HAZ width measured was 20 mm. It is important to bear in mind, that this represents the visible HAZ from the weld FZ, therefore, the "overall" HAZ is expected to be the double of the value presented.

II. Hardness variation

The weld hardness variation is known to be one of the easiest ways to determine weld quality [77]. Hardness measurements were performed using a load of 1kgN and a distance of 1 mm between indentation [78]. Indentations were performed from the weld FZ of the B360 up to 100 mm, as at that distance a total recovery of hardness was expected.

Both the hardness variation together and the microstructural development of the weld, are a function of the overall thermal cycle during welding; the dwell time, cooling rate and peak temperature reached in the dissimilar HAZ regions [79].

Figure 63 represents the Vickers hardness profile of the B360 rail, together with its corresponding gradient map. The rail hardness variations have helped to determine the dissimilar regions, Critical (C), Intercritical (IC), Subcritical (SC) and Parent, which are represented below.
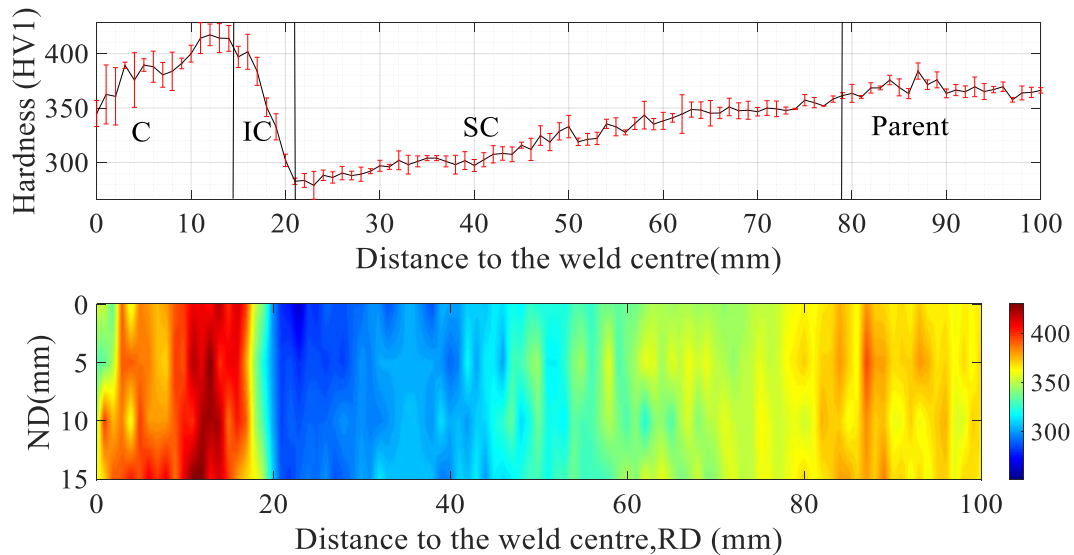

Figure 63. Hardness variation versus distance to the weld centre line of a B360 welded rail steel.

Those show the typical behaviour of a FBW hardness profile, showing the fall in hardness between the CHAZ and SCHAZ and the slow recovery in hardness produced in the SCHAZ. The parent region was selected once the hardness recovery was $\geq$ 360HB, this will be around 376 HV.

As previously mentioned, the visible HAZ width of B360 rails was of 20 mm, this corresponds to the distance from the weld FZ up to the end of the ICHAZ (~21 mm).

The hardness of the FZ was of 348.9±1.7HV1; slightly lower than the one of the parent steel (383.5HV1); this is a typical behaviour of FBW procedures, as carbon diffuses away to the FZ where is removed after the stripping process.

As a guidance, according to the European standard for pearlitic welds [18]; the rail hardness variation has to be between P+60 and P-30; in which P is the nominal hardness of the rail, which is of 383.5±2.5 HV1.

Table 14 represents a summary of the hardness values obtained in the FBW, together with the extension of the tempered SCHAZ.

87

Table 14. Hardness values of the HAZ of a CFB B360 FBW.

Visible HAZ width (mm)	20
Max Hardness (HV1)	415.5
Min Hardness (HV1)	282.5
Variation of hardness in the IC HAZ (HV1)	133
Extension of the SC HAZ (mm)	58
Max H – Parent (HV1)*[1]	41.2
Min H – Parent (HV1)*[2]	94.7

*[1] *Maximum hardness value in the HAZ – Hardness of the parent rail*
*[2] *Minimum hardness value in the HAZ – Hardness of the parent rail*

Maximum hardness levels are reached at 11 mm from the FZ, in the CHAZ weld, with values up to ~ 415.5HV1. This is 41.25 HV higher than the B360 parent rail hardness. Satisfying the previously mentioned maximum hardness criteria of P+60.

Otherwise, the minimum hardness levels are produced at 21 mm from the FZ, at the end of the ICHAZ; producing hardness variation of 94.75 HV1, which doesn't satisfy the minimum hardness criteria stipulated of P-30.

The observable differences in the CFB B360 HAZ could cause plastic deformation or uneven wear, which produces localised cupping on the rail running surface; in turn, reducing rail lifetime. However, previous reports made on pearlitic grades [58], believe that 15-20 mm of width is too narrow to produce any consequences during the wheel-rail contact; this is because the wheel-rail contact patch is generally of ~12mm.

III. Micrographic examination

The microstructural characteristics of the dissimilar regions of the HAZ (FZ, CHAZ, ICHAZ, SCHAZ) were analysed in this section. An extended microstructural characterisation of an FBW B360 with techniques such as TEM and EBSD has never been made before to the author knowledge, and can help to understand the mechanical properties of the weld.

The samples were cut towards the rails normal direction (ND), whose area was selected according to the hardness measurements previously obtained, as previously described in the experimental procedure.

Moving away towards the **CHAZ**, two main regions are usually found during FBW procedures, Coarse Grained HAZ (CGHAZ) and Fine Grained HAZ (FGHAZ). The rail hardness variation between these two regions together with OM of the regions presented is represented in Figure 64.

In the weld FZ, no visible porosity was found, meaning that a good fusion between the two metals was produced. Regarding welding problems with CFB, and as explained in the literature review, those are more related with its in-track performance than the weld joint quality itself.

A more in detail examination of the FZ, CGHAZ and FGHAZ was made with the use of SEM, as in Figure 65.

According to Tawfik et al. (2008) [55]; just after the upsetting stage and adjacent to the FZ, temperatures above 1400°C are reached; which leads to grain growth and coarser recrystallized grains . This behaviour is expected in both bainitic and pearlitic steels. Near the FZ a particularly coarser microstructure can be identified; consisting in bainitic ferrite laths surrounded by RA regions and some MA islands.

When moving away from the FZ, a reduction of the peak temperatures leads to a decrement of the recrystallized grain size; and a more acicular microstructure.
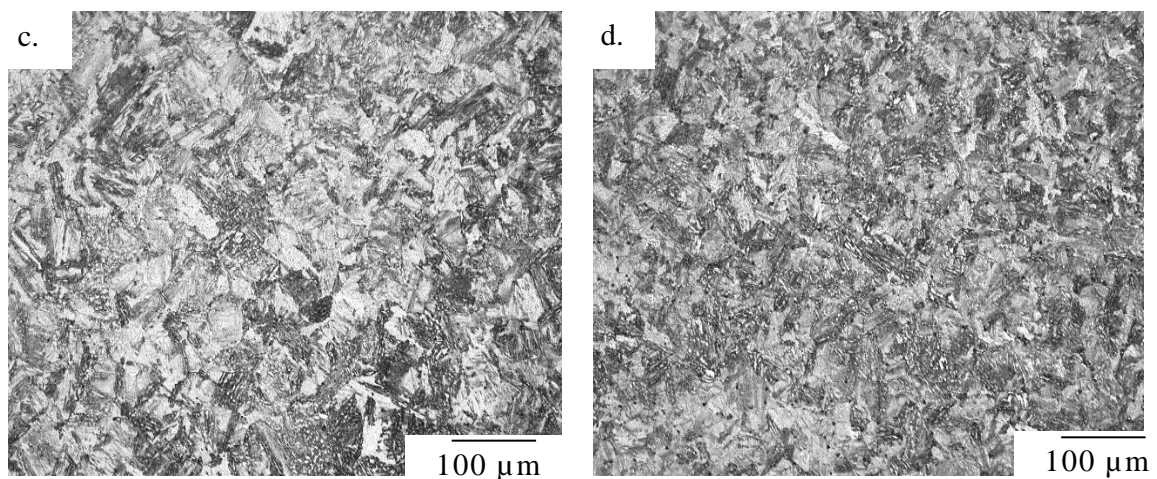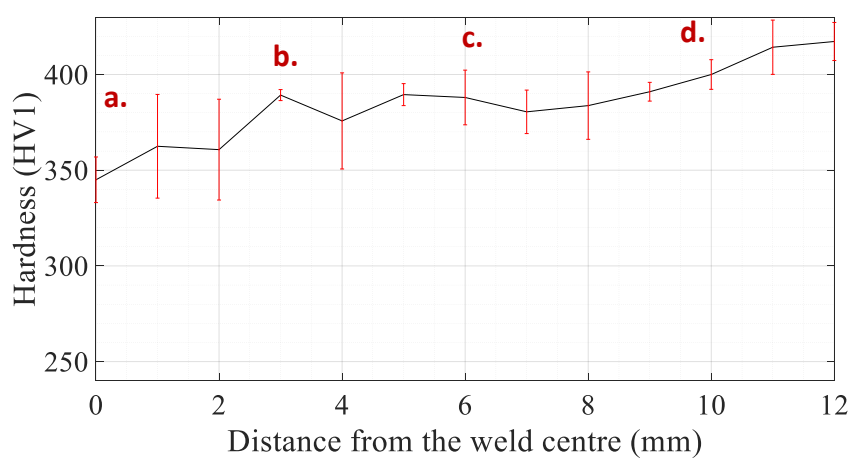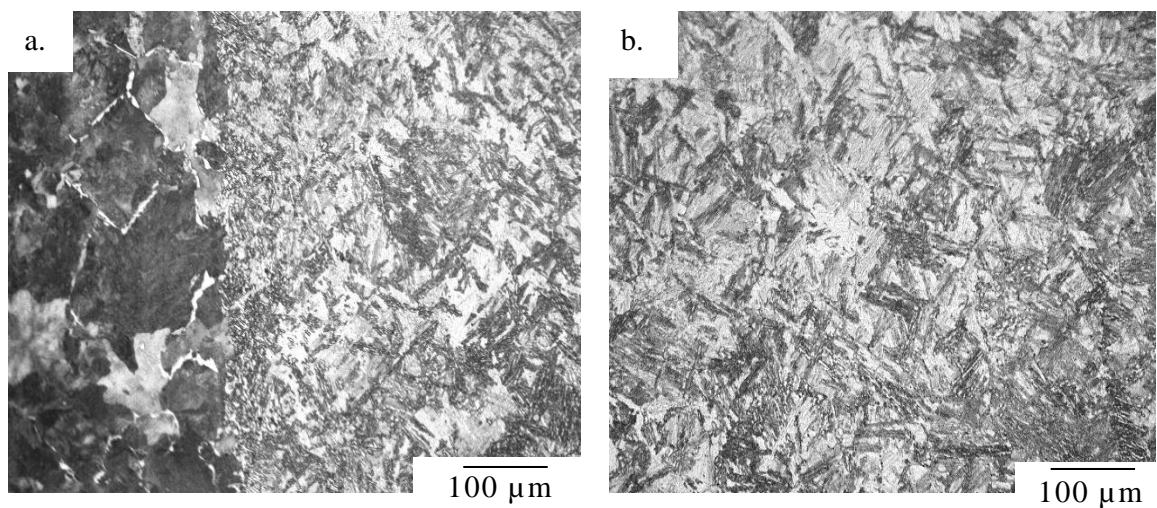
Figure 64. Hardness variation between the rail FZ up to the end of CHAZ, together with optical micrographs from specific locations.

In Figure 65 (a), (b); the pearlitic and bainitic HAZ regions are easily recognisable.
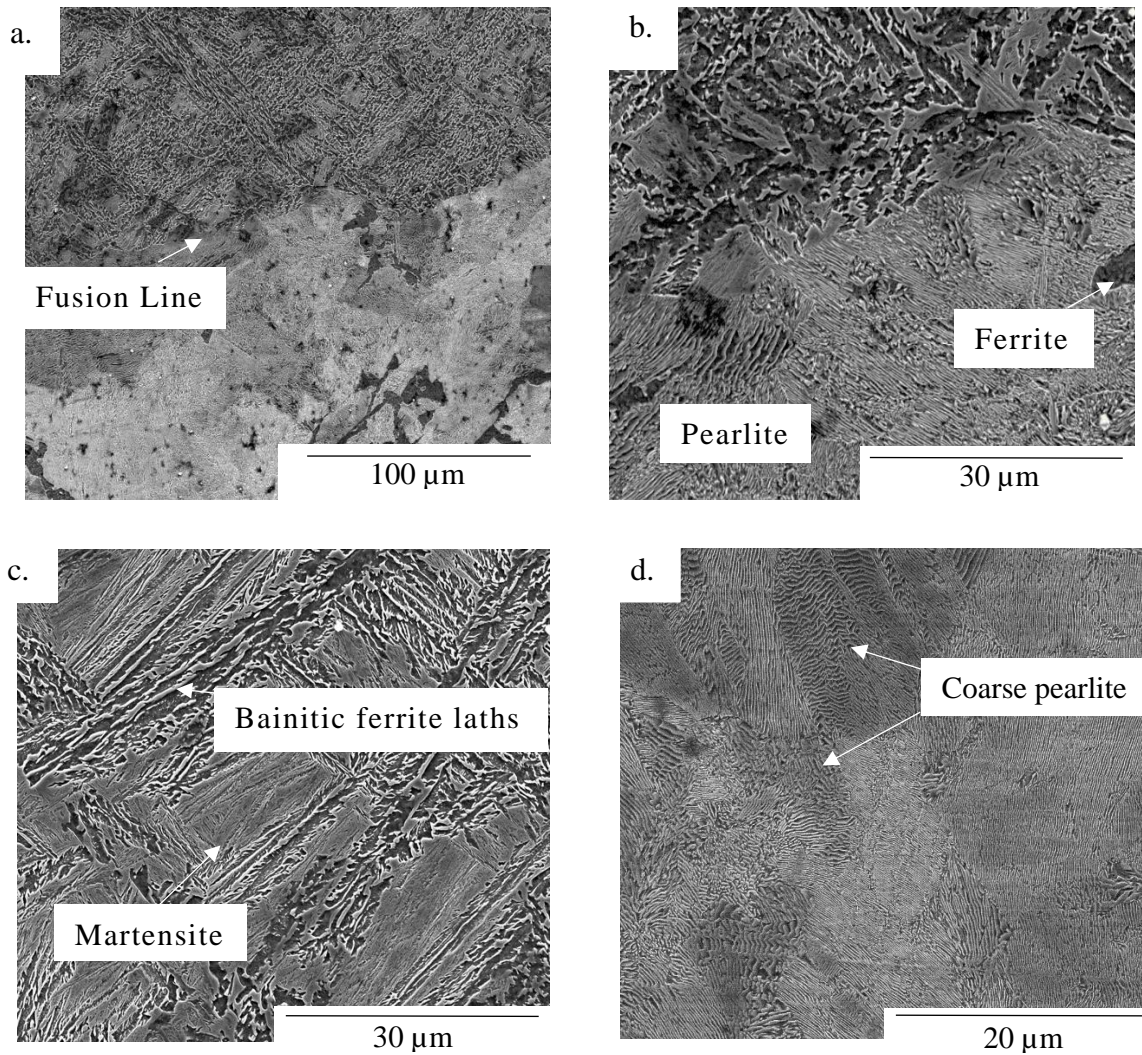
Figure 65. Scanning Electron Micrograph (SEM) of the FZ and CGHAZ (a), (b). FGHAZ (c) of a B360 grade, and HT350 FGHAZ (d) FBW with 8PH cycles.

In pearlitic grades, the grain size of the HAZ regions is directly related with its hardness due to a refinement of the pearlite interlamellar spacing. In the figure above, a very fine interlamellar spacing near the pearlitic FZ and FGHAZ can be observed.

Previous analysis on B360 FBW and ATW have shown similar increments in the rail hardness at the outer limit of the CHAZ [68],[79],[80].

Due to the relatively high cooling rates reached near the FZ, higher amounts of martensitic regions are expected. A more detailed examination was made on a nano-metric scale on a region of the B360 CHAZ with the use of thin foils on the TEM as in Figure 66, those were obtained in a mid-area of the CHAZ. Thus, helps us to distinguish the carbide distribution between the bainitic ferrite laths. Showing the presence of upper bainite laths and Martensite, these will increase considerably the

steel hardness from the parent material. Martensite can be easily distinguishable as dark regions due to its high density of dislocations.
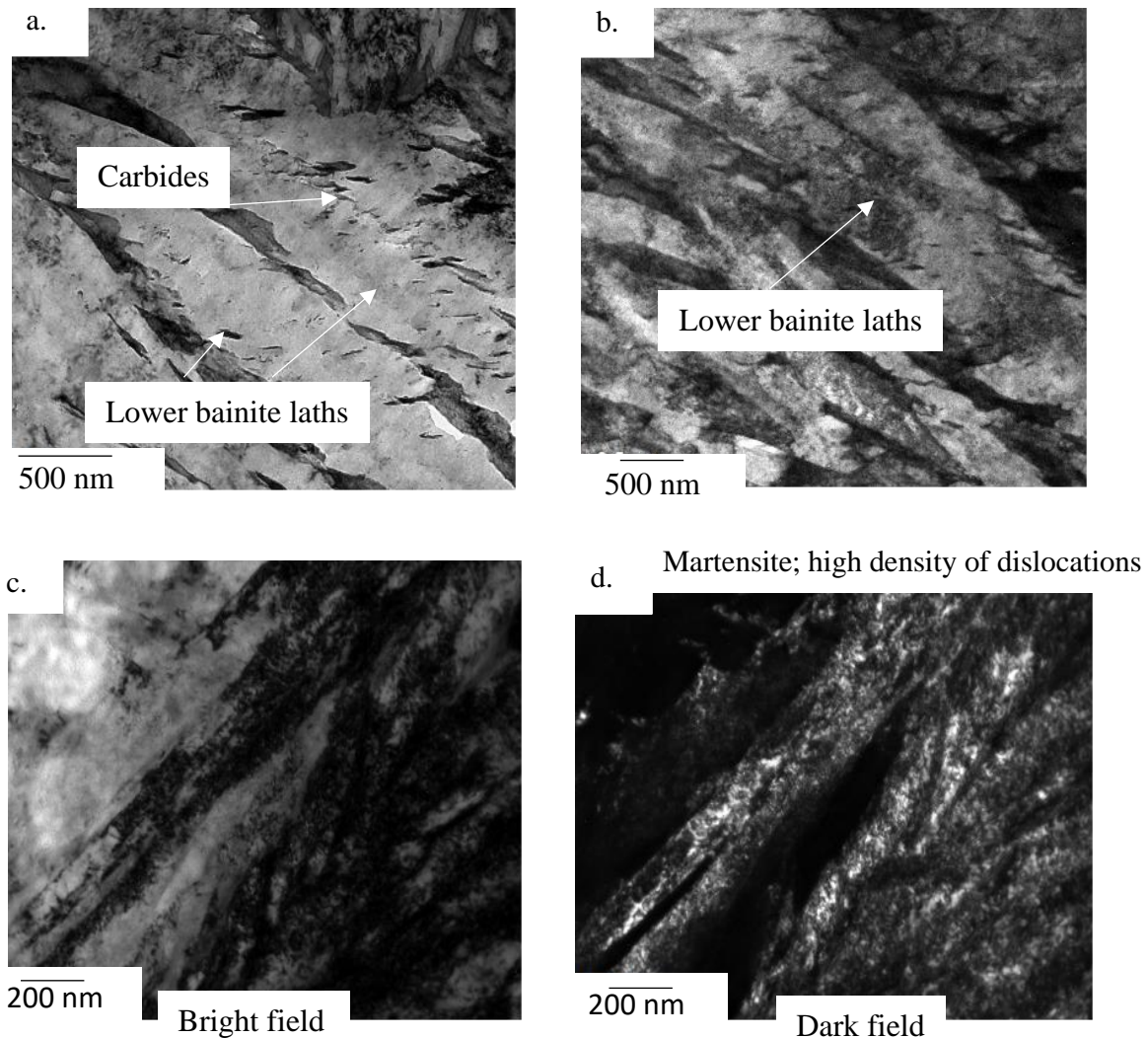

Figure 66. Transmission Electron Micrograph (TEM) of a region from the CHAZ, thin foils, bright field (a), (b), (c), and dark field (d)

Moving to the **ICHAZ** low peak temperatures up to 900°C are produced, leading to partial reaustenitisation of the steel. At this low peak temperatures, limited growth of the austenitic grains is produced, resulting in a refinement of the microstructure.

As observed in Figure 67, high variations are produced between 13 to 21 mm from the weld FZ, with a difference of 133.5 HV1 in only 8 mm of distance. These high hardness variations could result in differential plastic deformation when in track applications.

As in the CHAZ, temperatures are high enough for a redistribution of Carbon, leading to a decrement of RA regions for the formation of Martensite during cooling [81].

92

However, when moving away from the beginning of the ICHAZ, a drop in hardness is observed, which may be linked by both a decrement in the martensite content, and tempering of the microstructure.

Another factor that might influence the high drop in hardness will be the presence of acicular ferrite (AF) in some parts of the ICHAZ. AF nucleates in non-metallic inclusions such as MnS, as it can be observed in Figure 68 b. The presence of AF is known to improve the steel toughness, as the dissimilar directions of the ferrite laths are believed to be able to deflect cracks. As observed in the SEM examination, regions of MA islands together with AF and bainitic ferrite can be easily distinguishable.

The TEM specimens of Figure 69, showcase carbide precipitation between the laths, those carbides seem to be relatively large with sizes around 180nm, AF is also easily distinguishable.
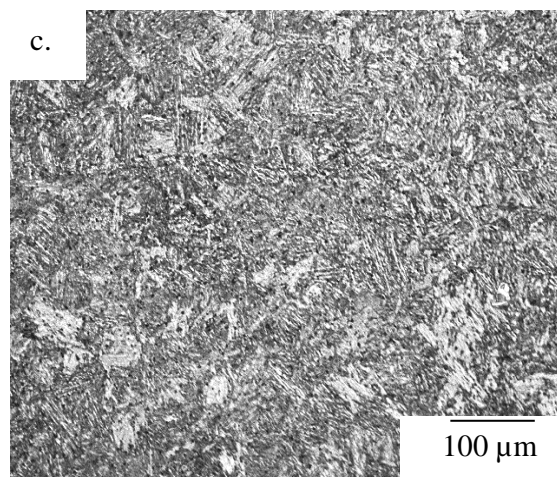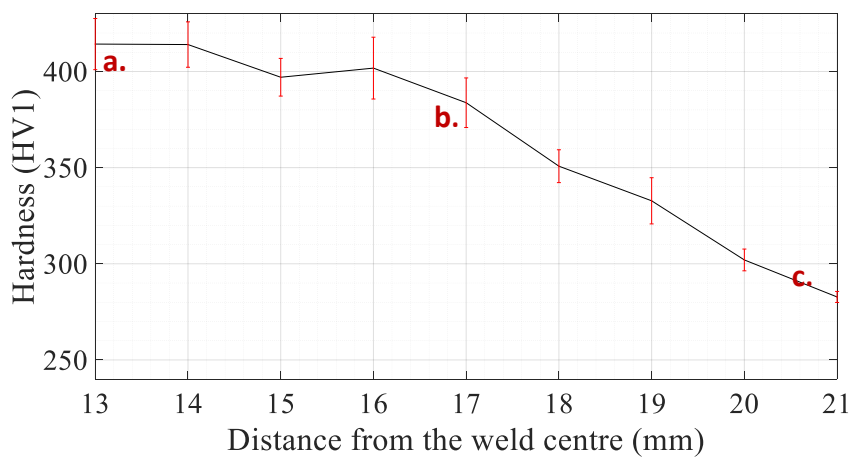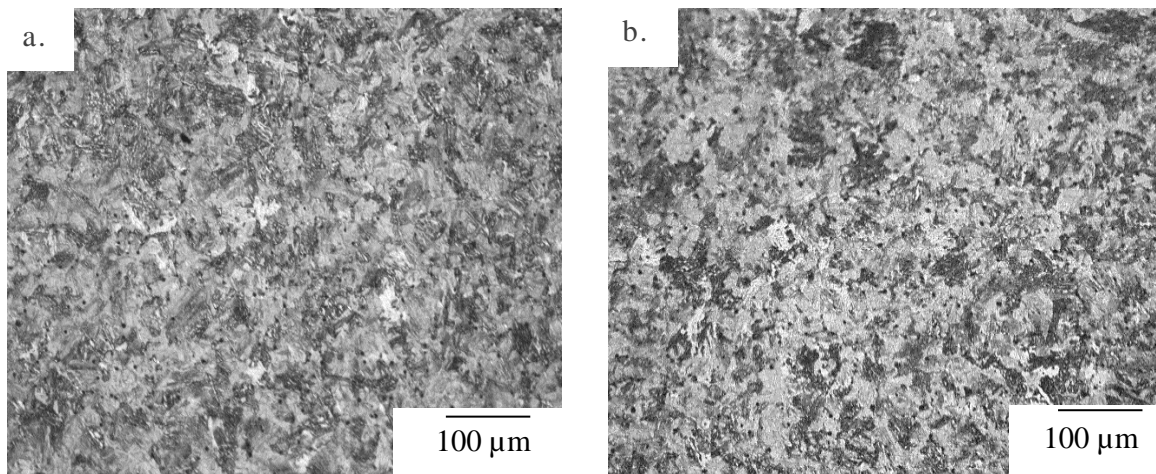
Figure 67. Hardness variation in the rail ICHAZ; together with light micrographs taken at specific locations.
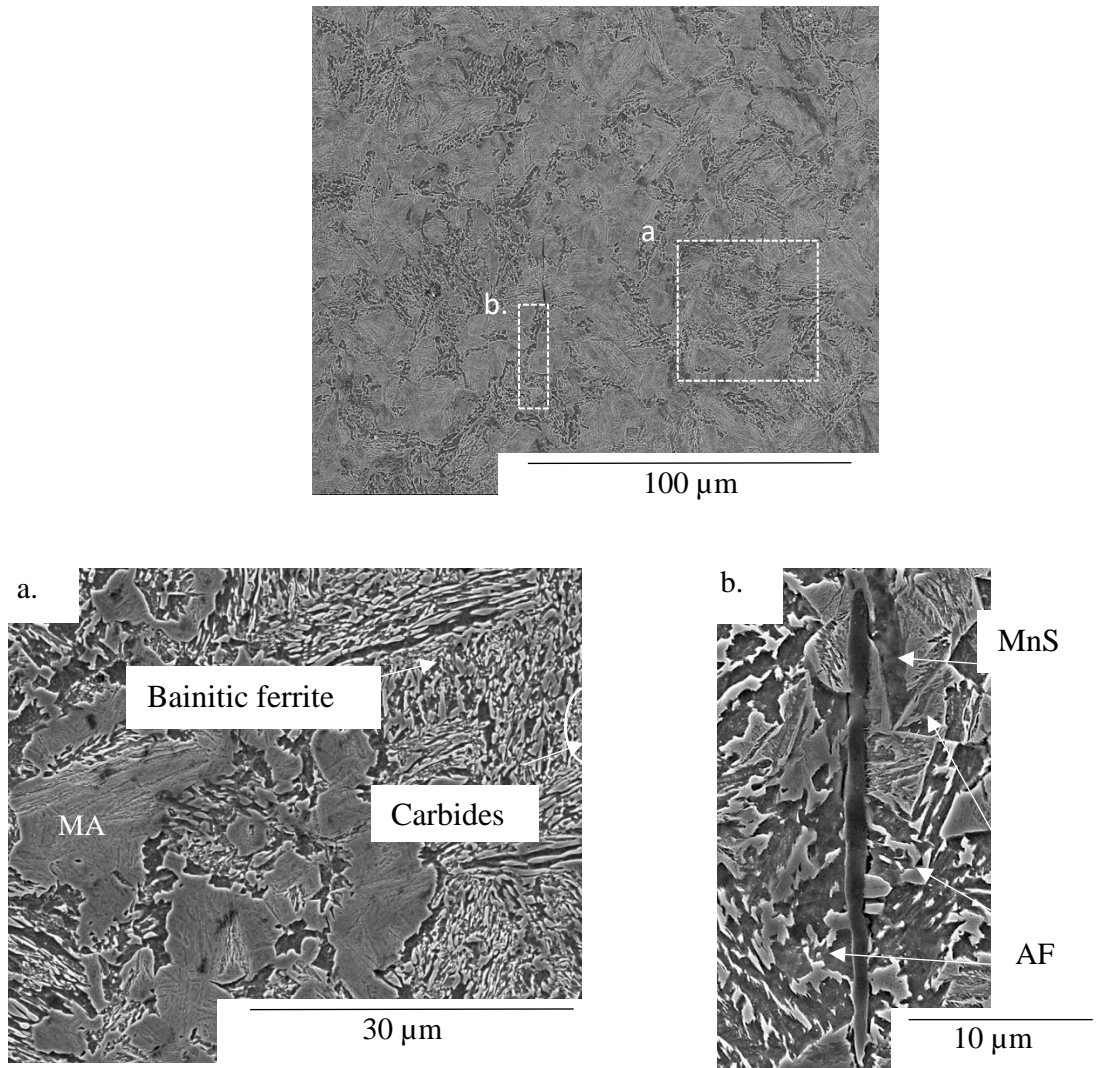
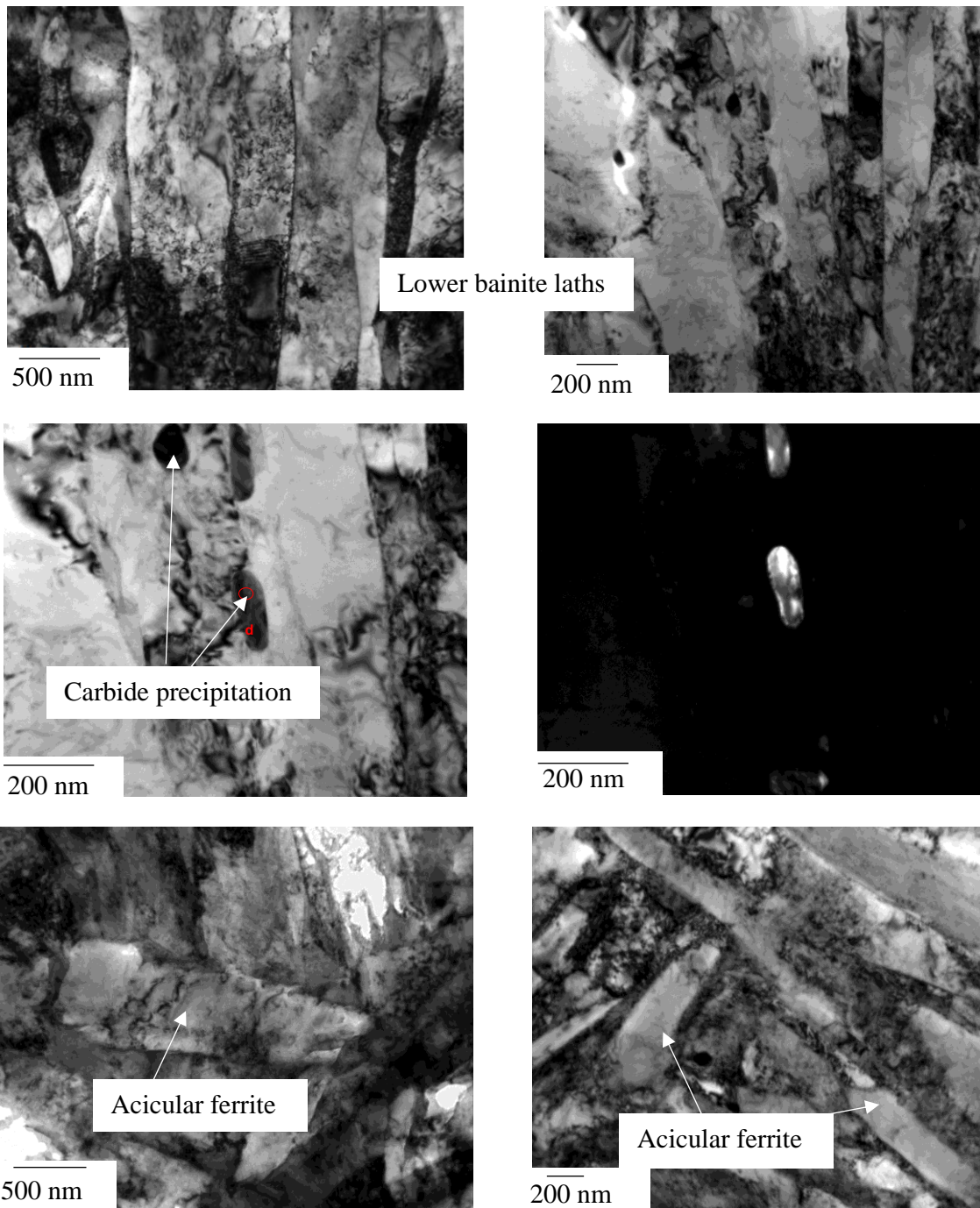**Figure 68.** Scanning Electron Micrograph (SEM) of the ICHAZ of a FBW B360-350HT.

Figure 69. Transmission Electron Micrograph (TEM) showing martensite laths, easily distinguishable by its high dislocation density, some carbide precipitation between the ferritic laths and acicular ferrite regions in the ICHAZ of a FBW B360.

When moving to the **SCHAZ**, the temperatures reached (from 400 to 700°C) were insufficient to produce reversion of the austenite to bainite, leading to an intense precipitation and coarsening of carbides and cementite at the Prior Austenitic Grain Boundaries (PAGBs) and between bainitic ferrite laths. Tempering of high carbon martensite regions could also take place.

The RA has almost completely discomposed, this together with the reduction of the steels internal stresses during tempering procedures, will lead to an overall softening of the microstructure. It can be easily observed in the hardness variation graph represented in Figure 70, in which the observable extent of tempering is of 58 mm.
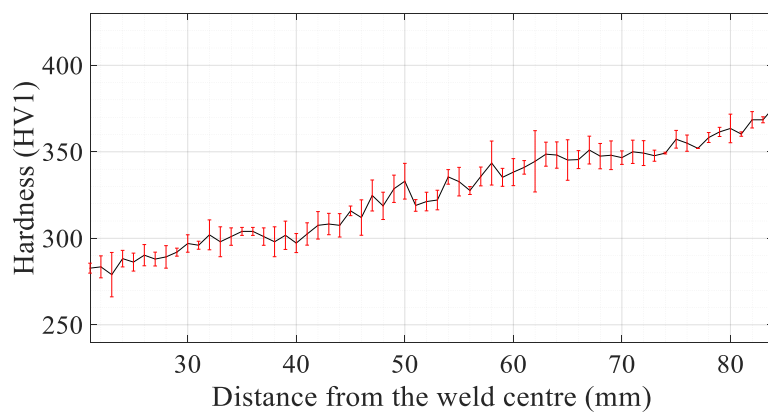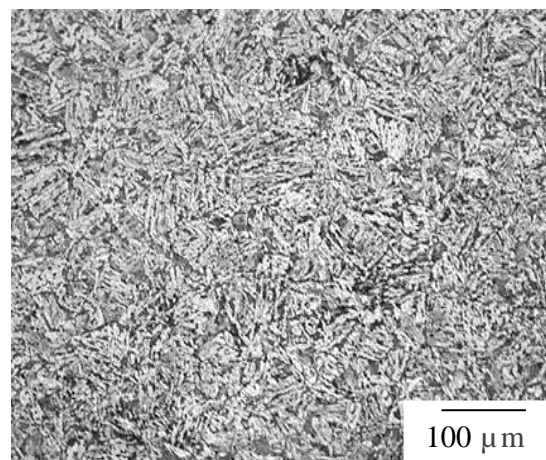

Figure 70. Hardness variation in the rail SCHAZ up until the hardness recovery; together with light micrographs taken at specific locations.

Softened HAZ regions are known to have a detrimental influence in the rail in track performance, producing weld batter, causing differential wear on the rail running surface.

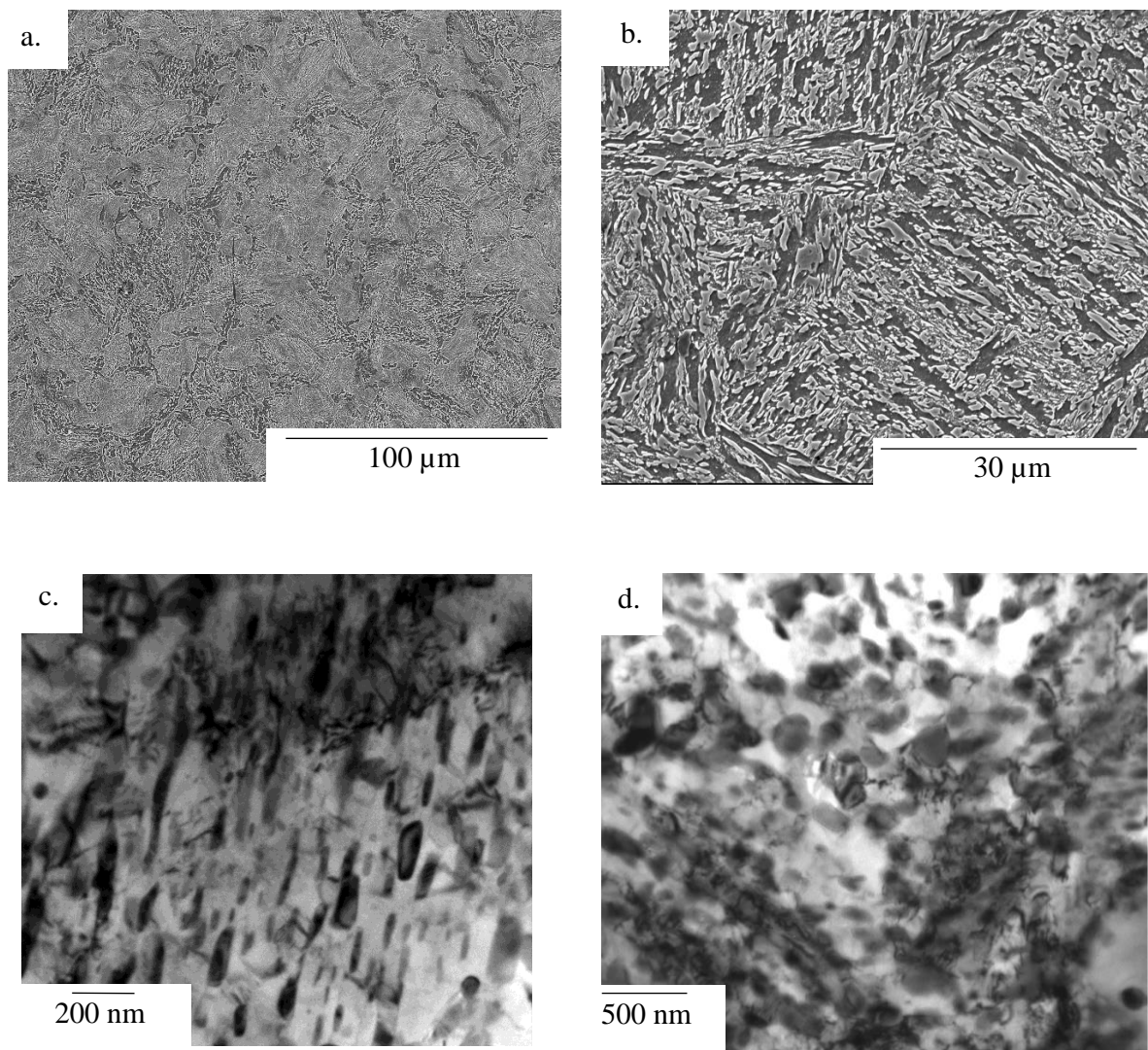Figure 71, represents a SEM and TEM examination of the softest region of the SCHAZ.

97

Figure 71. (a., b.) Scanning Electron Microscopy (SEM)of the SCHAZ, showing BF laths and carbide precipitation caused by the temperatures reached during tempering. (c., d.) Transmission Electron Micrograph (TEM) showing high amounts of carbide precipitation in the SCHAZ of a FBW B360, (beginning of the SCHAZ)

At tempering temperatures between 400 and 700 °C, coarsening of carbides will take place [40]. The extent of carbides growth is a direct function of its chemical composition; elements such as silicon, known to delay the coarsening process [82]. Although the steel under interest has high Si content (1,2 wt.%), large carbides up to 200nm were observed within the SCHAZ. The size of those will affect steel toughness.

When moving away only 10 mm from the SCHAZ, with a reduction of the tempering temperatures, the carbides seem to be smaller, with sizes of around 100 nm as in Figure 72.
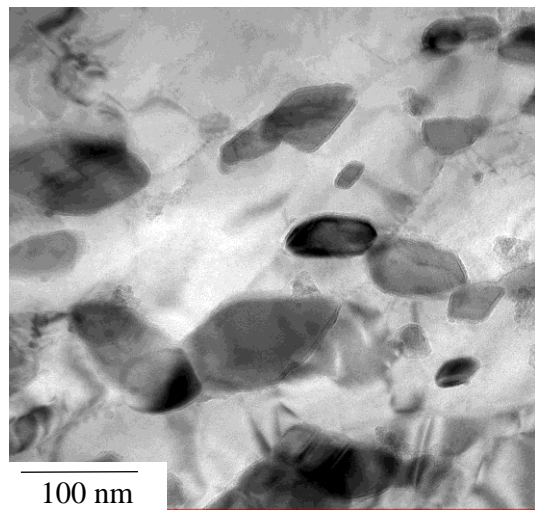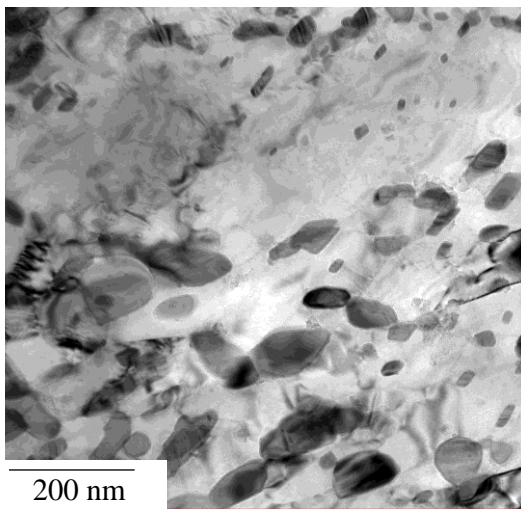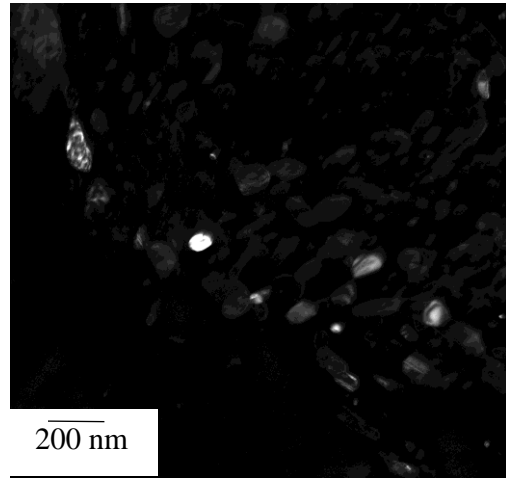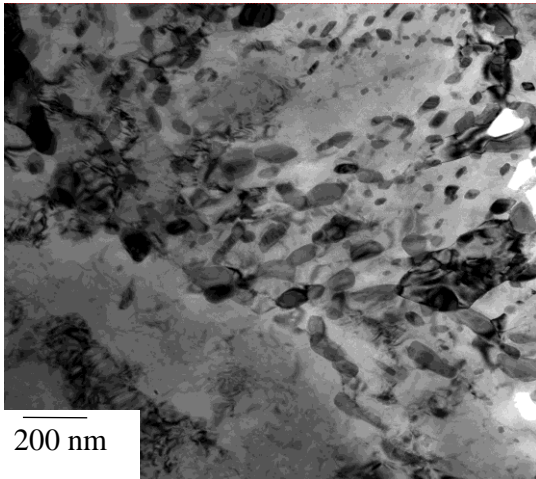
Figure 72. Transmission Electron Micrograph (TEM) showcasing high amounts of carbide precipitation in the SCHAZ of a FBW B360, (end of the SCHAZ)

IV. EBSD analysis

A further analysis was made with the help of EBSD, helping to identify more easily the amount of RA and MA constituents within the ferrite matrix. Starting with the "as rolled" material, Figure 73, represents the initial band contrast map (BC), representing image quality or intensity of the obtained Kikuchi pattern, together with a colour map showing the two phases present in the "as-rolled" grade; α-Fe and γ-Fe; and the grain boundary distribution of the B360 compared with Mackenzie distribution.
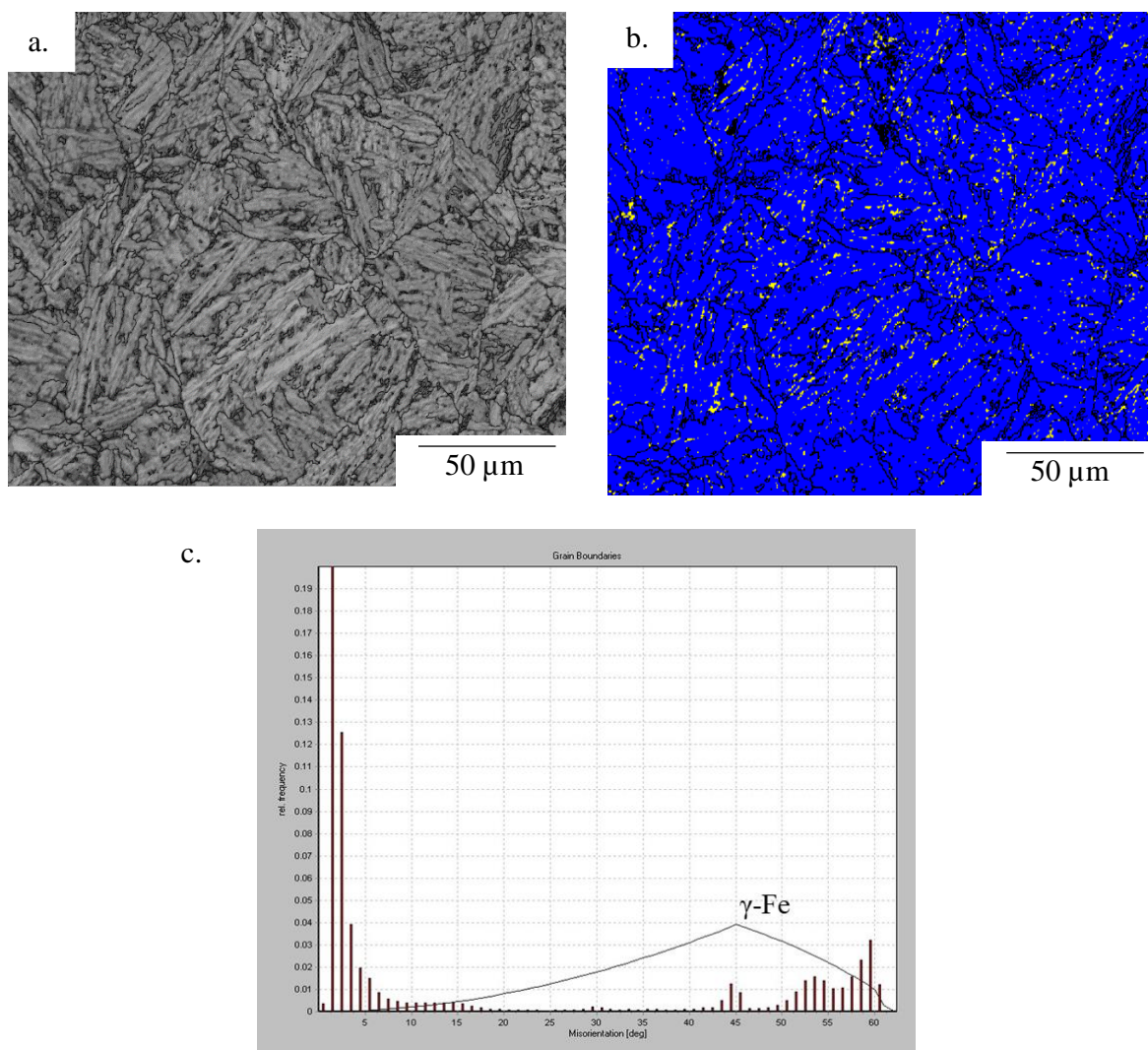

Figure 73. EBSD characterisation of "as rolled" B360. (a) Band Contrast (BC) + Band Slope (BS), (b) Representation of the RA content (FCC) in yellow and ferrite in blue. (c) Grain boundary distribution in a B360 steel, compared with Mackenzie distribution

The black lines represent the High Angle Grain Boundaries (HAGB) with a misorientation of <15°, as this is the critical disorientation for metallic materials.

100

Austenite, represented in yellow, seems to be present in form of both films, between the bainitic ferrite laths and blocks. Although, blocky austenitic regions are thermodynamically stable at room temperature, mechanical stresses on these regions could result on high carbon martensitic regions [48].

Only displacive transformations took place. As observed in the grain boundary distribution map in Figure 73, the majority of transformations were produced at either <15°, or between 50°-63°. A peak was found at 45°, corresponding to the presence of RA. A quantification of the amount of RA was made in all the dissimilar HAZ regions as in Figure 75.
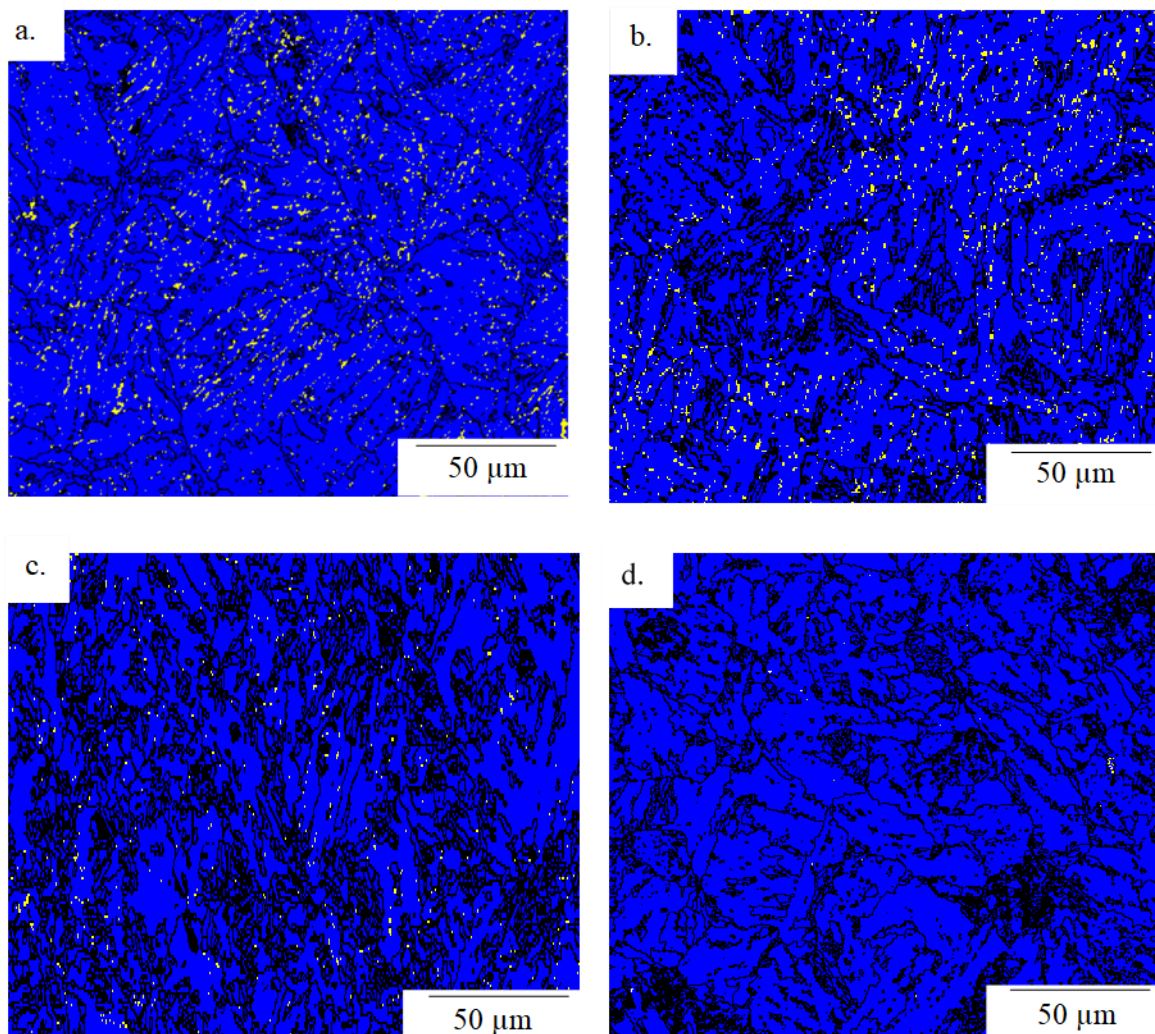

Figure 74. EBSD characterisation representing the dissimilar HAZ regions. A. "As rolled", b. Critical HAZ, c. Intercritical HAZ, d. Subcritical HAZ. In red the RA content (FCC).

It has to be borne in mind that RA laths have a length of 20-100 nm, thence, there is a limitation in the quantification of RA between the ferritic laths with EBSD, therefore XRD quantification would be more appropriate in this, however, the EBSD data will give us an idea of the amount of RA and its shape and morphology. As an example, according to the EBSD data, 12% of RA was present in the section under analysis, 5% less that the obtained with EDX analysis.

Further analysis was made to determine the amount of martensite in the selected regions of the HAZ and the "as rolled" steel. Knowing that martensite has a BCT crystal structure, EBSD will read it as a distorted BCC. This can be easily observable when using the previously mentioned BC map; in which brighter regions represent higher quality [83], meaning that, in the case under study, brighter regions will appear as ferrite and darker as martensite. A separation of the ferritic and martensitic regions was made on the HAZ regions under interest as in Figure 75.
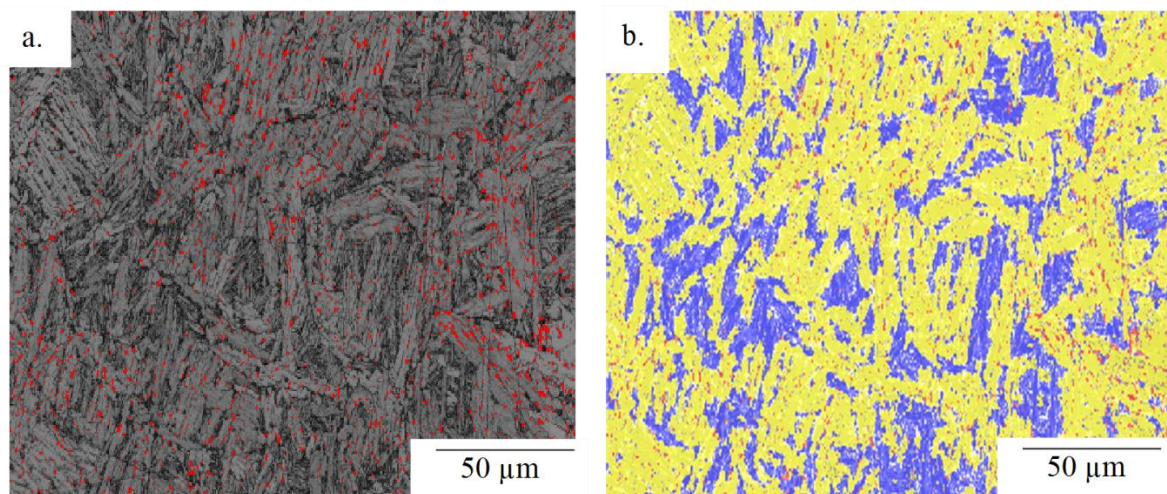

Figure 75. Determination of martensitic regions using BC. a. BC map showing darker regions as martensite and lighter as ferrite, b. Map performed using the internal statistics on Chanel 5, showcasing martensite as blue and ferrite as yellow.

As expected, a significant reduction of RA is present from the CHAZ up to the SCHAZ, being in all of them lower than in the "as rolled" B360. RA is expected to result in carbon dissolution in excess of ferrite to produce more carbon rich martensite, bainite or carbide precipitation which will result in potential damage on the steel mechanical properties. In the SCHAZ the RA has completely discomposed to the formation of bainite and carbides, as previously represented in the TEM images. Being the main cause of the softening behaviour of this part of the HAZ.

102

Figure 76 represents the phase segmentation map of the "as rolled", CHAZ and ICHAZ, no martensite was found in the SCHAZ.
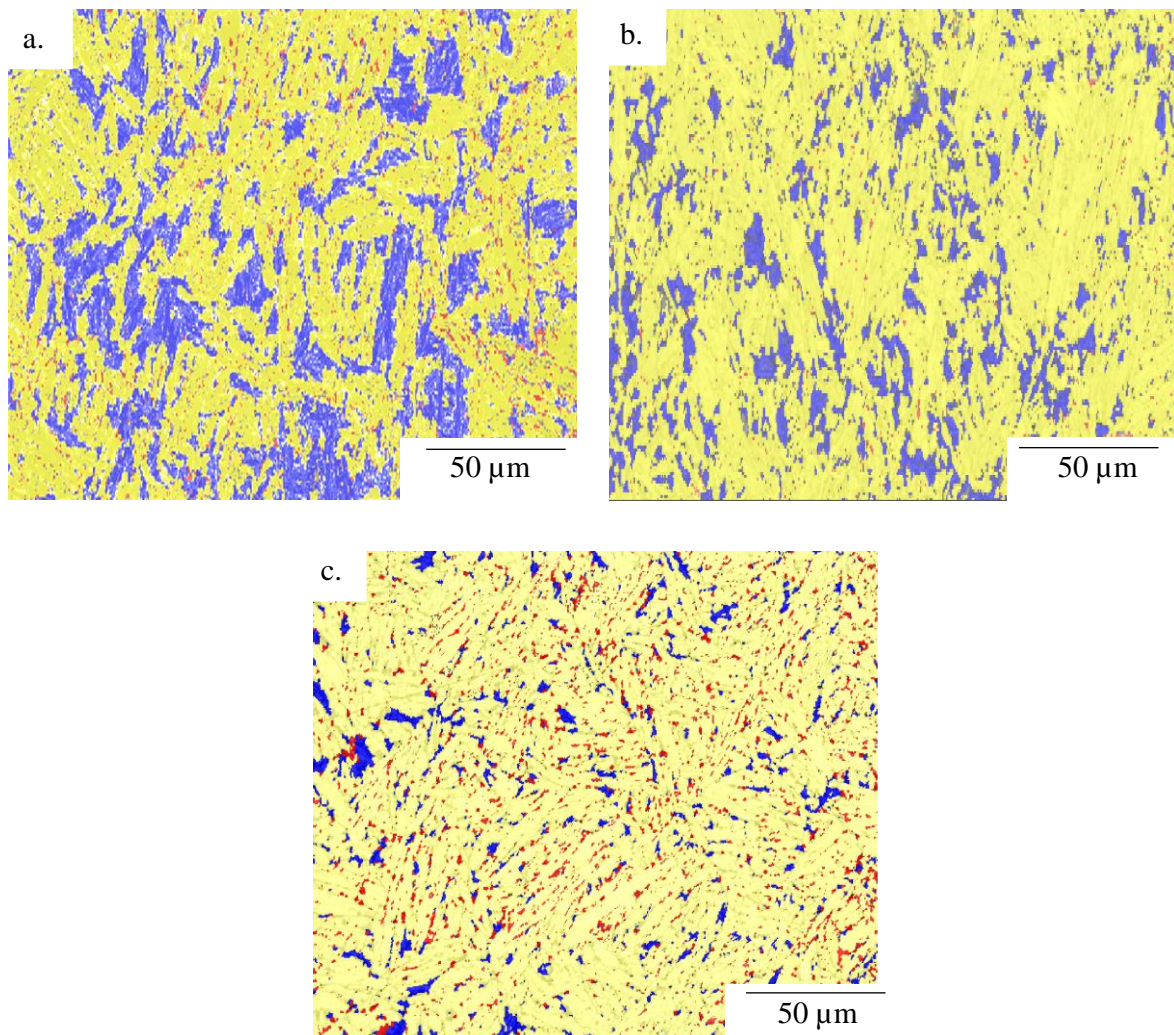

Figure 76. Phase segmentation map, showing martensite in blue, ferrite in yellow and retained austenite in red. A. CHAZ, b. ICHAZ and c." As rolled" B360.

The martensite-ferrite phases were later on quantified using its area fraction in imagej, the results of this quantification can be observed on Table 15.

As observed, in the rail SCHAZ, almost no RA and no Martensite was found, having predominantly a ferritic microstructure. When doing a more in-depth analysis in TEM we could observe intense amount of carbide precipitation or cementite. RA will decompose into carbides and ferrite, whilst the martensite constituents of the as-rolled steel will be metastable, losing is tetragonality during tempering and decomposing into cementite [84].

Table 15. Volume fractions of phases of the dissimilar regions.

Regions	Martensite	Retained austenite	Ferrite
Parent "as rolled"	9.7%	12.1%	78.2%
CHAZ	28.5%	5.3%	66.1%
ICHAZ	17.4%	1.0%	81.6%
SCHAZ	-	0.2%	99.8%

4.5. Analysis of other FBWs

A B320 rail was welded with a pearlitic R260 rail, supplied by British Steel. The chemical analysis of those rail steels was previously represented in Table 13.

A separate analysis was made on the two welded regions. Those were welded as the B360 with a "standard" FBW procedure with 8PH cycles, 4.6 s of preheating time "ON" and 1.1 s of delay period "OFF"

I.B320

The microstructure of the "as rolled" rail can be observed in Figure 77; consisting on BF laths surrounded by RA regions, as in the B360 grade. Hardness measurements were performed on the rails head RD, obtaining a value of 356.9 ± 5.0 HV1.
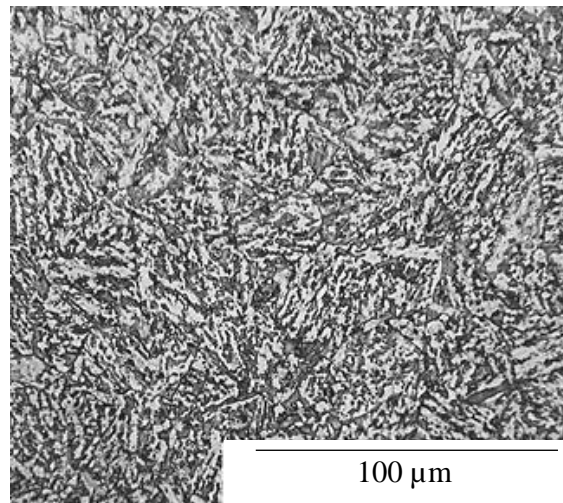

100 μm

Figure 77. OM of an "as rolled" B320 grade

The visible HAZ width of the weld had a value of 18 mm. Hardness measurements were made from the weld FZ up to 60 mm, as at that distance the recovery of hardness was expected to be completed. Figure 78, represents the Vickers hardness profile of the B320 rail, together with its corresponding gradient map.
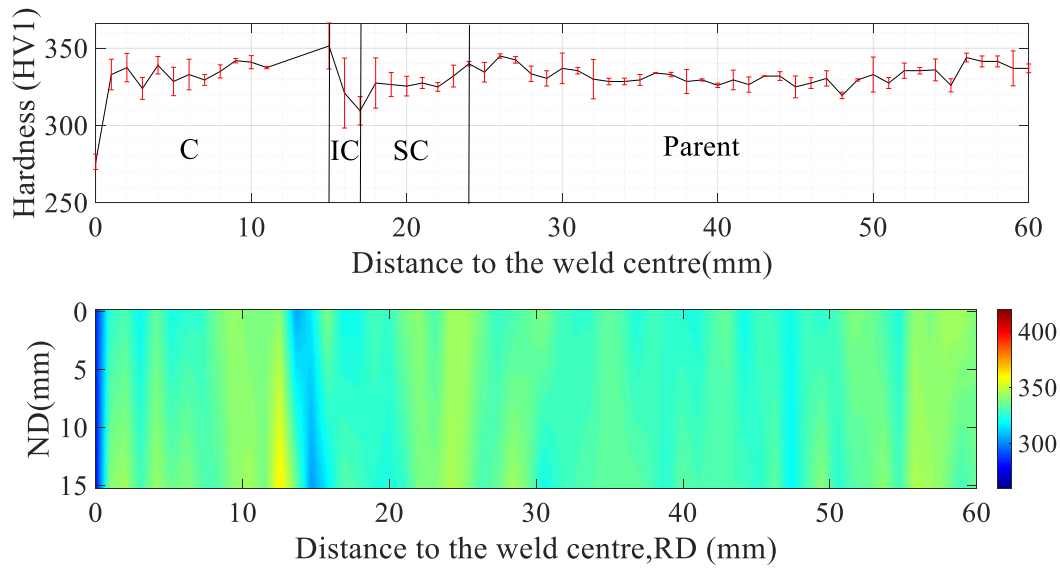
Figure 78. Hardness variation versus distance to the weld centre line of a B320 welded rail steel.

As before, Figure 78 shows the typical behaviour of a FBW hardness profile, with the dissimilar HAZ regions, C, IC, SC and Parent. The parent region of the HAZ was selected once the hardness values reached ≥ 335 HV1. Table 16 represents a summary of the hardness values obtained in the B320 FBW, together with the extension of the tempered SCHAZ.

Table 16 Hardness values of the HAZ of a CFB B320FBW.

Visible HAZ width (mm)	18
Max Hardness (HV1)	351
Min Hardness (HV1)	309
Variation of hardness in the IC HAZ (HV1)	42
Extension of the SC HAZ (mm)	7
Max H – Parent (HV1)*[1]	22
Min H – Parent (HV1)*[2]	17

*[1] *Maximum hardness value in the HAZ – Hardness of the parent rail*
*[2] *Minimum hardness value in the HAZ – Hardness of the parent rail*

At 12 mm from the FZ, maximum hardness values were found through the CHAZ, with a peak at 351 HV1, which is 22 HV1 higher than the parent rail hardness of 326 HV1.

Therefore, as B360, B320 also satisfies the maximum value for pearlitic steels according to the European standard [67] of P+60. The minimum hardness measurement of the HAZ is of 309 HV1, 17 HV1 lower than the parent hardness of 326 HV1. In this case, B320 does satisfy the minimum hardness requirement of P-30.

Whilst the extension of the visible HAZ was similar to the B360 grade, the main difference on these two welds will be the extension of the tempered SCHAZ, which is much narrower in the B320 grade. Figure 79, represents a micrographic examination of the B320 FBW.
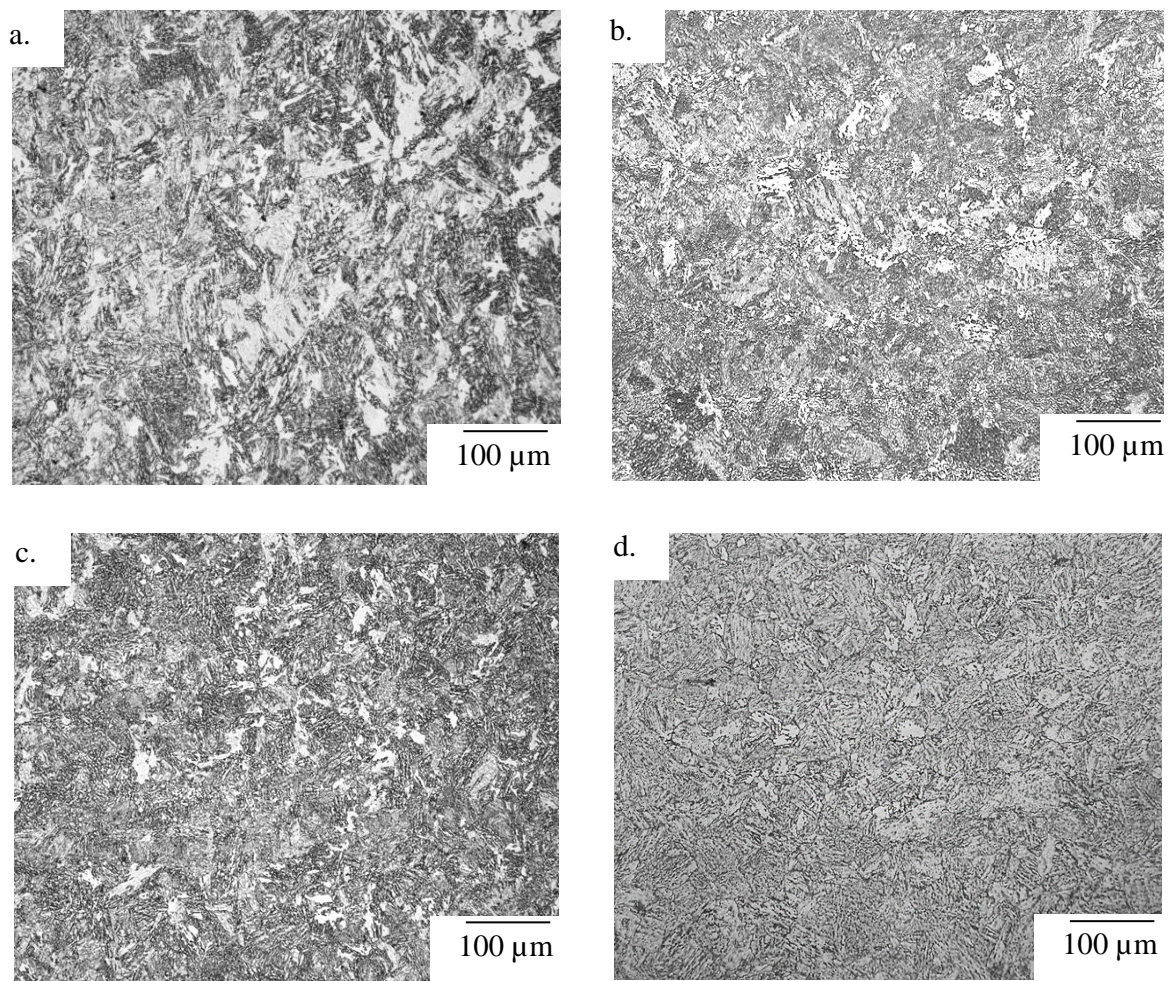

Figure 79. Micrographic examination of a B320 weld, a. CGHAZ, b. FGHAZ, c. ICHAZ, d. SCHAZ.

From the B320 HAZ microstructural variation, a very similar evolution as in B360 can be observed, with the typical progressively finer microstructure of FBW procedures, whose extension goes from the weld FZ up to 14 mm from the weld centre.

Regions of martensite, lower bainite and AF in both the CHAZ and ICHAZ and a tempered microstructure in the beginning of the SCHAZ up to 24 mm were observed.

A more in-depth analysis on the SCHAZ of B320 grades was made with the use of carbon replica, we could observe high amounts of spherical vanadium precipitates through the softest region of the SCHAZ, as in Figure 80.

Also, there is visible reduction in the number of larger carbides from the previously examined B360 grade. Therefore, there not only is an increment on steel hardness due to precipitation hardening, but Vanadium seems also to slow down austenite decomposition into carbides; this behaviour is currently being investigated by British Steel [85]
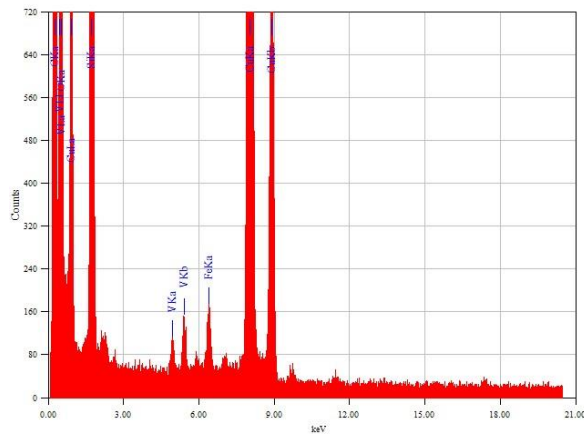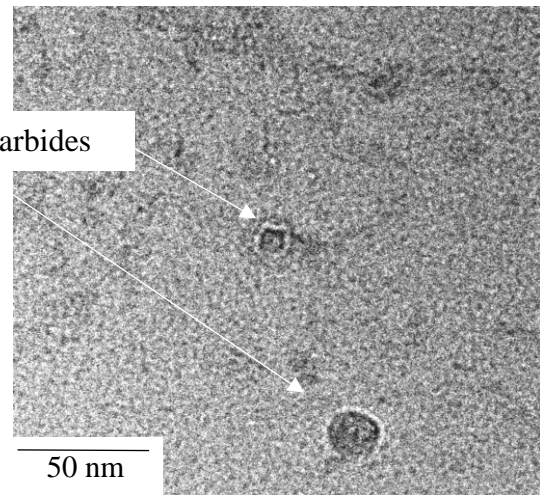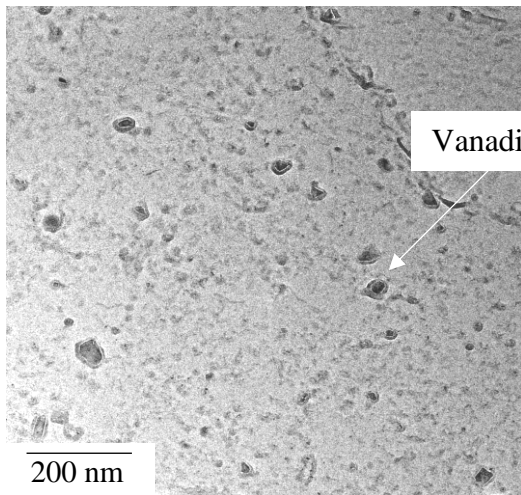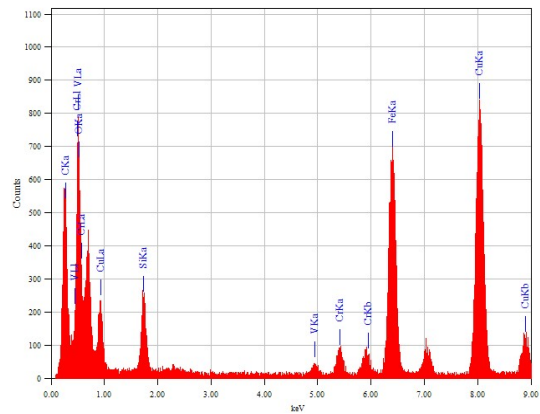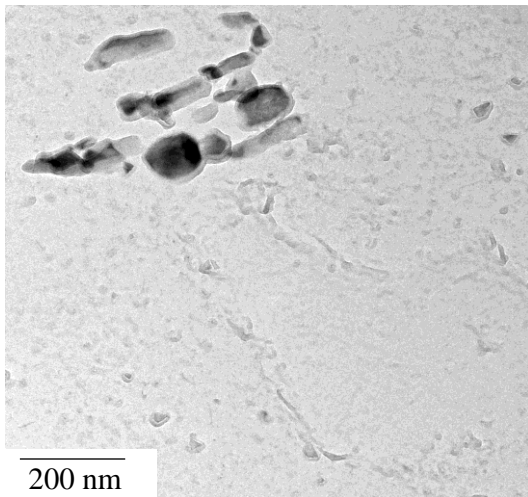
Figure 80. Transmission Electron Micrograph (TEM) showcasing high amounts of vanadium carbide precipitation in the SCHAZ of a FBW B320. Carbon extraction replica

II.R260

Pearlitic steel R260 with a hardness of 273 ± 1.9 HV1, displays a fully pearlitic microstructure; with an alternating lamella of pearlite and cementite as in Figure 81. This is in accordance with previous work made on this grade [16].
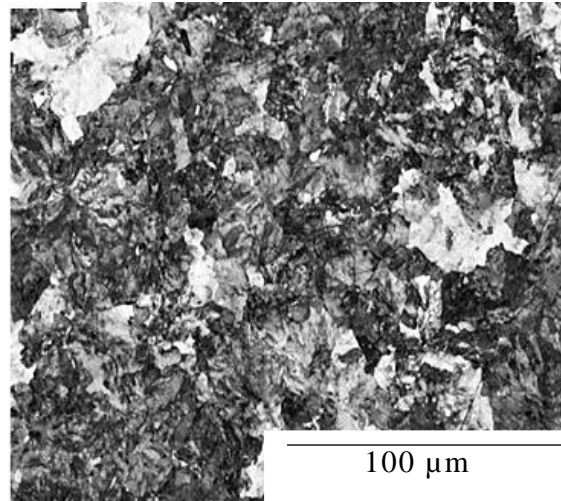

Figure 81. OM of an "as rolled" R260 grade.

Measurements of the R260 welded region, were made from the weld FZ up to 60 mm, as at that distance the recovery of hardness was expected to be complete. Figure 82, represents the Vickers hardness profile of the R260 rail, together with its corresponding gradient map. It shows the typical behaviour of a FBW hardness profile, with the dissimilar HAZ regions, C, IC, SC and Parent. The parent rail was selected once the hardness values achieved were of ≥ 274 HV1.

The maximum hardness measurement of 320.7 HV1 corresponds at 2 mm from the FZ; which is 46.2 HV1 higher than the parent rail hardness (273.8 HV1).

The minimum hardness measurement is of 247 HV1 at 13 mm from the FZ; which is 26.8HV1 lower than the parent rail. Therefore, it satisfies the maximum and minimum hardness profiles for pearlitic steels, P+60, P-30. All the values obtained on the FBW R260 are in accordance with expectation, satisfying the standard [67].

During recent years, numerous attempts have been made in order to understand the hardness and microstructural evolution of pearlitic FBWs [16] . As the microstructure produced on pearlitic steels during FBW procedures is mainly pearlite, the differences in hardness are mainly a function of its PAGS and therefore, its interlamellar spacing.

110

As when increasing pearlite interlamellar spacing there is a decrement of the steel hardness.

Near the FZ high peak temperatures are reached, up to 1500-1200°C, leading to a complete reaustenitisation of the steel. This region is also subjected to large amounts of plastic deformation due to the upsetting process [16]. At these temperatures, an increment of the PAGS is produced, leading to a coarse grain region.

When moving away from the weld FZ, as peak temperatures decrease below 1200 °C, grain growth is limited due to partial reaustenitisation of the steel, leading to a decrement on the grain size, a possible spherodization of pearlite and a reduction of the steel hardness in pearlitic R260.

The HAZ regions in which temperatures reached are below A_{c3}, the visible reduction of hardness in the subcritical HAZ could be attributed to partially spheroidised pearlite structure, which consists of a partially spheroidised cementite in a soft ferrite matrix. [16]
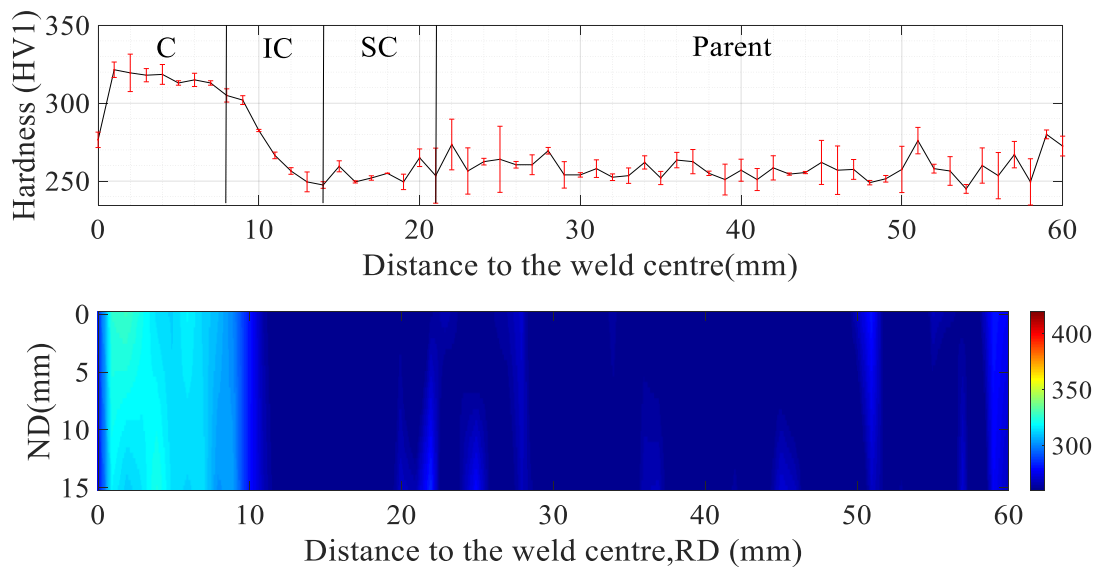
Figure 82. Hardness variation versus distance to the weld centre line of a R260 welded rail steel.

In the R260 region of the FBW, variations in hardness were found before 20 mm from the FZ. With an extension of the softened HAZ region of 7 mm.

Table 17 represents a summary of the hardness values obtained in the R260 FBW, together with the extension of the tempered SCHAZ.

111

Table 17. Hardness values of the HAZ of a R260 FBW.

Visible HAZ width (mm)	15
Max Hardness (HV1)	320.7
Min Hardness (HV1)	273.8
Variation of hardness in the IC HAZ (HV1)	46.9
Extension of the SC HAZ (mm)	7
Max H – Parent (HV1)*[1]	16.2
Min H – Parent (HV1)*[2]	26.8

*[1] *Maximum hardness value in the HAZ – Hardness of the parent rail*
*[2] *Minimum hardness value in the HAZ – Hardness of the parent rail*

4.6. Summary and discussion of results

On this chapter, an analysis of three 60E2 rail steels was made; B360, B320 and R260. Emphasising on the B360 characterisation.

B320 and B360 present a bainitic microstructure consisting on CFB laths surrounded by RA in the shape of both laths and blocks, whilst R260 is fully pearlitic.

After welding, using the same welding program with 8PH cycles, 4.6 s of preheating time "ON" and 1.1 s of delay period "OFF". The weld hardness variation of the three rails was analysed at 5 mm below the rail running surface; as this is the easiest way to determine the weld quality [77]. Also, the dissimilar HAZ regions could be easily identified, C, IC, SC.

Figure 83, represents the hardness variation produced from the FZ on the three rails under examination: R260, B320 and B360.
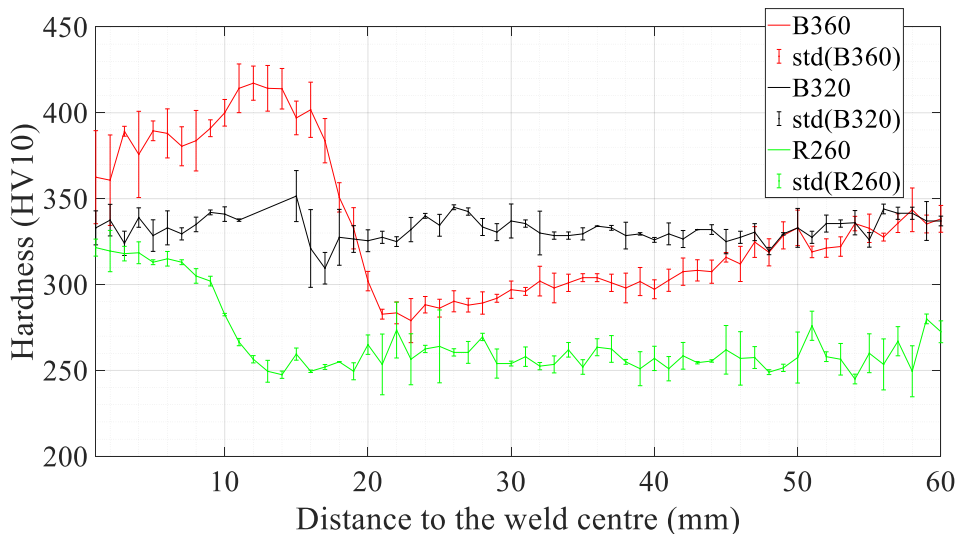
Figure 83. Rail hardness variation of the three rails under study: B360, B320 and R260.

As observed in Figure 83, The extension from the weld FZ up to the beginning of the softening SCHAZ seems to be more extended on the B360 steel; however, this extension is believed to be too narrow (20 mm) to produce any detrimental effect in track applications [58]. Therefore, the major concern will be more focused on the much wider extension of the B360 tempered SCHAZ.

The width of the softened HAZ together with the ICHAZ hardness variation of the B360 steels is greater than in B320. Variations in B320 and B360 FBWs have been seen previously and are believed to be produced due to; both, the presence of vanadium in the B320 grade, which could reduce softening in the tempered HAZ by precipitation hardening, and its lower carbon content, 0.23wt%, which will limit the maximum hardness obtained in the fine-grained HAZ.

Table 18, represents a summary of the maximum, minimum hardness values of the HAZ, together with the hardness variation in the ICHAZ and the extension of the SCHAZ; of the three steels under examination: B360. B320 and R260.

Table 18. Review of measurements obtained in the rail-running surface

	B360	B320	R260
Visible HAZ width (mm)	20	18	15
Max Hardness (HV1)	415.5	351	320.7
Min Hardness (HV1)	282.5	309	273.8
Variation of hardness in the IC HAZ (HV1)	133	42	46.9
Extension of the SC HAZ (mm)	58	7	7
Max H – Parent (HV1)[1]	41.2	22	16.2
Min H – Parent (HV1)[2]	94.7	17	26.8

1 Maximum hardness value in the HAZ – Hardness of the parent rail
2 Minimum hardness value in the HAZ – Hardness of the parent rail

As it can be observed, the welded rail section showing a less accentuated hardness variation seems to be the B320 FBW.

From all the welds under examination, only the B360 doesn't satisfy the minimum hardness criterion of P-30, however, this is only a criterion for pearlitic grades R260, R220 and R260Mn [67]. There is not current standard for bainitic grades.

Whilst, according to the literature, R260 microstructural evolution seems to be fully pearlitic, B320 and B360 show a much more complicated evolution.

An in-depth analysis was made in the dissimilar HAZ regions of the B360 grade. Starting in the weld CHAZ, where high amounts of martensite and upper bainite were present leading to the observable increment in the steel hardness.

When moving to the weld ICHAZ, a considerable drop in hardness was observed in only 8 mm of distance, with a hardness difference of 133 HV1. A more in-depth examination has shown regions of martensite, acicular ferrite and tempered bainite, starting to see first sights of carbide precipitation between the bainitic ferrite laths.

Finally, the rail SCHAZ has shown a steady increment in hardness, up to the rail parent hardness of 360HV. The hardness recovery started at 79 mm. Softened HAZ regions in rail steels are known to wear, reducing rail lifetime. An intense carbide precipitation was observable in the tempered HAZ region, with large carbides up to 200nm in size.

Chapter 5

Narrower FBW of a B360 60E2 rail

5.1. Introduction

A series of 12 Flash Butt Welds (FBW) in B360 60E2 rails were produced at the stationary FBW GAAS 80 / 580 Schlatter [58] in British Steel Scunthorpe, UK. These were made with the purpose of producing a narrow HAZ. Thus, eliminating the probabilities of preferential wear associated with the existed wide standard welds or "weld batter" and, reduce the extension of the detrimental tempered HAZ region of CFBs [68].

Previous attempts were made back in 2006 and 2008 by British Steel [53],[80],[86], showing that reducing the number of preheat cycles (PH) during the FBW of CFB B360, will produce a narrower extension of the HAZ. In addition, this will reduce both power consumption and welding time, lowering costs by increasing production rates[60].

In order to continue with this previous work, an analysis of four dissimilar values of PH cycles within the FBW procedure were made. Differently, one analysis was made adding post weld heat pulses (PWHP) at the end of the weld in order to observe the influence this may produce, looking for a reduction of the weld-cooling rate.

When selecting the FBW parameters, it is important to bear in mind that, reducing the number of PH cycles and time could result in not enough heat for a proper

consolidation of the weld, and in problems during the stripping process. Additionally, an increment of the rails cooling rate is known to lead to a more ductile microstructure [87]. Therefore, the aim of these trials was to reduce the width of the HAZ whilst retaining weld integrity.

As previously described in the experimental procedure, the preheat cycles used were 3,4,5,6 and 6 + 3PWP; with a preheating time (s) (ON) and delay period (s) (OFF) of 2.0 and 0.5 respectively. In conventional welds these times are of 4.5s ON and 1.1s OFF [68]. The short OFF time selected, is believed to limit the amount of heat that diffuses away from the weld, whilst the short ON time will limit the heat input; therefore, a reduction of the HAZ width extension is expected when comparing with conventional welds.

On this chapter, an analysis of the data obtained after the FBW procedures and how this will influence the final mechanical properties of the welds was made. Furthermore, an investigation of the HAZ width, the welds hardness variation and its relationship with the microstructural changes produced is discussed.

A further analysis of the welds longitudinal and transverse residual stresses as a function of the number of PH cycles was investigated, together with an analysis of the weld integrity with the use of a three-point bend tester.

5.2.   As rolled material

As previously discussed in the experimental procedure, two B360 rails of 20 meters each were used for FBW. Those were welded together and cut at dissimilar distances in order to generate a total of 12 welds. A section of the parent rail was separated for metallographic analysis, hardness and mechanical testing.

The hardness of the parent rail measured was of 383.26 ± 3.5 HV1. The chemical composition of the B360 has been discussed in both the experimental procedure and Chapter 4.

The parent material of the welds displays a typical microstructure of a CFB B360, with upper bainitic ferrite laths surrounded by retained austenitic regions (RA), and some martensite-austenite (MA) islands. Figure 84, displays a SEM microstructure of the CFB B360.
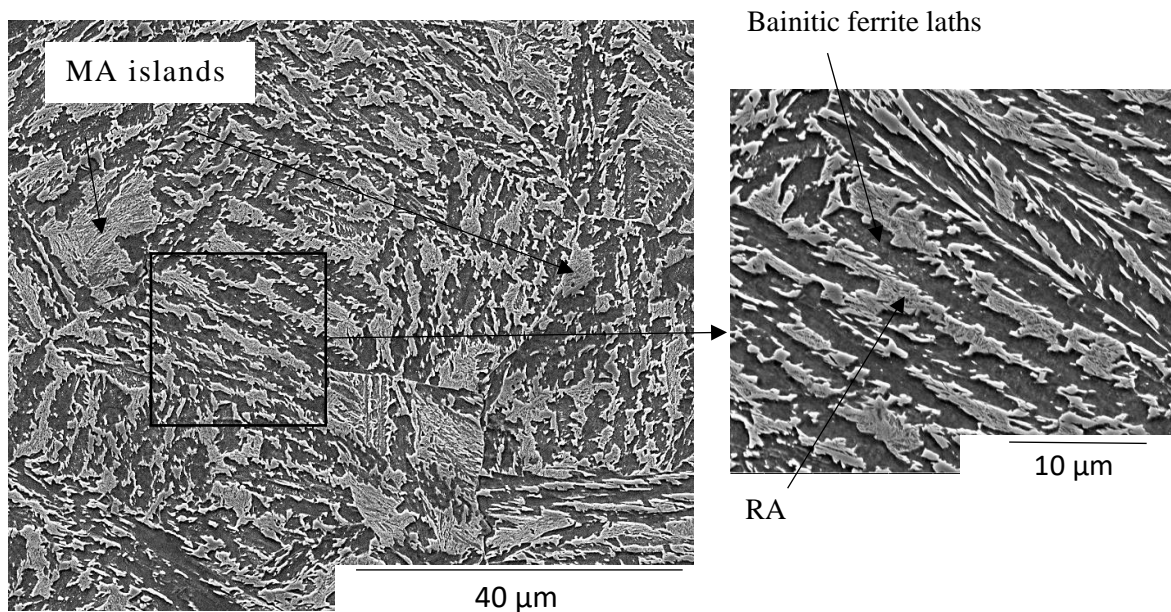

Figure 84. Scanning Electron Microscopy (SEM) of an "as rolled" CFB B360 rail.

5.3. Welding trials

After the welding procedure, an analysis was made with the help of an obtained SWEP chart. These display the steps involved in the weld process: burn off, preheating, flashing and upsetting in terms of its current (A), force (kN) and travel (mm) [58],[16]. An example of a SWEP chart obtained for the welds in which only variations of PH cycles were produced can be observed Figure 85. The other weld charts obtained after the FBW can be found in the appendix.
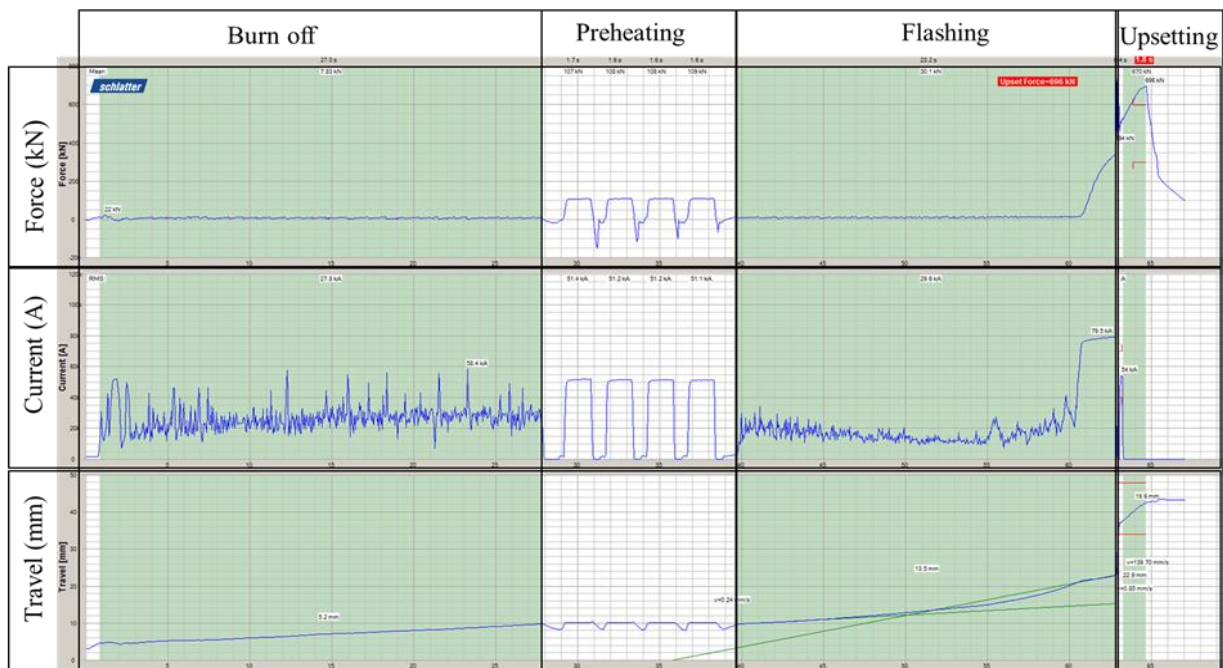

Figure 85. Representation of a weld chart obtained after the FBW process. 4PH weld.

For conventional pearlitic steels, rails are naturally air cooled down to a temperature of ~500 ⁰C to allow fully pearlitic transformation in the CHAZ. As an example, the hardness levels achieved in a R260 CHAZ are of approximately 300HB (320HV) [58]. Once the temperature reaches 500°C; welded rails are automatically quenched with water spray [58] this is made in order to speed up the welding process to increase production rates [16],[88].

However, in order to avoid the formation of detrimental microstructures on bainitic steels; and as it was previously recommended by H.M. Smith [73], they have to be air cooled down to 200⁰C following by water quenching.

Figure 86 represents the temperature control panel of one of the B360 welds in the Schlatter; just before water quenching.

Figure 86. Fixed FBW, temperature control before water quenching

After the welding procedure, parameters such as the welding current, upset force and material displacement have a direct influence on weld consolidation [16],[89]

Table 19 and Table 20 represent a summary of the obtained current (kA), upset Force (kN) together with the selected preheat cycles, at the dissimilar quenching temperatures used: 300 and 200°C. The lower quenching temperature of 200°C versus 300°C is not expected to have any significant variations in the HAZ microstructure and hardness variation, as observed in the CCT diagram found in Chapter 2.

Table 19. Summary of parameters obtained after the welding procedure for the dissimilar PH cycles. Rails quenched at 200 °C.

PH cycles	PH Current (kA)	Maximum upset Force (kN)
3	53.7	692
6	55.2	694
6 + 3PWP	54.9	692

Table 20. Summary of parameters obtained after the welding procedure for the dissimilar PH cycles. Rails quenched at 300 °C.

PH cycles	PH Current (kA)	Maximum Upset Force (kN)
4	51.4	696
4	48.4	726
4	50.7	642
5	53.4	612
5	49.8	621
5	50.4	614
6	51.2	584
6	49.6	607
6	50.9	624

Two of the rails welded could not be repeated; 3PH and 6PH+3PWP, and were only used for examination of the rail running surface and its longitudinal-axial section. In both cases, the extruded material that holds oxides and impurities could not be stripped away.

For the case of the rail with 3PH cycles, the weld was too cold when the strippers went through, generating an impact. For the weld with the use of PWHP, the strippers could not remove the excess of material produced after the welding procedure, the cause of this is not entirely clear.

Figure 87, represents both, a weld that has been stripped automatically after the welding process, at a length of 20cm; and a weld after surface polishing, that suffer problems during the stripping process; in which excess of material is still present.
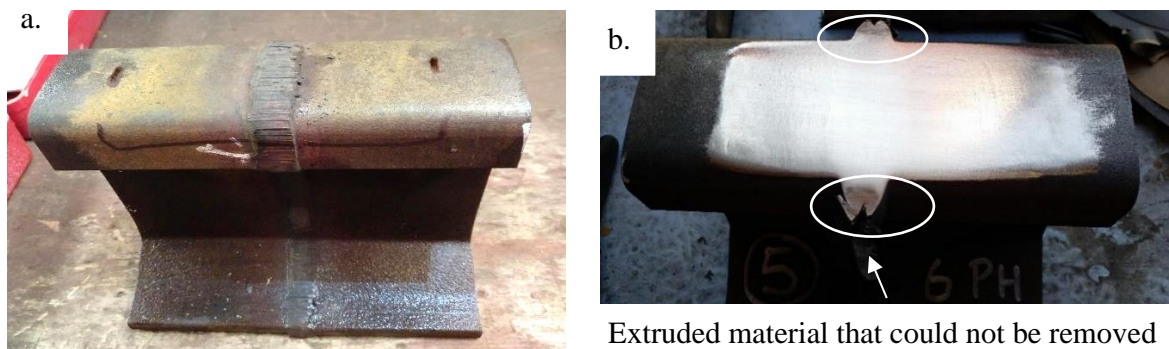

Extruded material that could not be removed

Figure 87. Section of 20 cm of a rail welded with 6PH cycles and quenched at 200ºC, a. 6PH weld quenched at 200 °C, after cutting; b. 6PH+3PWP weld quenched at 200°C, after cutting and polishing.

Whilst only changes in the number of PH cycles were made, slight variations were found within the first PH current (kA), even in the welds with the same welding programs.

The welding current will have a direct influence in the HAZ width, and the final weld upset [58],[60]. Variations on the PH current using the same welding program were previously observed within British Steel and are believed to be produced because of poor cleanliness in the rail end or copper die. This could mean that there might be slight alterations on the HAZ width even when using the same welding procedure.

Moreover, there are slight variations in the upset force (kN). The upsetting force is the force required to push the rails together before the stripping process. It has been

well established that at higher upset force, higher displacement (mm) and; therefore, more material is heated up and extruded [16].

Consequently, it is expected that a higher upsetting force (kN) will lead to a narrower visible HAZ. Therefore, the programs in which the same number of PH cycles were employed, the weld with higher upsetting force is expected to have a slight narrower visible HAZ. As observed in Table 20, the upsetting force seems to increment when lowering the number of PH cycles.

5.4. Macrographic examination.

Measurements of the visible HAZ width were made on the etched railhead, as mentioned in the experimental procedure. Table 21, represents the rail running surfaces after polishing, etching; with its corresponded HAZ width measurements.

Table 21. Railhead etched for HAZ width measurement of all the welds under analysis.

3PH (Quenched 200°C)	4PH (Quenched 300°C)

6PH (Quenched 200°C)	5PH (Quenched 300°C)

6PH+3PWP (Quenched 200°C)	6PH (Quenched 300°C)

Table 22, represents the HAZ width measurements obtained as a function of the number of PH cycles, the quenching temperature (ºC) and the upset force (kN).

Table 22. HAZ width measurements as a function of weld.

PH cycles	PWHP	Quenching T ($^{\circ}$C)	HAZ width (mm)	Upset Force (kN)
3	_	200	27	692
4	_	300	25	696
5	_	300	29	612
6	_	300	30	584
6	_	200	29	694
6	3	200	34	692

As previously mentioned, during FBW procedures, two main aspects are known to have a direct influence in the visible HAZ width; the number of preheats and the upset force (kN).

As expected, if only considering the lower number of PH cycles, a slightly narrower visible HAZ is generated. However, variations can also occur due to machine variations, as the welds were produced with a period of six months apart from each other.

As previously stated, high upsetting force (kN) generally leans to a higher forging force, meaning that more material is extruded during the stripping process, leading to narrower HAZs [16],[58]. This is evident when looking at the two welds in which 6PH were used, having a slightly narrower HAZ the one in which a higher upset force was employed.

Otherwise, adding Post Weld Heat Pulses (PWHP) seems to increase the visible HAZ width, obtaining the largest width of 34 mm, which could be an expected behaviour as the rail is being heated for a longer period of time. The author up to date found no literature about the effect of PWHP after FBW.

The narrowest visible HAZ width is of 25 mm for the FBW procedure in which 4PH cycles were used, thus is 35 mm lower when comparing with the previous "standard" weld analysed in Chapter 4, in which 8PH cycles were used.

Another aspect to take into consideration is that the visible HAZ width of the rail running surface falls between the values of 25 mm minimum and 45 mm maximum according to the standard EN14587-1:2018 [67].

Due to limited time, it was decided to do a macrographic examination of the longitudinal-axial section of only three of the welds: 3PH, 6PH and 6PH+3PWP. However, similar behaviour is expected in the other welds.

A macrograph of the longitudinal-axial section of the FBWs following etching with 2% Nital revealed the HAZ width variation across the rail, showing a typical profile of the visible HAZ of a FBWs [88],[68],[90]. Thus, displays the weld centreline and the extension of the visible HAZ, as represented in Figure 88.
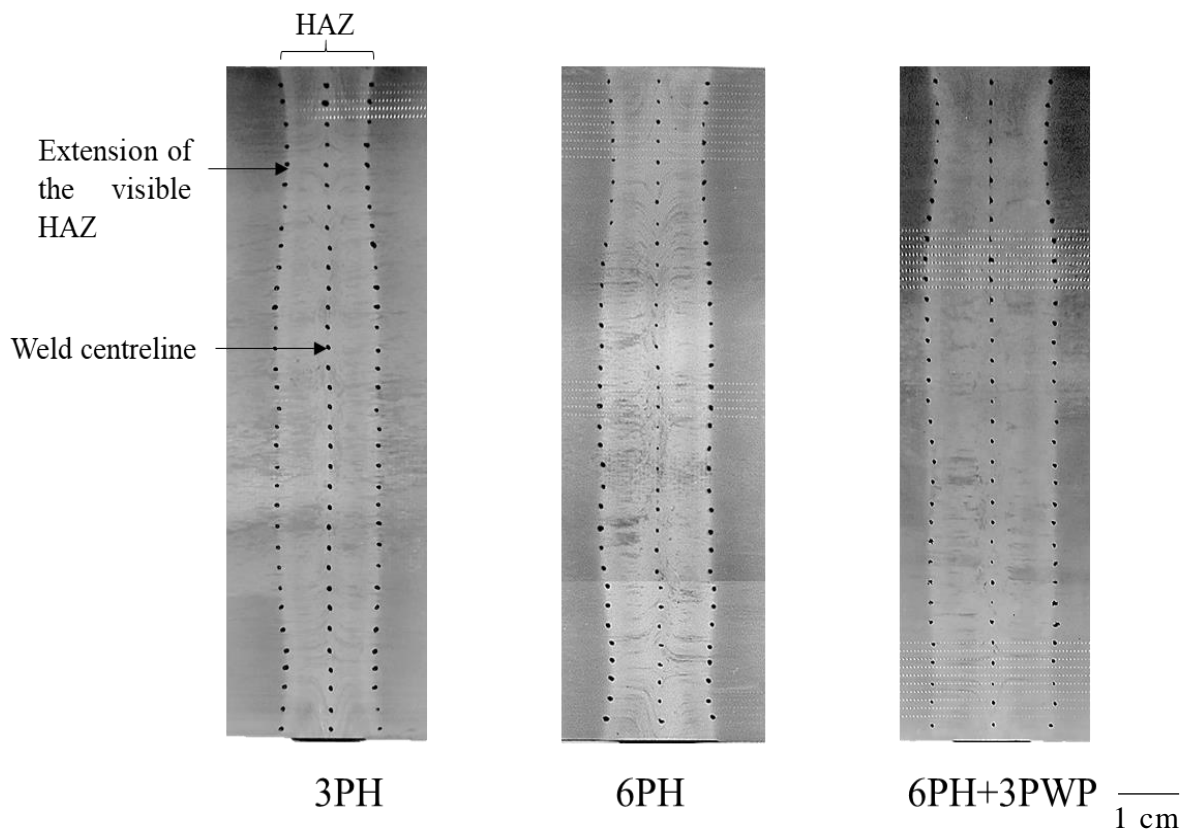

Figure 88. Macrographs of the longitudinal-axial section of three FBW: 3PH,6PH and 6PH+3PWP

No visible porosity was observed within the FZ of all the FBWs. A more in-depth macrograph of the sections reveals the flow of material near the weld FZ in Figure 89.
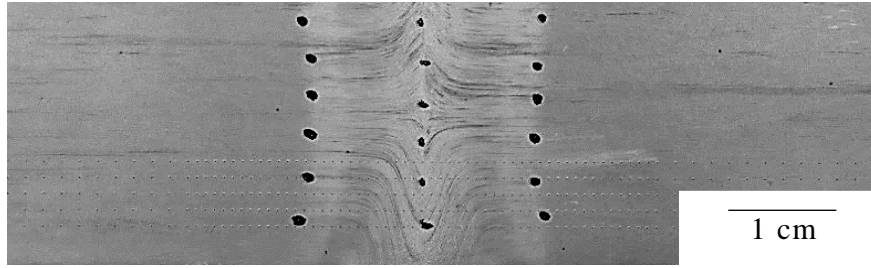
126

Figure 89. Macrograph of the longitudinal-axial section of one weld.

The previously observed macrographs, revealed a narrow HAZ in the railhead with slight broadening within the web region; similar behaviour has been found in the literature[88],[68],[16].

Figure 90; represents the measurements of the HAZ width, every 5 mm from the rail running surface up to the base foot. Observing that the overall width was narrower than even the one achieved by standard FBW procedures in pearlitic grades, which is typically in the region of ~ 40 mm [58].

As it can be observed, slight variations were found through the entire longitudinal-axial section of the HAZ, however, these alterations were within the permitted minimum to maximum variation limit of 10 mm specified in [67]. Likewise, 6PH+3PWHP was the only weld that fell between the 45 mm maximum and 25 mm minimum standard per EN 14587-1 [67]. Nevertheless, it is important to consider that this standard only covers conventional pearlitic rail steels such as R220 and R260.
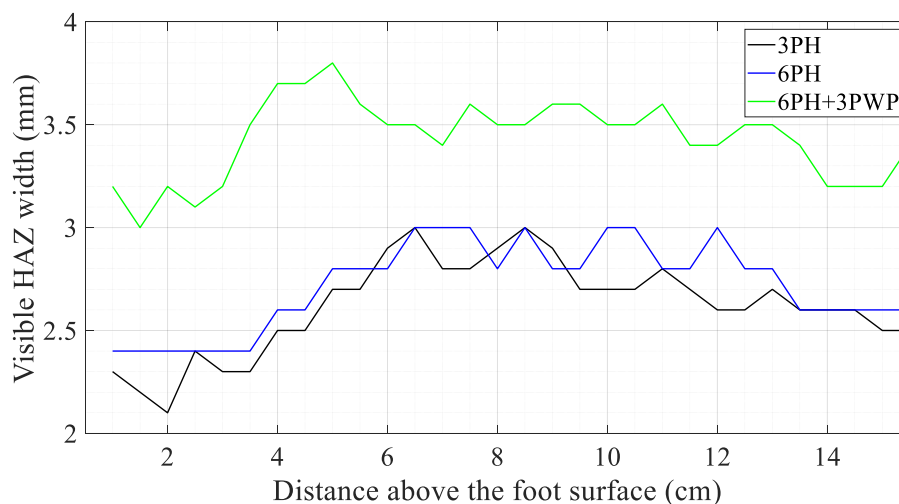

Figure 90. Variation of the HAZ width of three welds analysed.

It is also observed, that the rail web HAZ is considerably wider than in the head and foot regions; this is a typical behaviour during FBW procedures. When applying alternating electric current (AC) during FBW, the electrical current generated will be higher within the rail surface than in the interior, due to a phenomenon called "skin effect" [91]. As the web occupies a lower volume in a larger surface area; when comparing with the head and foot; the current and; by extension; heat generated, will be higher. Therefore, and according to Mansouri et al. [92], the HAZ width of the web should be wider than in the rest of the rail.

5.5.   Hardness variation

Vickers hardness measurements were made every 1 mm from the weld centreline up to 40 mm, as at that distance the hardness recovery of the SCHAZ is expected to be complete. Although, according to the specification [67], in standard welds the common load used is 30 kg, 1kg was selected to obtain a better observation of the rail hardness variation, as when using a lower load the indent space will be closer, obtaining a better resolution.

Both a hardness graph and a gradient map made the representation of the rail hardness variation; this can be observed in Figure 91- Figure 96, the dissimilar regions of a weld are also represented: Critical (C), Intercritical (IC), Subcritical (SC) and parent. The extension of the SCHAZ was considered as the region until the hardness recovery was ≥ 376 HV.

The hardness variation vs distance from the FZ observed in all the welds shows a typical profile for FBW [90],[16] ; showing the fall in hardness between the C and SC region of the HAZ and the slow recovery in hardness produced in the SCHAZ. The hardness levels achieved within the weld centreline were of around 365 HV1, slightly lower than the hardness of the parent material of 385.5 HV1. This variation is produced as during flashing, the carbon is diffused to the molten region and pushed out by the stripping tool [93]. When moving away from the FZ, maximum hardness values of ~468 HV1 on average were produced in the CHAZ region, which is situated between 5 to 11 mm from the weld FZ. A much-accentuated drop in hardness was produced within the ICHAZ until the hardness values reached were around 305.5 HV1. From the SCHAZ minima, with values around 300HV1, there was a rise in hardness until a recovery of 376HV1, this was produced at an average distance of 17.5 mm.

The profile of hardness variations produced in bainitic FBW is very similar to the one of pearlitic steels [16], however both the hardness variations and the distance in the SCHAZ is larger in bainitic steels.
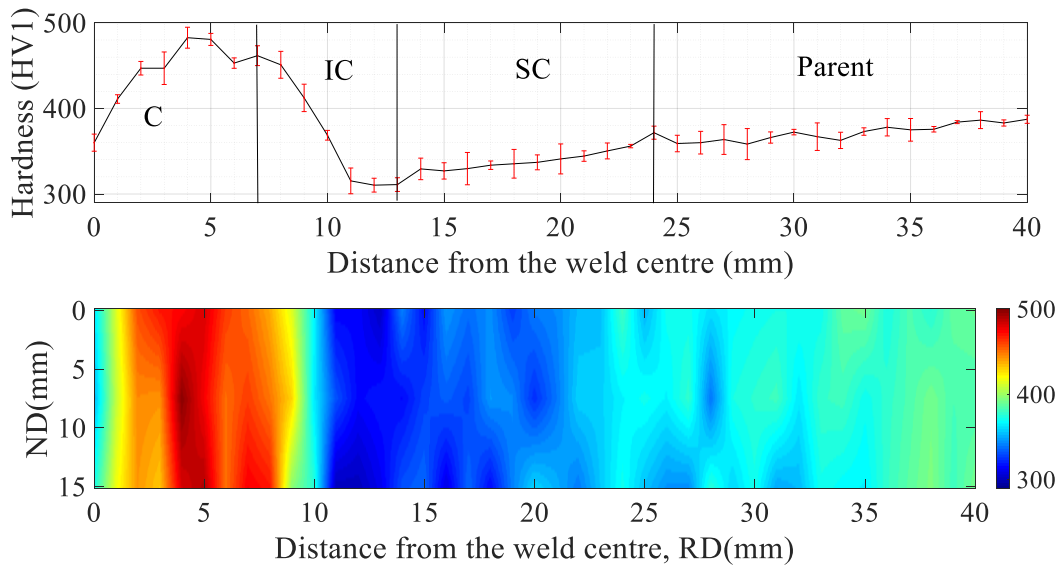
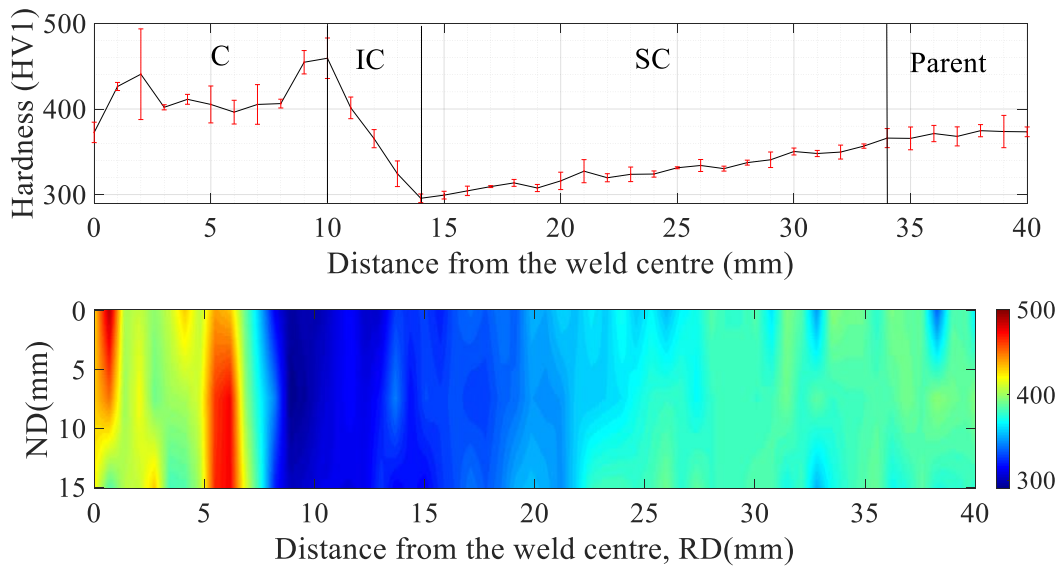**Figure 91.** Hardness variation and gradient map of weld with 3PH and quenching temperature of ~200°C

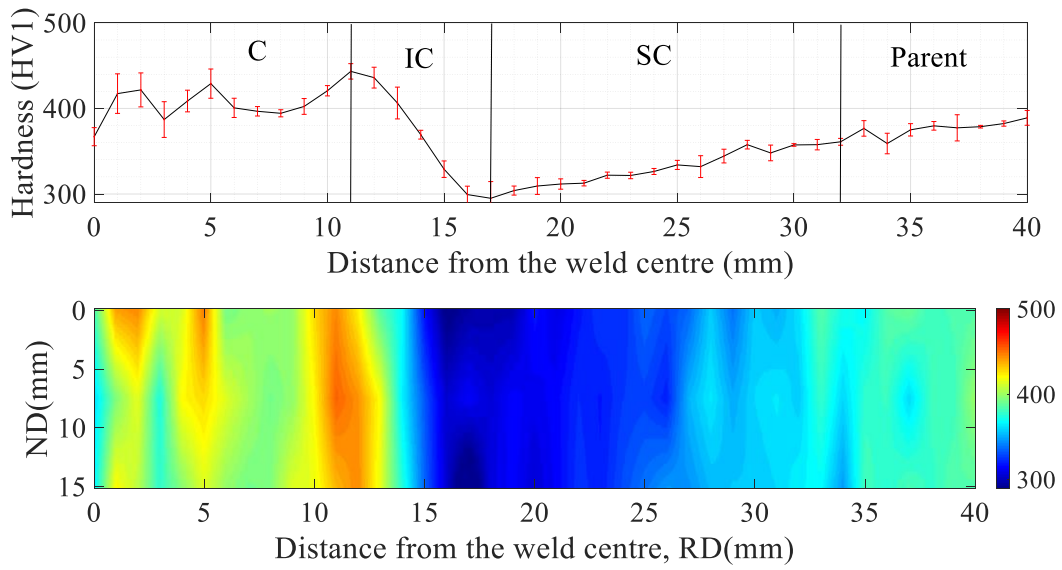**Figure 92.** Hardness variation and gradient map of weld with 6PH and quenching temperature of ~200°C

Figure 93. Hardness variation and gradient map of weld with 6PH+3PWP and quenching temperature of ~200°C

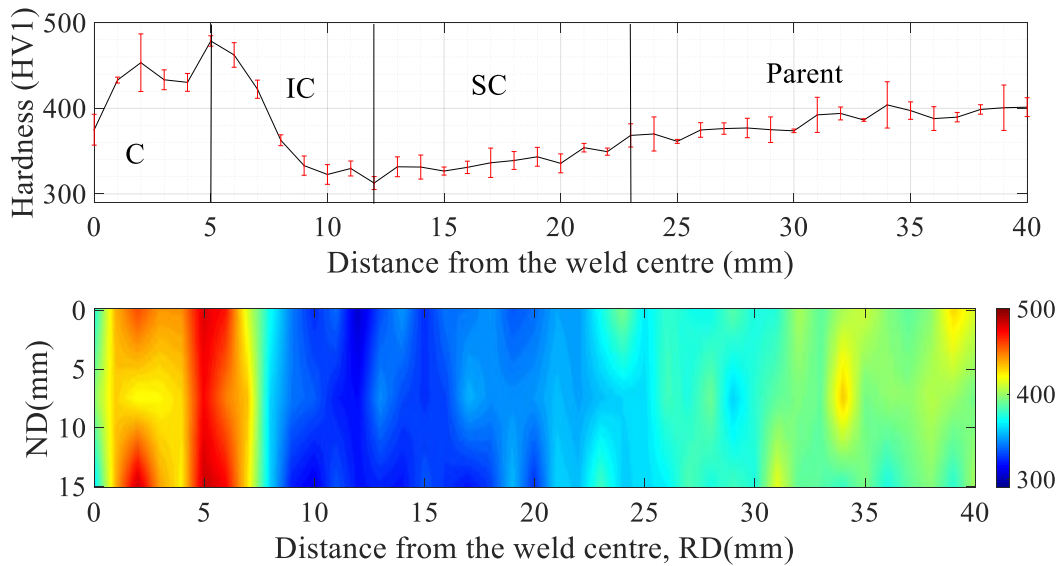**Figure 94.** Hardness variation and gradient map of weld with 4PH and quenching temperature of ~300°C

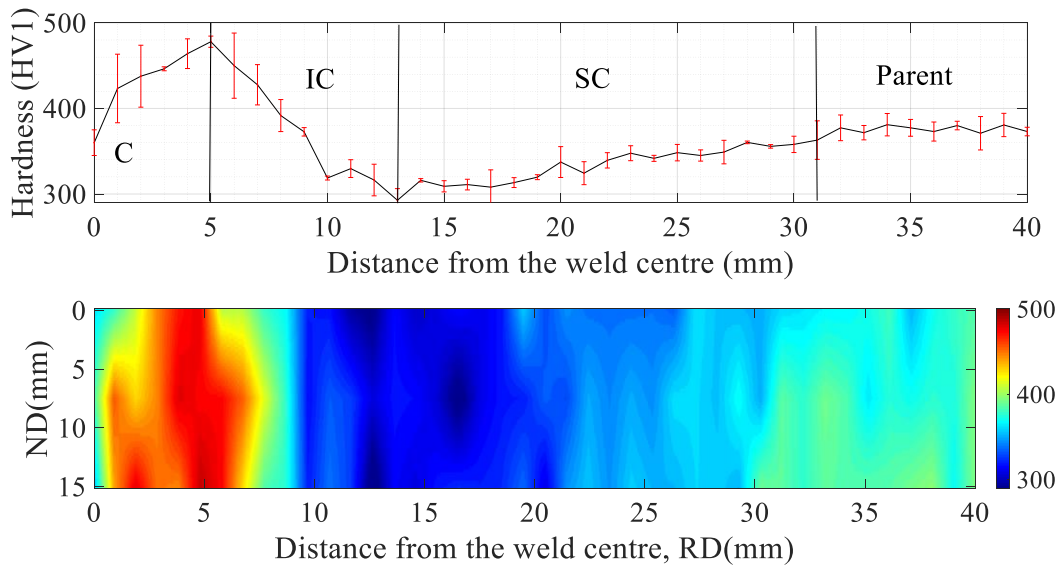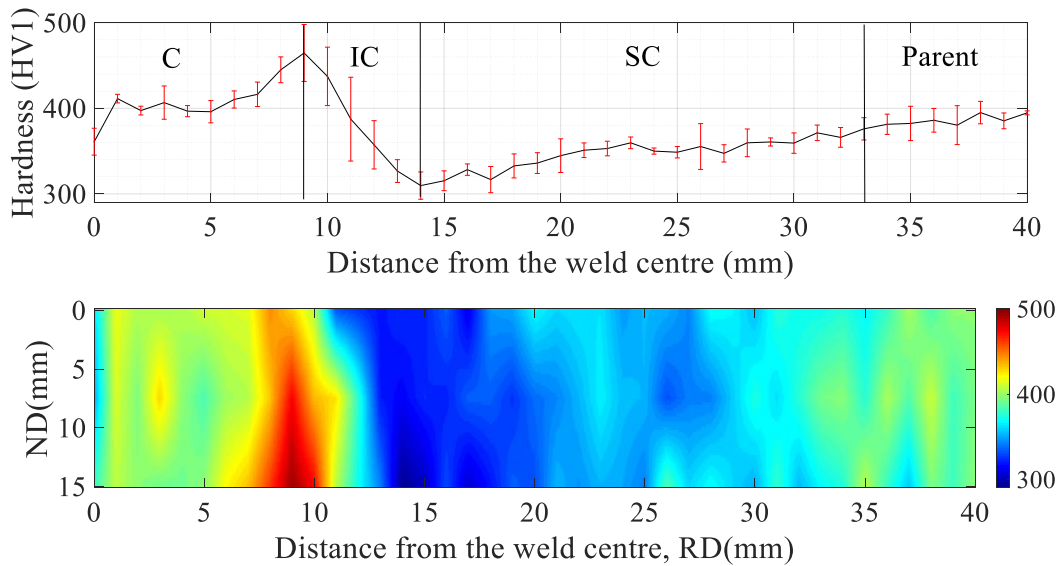**Figure 95.** Hardness variation and gradient map of weld with 5PH and quenching temperature of ~300°C

Figure 96. Hardness variation and gradient map of weld with 6PH and quenching temperature of ~300°C

Table 23 and Table 24, represent a summary of the maximum, minimum hardness values of the HAZ, together with the hardness variation in the ICHAZ and the

extension of the SCHAZ; as a function of the number of PH cycles and the quenching temperature (°C).

Table 23. Review of measurements obtained in the rail-running surface, 200°C

	3PH	6PH	6PH+3PWP
Visible HAZ width (mm)	27	30	34
Max Hardness (HV1)	482.7	459.3	443.3
Min Hardness (HV1)	310.3	295.7	299.3
Variation of hardness in the IC HAZ (HV1)	180.4	163.6	144
Extension of the SC HAZ (mm)	15	20	15
Max H – 385.5 (HV1)[*1]	97.2	73.8	57.8
Min H – 385.5 (HV1)[*2]	-75.2	-89.8	-86.2

Table 24. Review of measurements obtained in the rail-running surface,300°C.

	4PH	5PH	6PH
Visible HAZ width (mm)	25	29	29
Max Hardness (HV1)	478.7	478.2	464.7
Min Hardness (HV1)	312.7	292.7	309.7
Variation of hardness in the IC HAZ (HV1)	166.0	186	155.0
Extension of the SC HAZ (mm)	13	17	17
Max H – 385.5 (HV1)[*1]	93.2	92.7	79.2
Min H – 385.5 (HV1)[*2]	-72.8	-92.8	-75.8

*[*1] Maximum hardness value in the HAZ – Hardness of the parent rail*
*[*2] Minimum hardness value in the HAZ – Hardness of the parent rail*

As it can be observed from the data represented in the tables above, none of the welds had satisfied the standard of P+60, P-30 in which P is the hardness of the parent rail [67], which is 385.5 HV1. However, it is important to bear in mind that this is only a standard for pearlitic grades such as R260, R220 or R260Mn; as there is not current standard for bainitic grades B320 and B360.

As expected, the welds with the narrower visible HAZ have also a narrower extension of the SCHAZ, or tempered bainite region. The determined visible HAZ width is defined by the positions of the beginning of the SCHAZ zone (mm), as represented in Table 25.

Table 25. Visible HAZ width versus SCHAZ minima values from the weld centre-line

PH cycles	PWHP	Quenching T (^{0}C)	HAZ width(mm)	SCHAZ minima(mm) From weld FZ
3	_	200	27	13
4	_	300	25	12
5	_	300	29	13
6	_	300	30	14
6	_	200	29	14
6	3	200	34	17

High hardness variations are produced through all the welds, which could be detrimental and lead to preferential wear and differential plastic deformation during in track performance. The highest hardness variation appears within the narrowest HAZ weld; 4PH. Therefore, it seems to be a trade-off between the HAZ width and the hardness.

Only three variables were changed during the FBW trials: The quenching temperature, the number of PH cycles and the use of PWHP; the effect of each of the parameters selected on the hardness variation of the HAZ is discussed below.

I. Effect of quenching temperature (°C)

As previously mentioned, two dissimilar quenching temperatures were utilised, the rails were naturally air-cooled and water quench at 300 or 200 °C, however no major differences are expected. Figure 97, represents two welds made using the same welding program with 6PH cycles, but with dissimilar quenching temperatures.
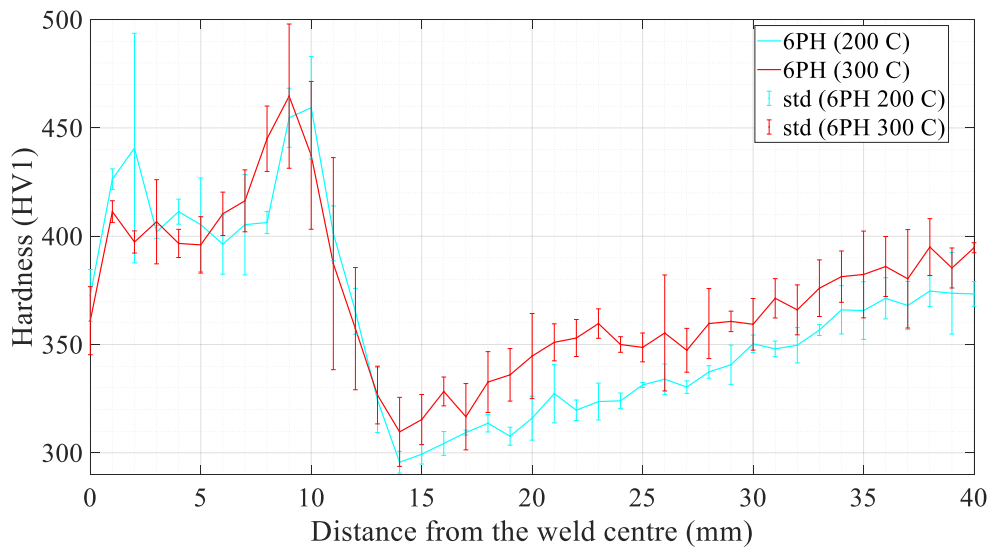

Figure 97. Hardness variation of rails welded with the same welding program (6 PH) but dissimilar quenching temperature (200°C and 300°C)

There is a variation of 5.4 HV1 on the maximum hardness of the CHAZ, and 14 HV1 in the minimum hardness of the SCHAZ. However, this variation comes with an expense of the extension of the SCHAZ, being wider in the weld quenched at 200 C.

The maximum HAZ hardness value is situated at 8 mm from the FZ in both welds, the starting point of the SCHAZ is situated at 14 mm from the weld centre-line, having both similar visible HAZ width (29-30 mm).

II.Effect of number of PH cycles

Figure 98, represents three welds with only variations on the number of PH cycles, using 4, 5 and 6 PHs at a quenching temperature of 300 °C.
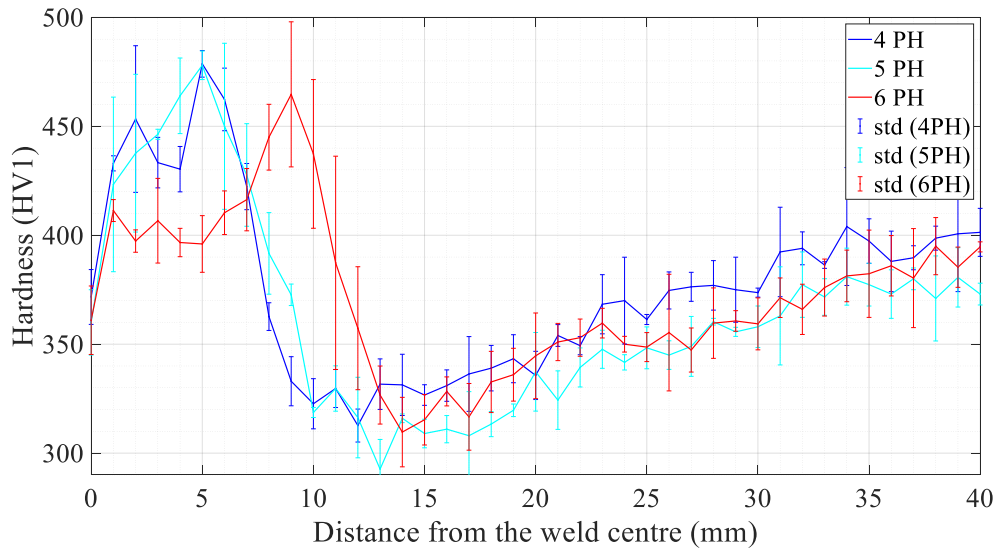

Figure 98. Effect of PH cycles on hardness variation of the HAZ. Use of 4, 5 and 6 PH, quenching at 300 °C.

Figure 99, represents two welds with only variations on the number of PH cycles, using 3 and 6 PH, at a quenching temperature of 200 °C.
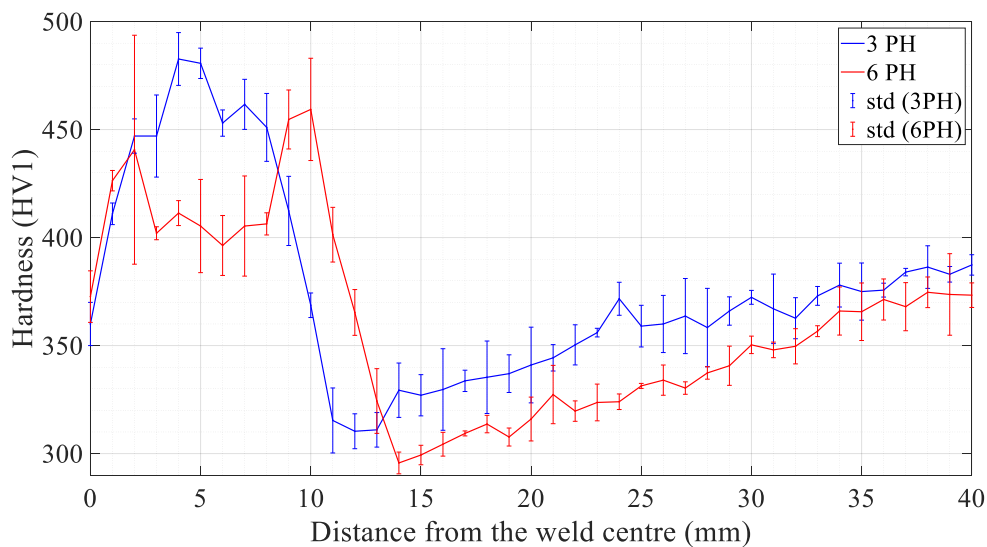

Figure 99. Effect of PH cycles on hardness variation of the HAZ. Use of 4, 5 and 6 PH, quenching at 200 °C

As expected, lowering the number of PH cycles has led to a narrower extension of both; the visible HAZ (covering the CHAZ and ICHAZ); and the tempered SCHAZ. The shorter welding time, will limit the extension of tempering, even with 1PH of difference. The highest difference between the SCHAZ extension is found between the welds quenched at 300°C; 4PH and 6PH; with a variation of 7 mm. The same behaviour was found on the rails quenched at 200 °C; the width of the SCHAZ is narrower with 3PH cycles (16 mm) than with 6PH cycles (20 mm).

However, as observed in the figures above, this narrower HAZ comes with a more accentuated difference between both the maximum and minimum hardness levels of the weld; as the cooling rate of the rails in which lower current was applied will be faster. Obtaining a difference of even 18.7HV1 between the narrowest and wider HAZ. This was not the case with the weld in which 5PH were used.

III. Influence of the use of PWHP

Adding PWHP resulted in a steady hardness distribution across the HAZ, satisfying even the maximum hardness of P+60, with hardness up to 443.3HV1, 26HV1 lower than welds with 6PH cycles but none PWHP.

Figure 100, highlights the hardness variation of three welds in which the same welding program was used (with 6 PH cycles), PWHP were added in one of the rails.
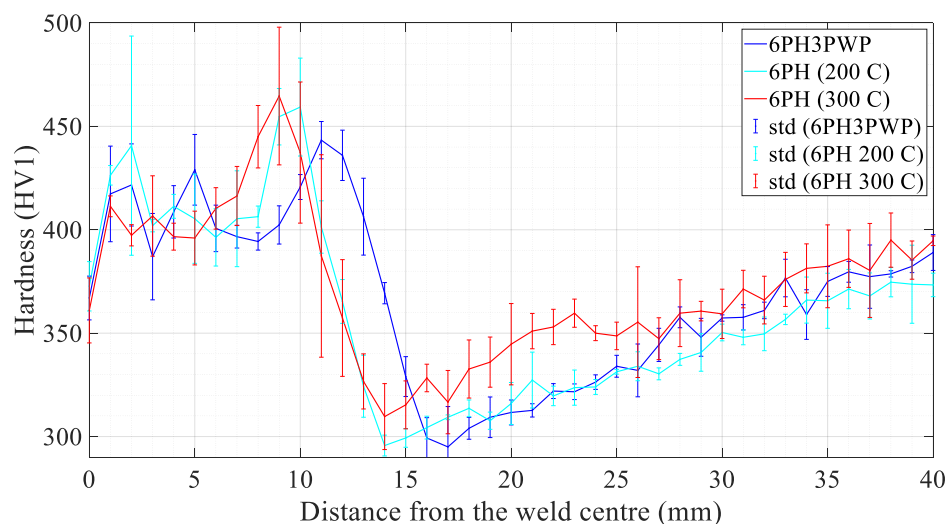

Figure 100. Effect of PWHP on hardness variation of the HAZ. Use of 6 and 6+3PWP, quenching at 200 °C.

In this case, and in opposition from expectation, there is not a trade-off between the reduction of the CHAZ maximum hardness and the extension of the SCHAZ; having even slight narrower SCHAZ than the other welds in which PWHP was not performed. Moreover, it seems to be a difference in the extension of the CHAZ; covering a wider region; and therefore, an extended visible HAZ. Up to date, the author has not found any work related to adding PWHP after the FBW procedure.

IV. Hardness variation of the rails longitudinal-axial section

Vickers hardness measurements were obtained from the longitudinal-axial section of the head, web and foot regions of the HAZ of three of the welds: 3PH, 6PH and 6PH+3PWP, quenched at 200°C. Summary of the data obtained is observed in Table 26, representing the maximum, minimum hardness values of the HAZ, together with the visible HAZ width (mm) and the extension of the SCHAZ (mm).

Table 26. Hardness values from the head, web and foot of three rails under analysis.

PHs	Region	Extension C+ICHAZ (mm)	Max Hardness (HV1)	Min Hardness (HV1)	IC HAZ Variation (HV1)	SC HAZ extension (mm)
	Head	14	483.8	296.8	187	23
3	Web	17	458.8	281.0	177.8	-
	Foot	15	477.8	295.3	182.5	25
	Head	14	455.8	289.2	166.6	33
6	Web	16	445.6	297.1	148.5	-
	Foot	15	452.4	292.8	159.6	37
	Head	17	449.7	299.5	150.2	31
6+3PWP	Web	20	390.3	291.3	99	-
	Foot	18	437.2	279.8	157.4	36

Similar behaviour was found in the welds running surface and 5 mm below its longitudinal-axial section; with slight differences in terms of SCHAZ extension; being wider in the longitudinal-axial section than in the running surface. A non-uniform hardness distribution across the rail longitudinal-axial section is observed; having slightly higher hardness values in the head and foot than in the rail web, Figure 101 displays the maximum hardness variation within the CHAZ as a function of the distance from the rail head, showing a minimun hardness in the web in comparison with the head and foot.
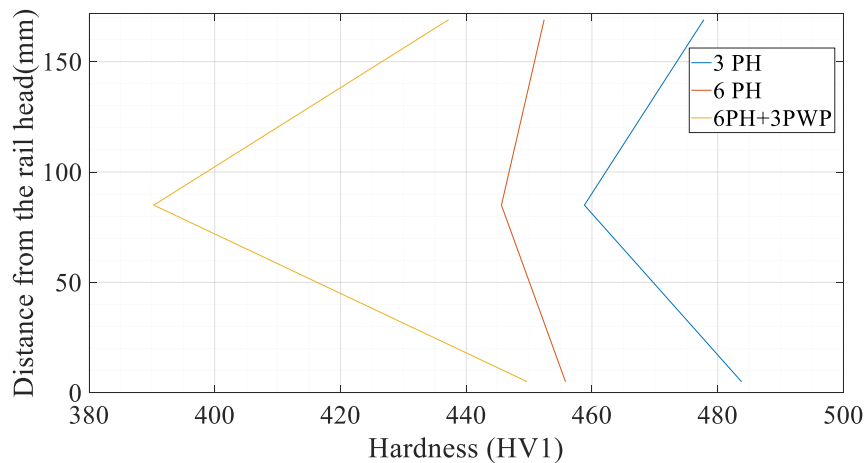

Figure 101. Max. hardness (HV1) as a function of rail head distance (mm).

As previously mentioned, the amount of heat generated in the web is superior than in the head and foot regions, therefore, it is expected that its cooling rate will be lower and, consequently, higher hardness values are usually found on the web after FBW procedures [92],[16]. However, when comparing the rail web hardness at 80 mm from the weld FZ (~350HV1) to the one of the head and foot (~380HV1) a slight decrement can be observed; an explanation of this behaviour could be related to the parent rail web having slightly lower hardness.

H.M. Smith studied the microstructure on the rail web of B360 grades [80], finding highly segregated areas with martensitic and upper bainitic microstructures, which led to a much higher hardness in the web (480 HV1) than in the head and foot; which does not relate with the aforementioned behaviour. Therefore, a further microstructural characterisation on the rail web HAZ of B360 rails seems necessary. Table 27 displays hardness variation and gradient maps of the three rails under analysis; 3PH, 6PH and 6PH+3PWP.

Table 27. Hardness variation in the rail longitudinal-axial section
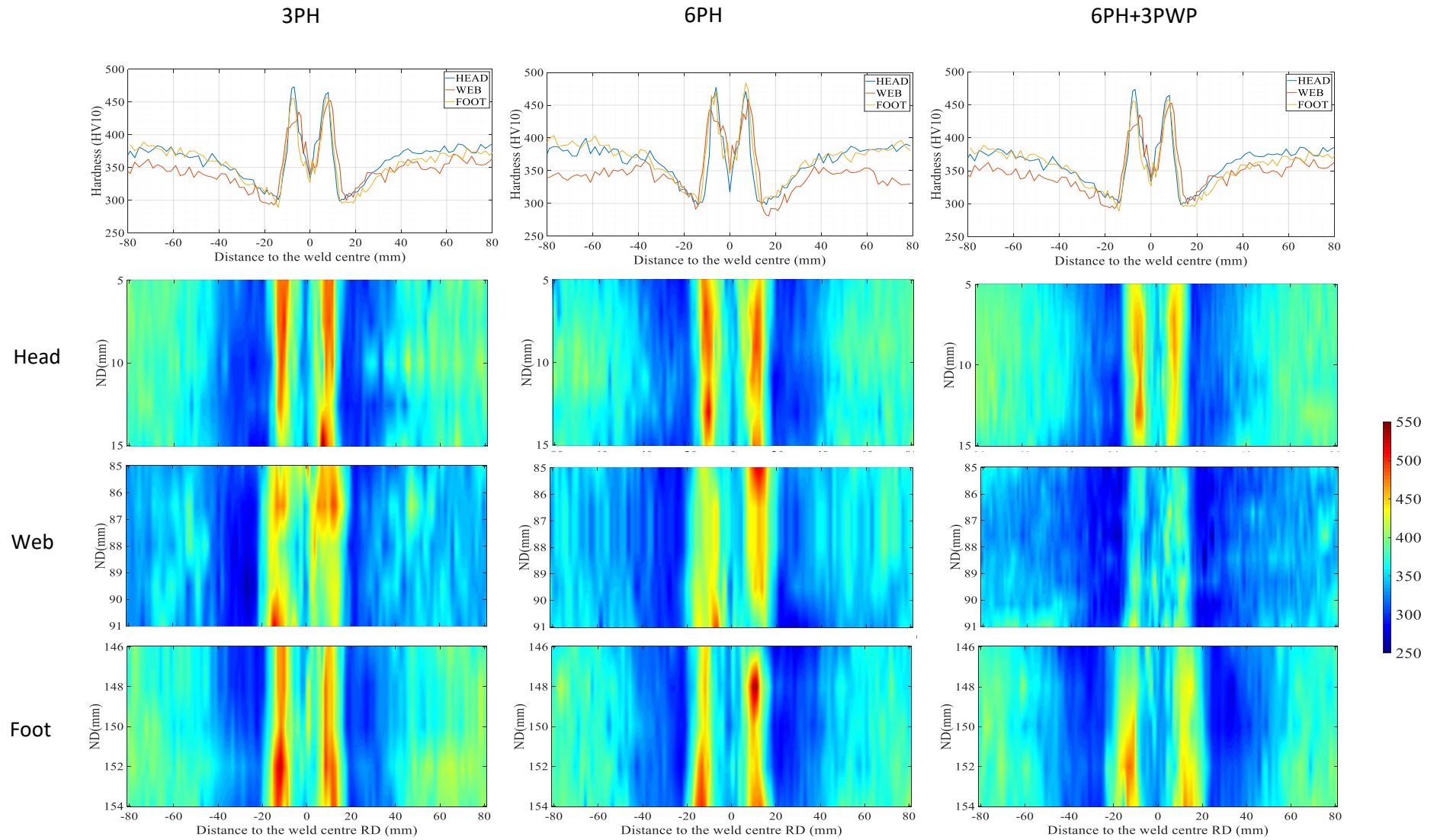
5.6.   Metallographic examination

The hardness variation produced in pearlitic FBW can be easily understood by variations in the interlamellar spacing, as a reduction of the pearlite interlamellar space will increase the rail hardness, however this is not as simple in bainitic steels as a much more complicated microstructural evolution is found during welding.

A metallographic examination was made in all the welds at 5 mm below the rail running surface. Table 28 and Table 29, represent a microstructural examination of the welds at dissimilar distances from the weld centreline, corresponding with the C, IC and SC HAZ regions. The micrographs showcase a typical microstructure of a B360 FBW, which was more extensively discussed in Chapter 4.

Very similar microstructures were found through all the welds under examination. Slight differences are observed when comparing the CHAZ of 4PH weld in which the highest hardness levels were achieved (478.7 HV1) with the 6PH3PWP weld, in which lower maximum hardness were reached (443.3 HV1). Figure 102, represents an optical micrograph of both. In the represented, martensite appears as the white phase, surrounded by darker bainitic ferrite regions.
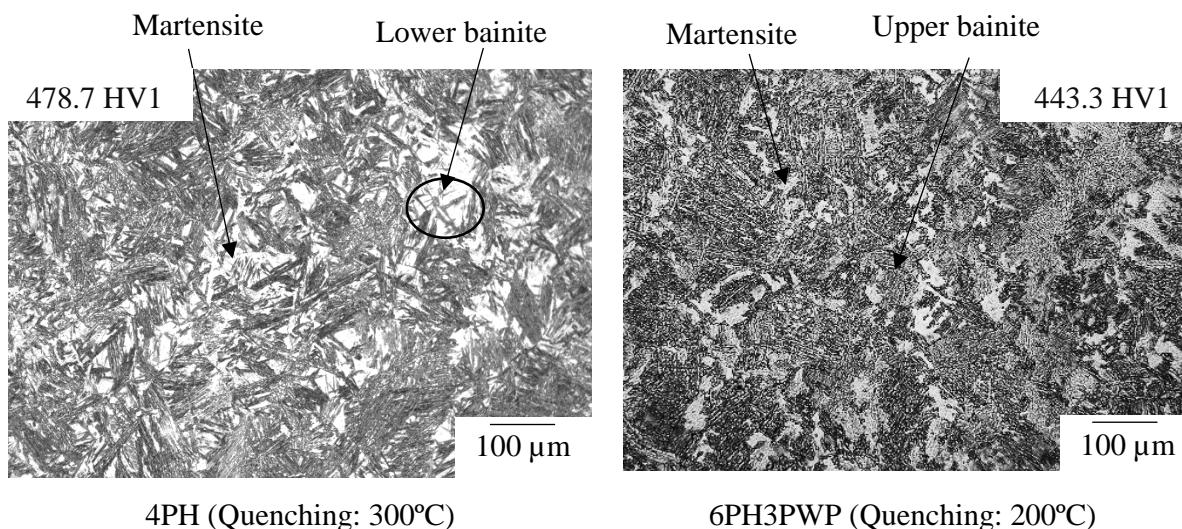

4PH (Quenching: 300ºC)   6PH3PWP (Quenching: 200ºC)

Figure 102. Light micrographs from the CHAZ of two welds: 4PH and 6PH; with its corresponded hardness (HV1).

After upsetting, in the CHAZ, temperatures around the melting point of the steels are reached, leading to a complete reaustenitisation of the steel. As the cooling rates

achieved within the CHAZ are high, it is difficult for the carbon atoms to diffuse, which leads to the formation of harder, low temperature transformation products; upper, lower bainite and martensite. As observed, higher amount of martensite and lower bainite are presented in the 4PH weld, whilst a more upper bainitic microstructure with some martensitic regions can be distinguished in the 6PH3PWP weld. The lower number of PH, together with the slow cooling rates expected on the weld in which PWHP were applied, could be an explanation for these variations.

In the ICHAZ (398.7 HV1), just partial reaustenitisation of the steel is expected, with temperatures between A1 and A3 [94], resulting in limiting growth of austenite and a very fine grained microstructure [92]. Figure 103, represents a light micrograph of a typical microstructure of the ICHAZ of B360 steels. Displaying a combination of AF, martensite, lower and upper bainite. Whilst upper bainite and martensite produce an increment in the steel hardness; softer needle-like acicular ferrite regions are known to increase the steel toughness [95]. Those, generally nucleate in non-metallic inclusions such as MnS [95],[96].
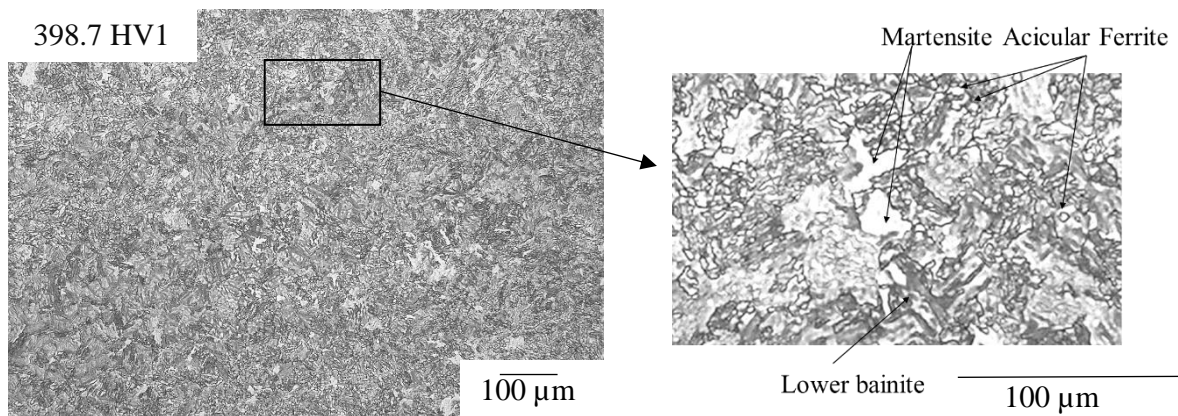

Figure 103. Light micrographs of the ICHAZ of 6PH weld, quenched at 200ºC, with its corresponded hardness (HV1).

Presence of MnS was observed mainly in the IC and SC regions of the HAZ. Evident segregation was found near MnS inclusions in the tempered HAZ region of the 6PH weld as in Figure 104.

Heavily tempered microstructures were found within the SCHAZ region, in which a drop of RA regions is produced, leading to coarsening of carbides, which could have a detrimental effect in terms of the rail mechanical properties, further information can be found in Chapter 4. Figure 105, shows a bright field TEM image of the very intense precipitation present on the SCHAZ of B360 grades.
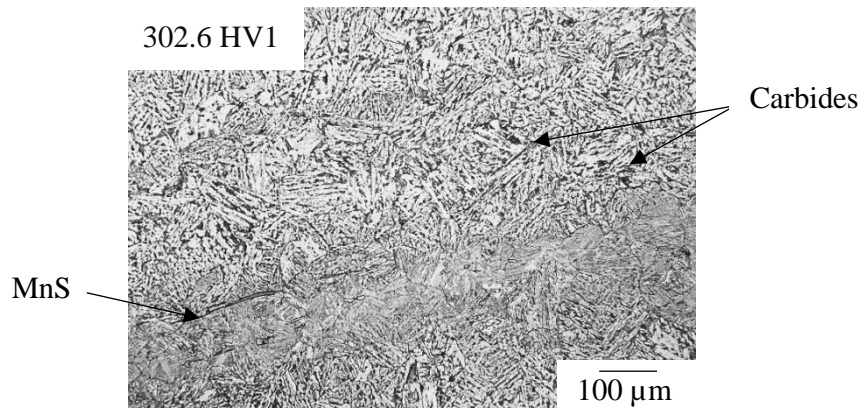
142

Figure 104. MnS inclusion in tempered HAZ region, with its corresponded hardness.
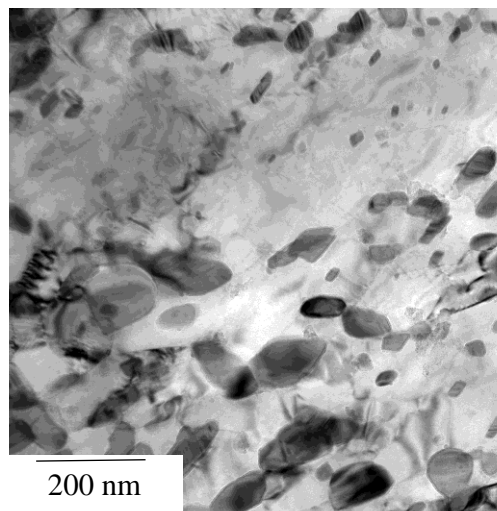

Figure 105. TEM Bright field image showing the intense carbide precipitation in the SCHAZ of a B360 FBW.

The main difference observed in the OM of the welds will be the extension of the SCHAZ; which seems to be narrower in the weld in which 4PH cycles were utilised, being of 13 mm, whilst when using 6PH the SCHAZ extension was of 21 mm. However, in the CHAZ of the 4PH weld, higher hardness values were reached in comparison with the other welds analysed.

Table 28. Light micrographs of selected regions of the HAZ, as a function of the number of PH cycles. Quenched at 200°C.
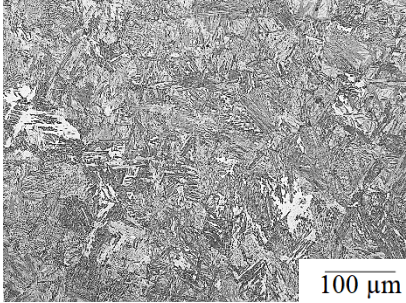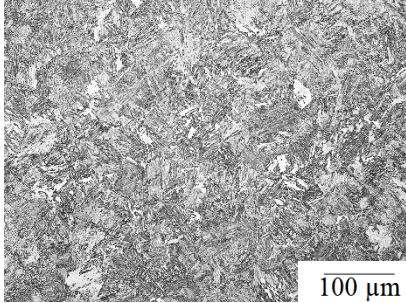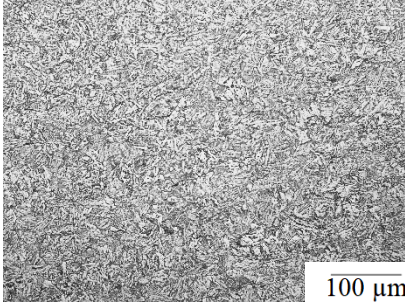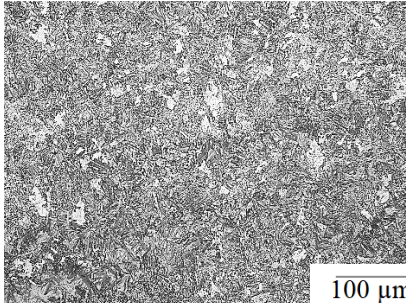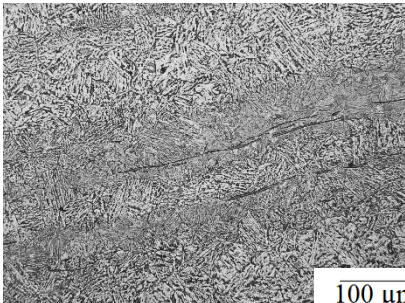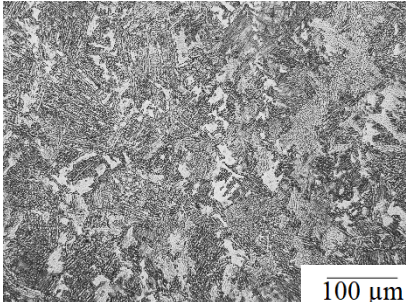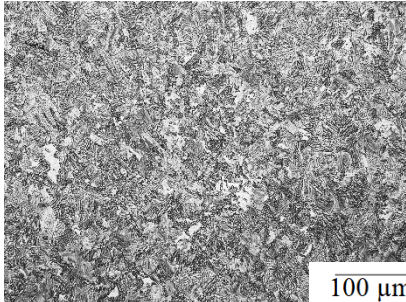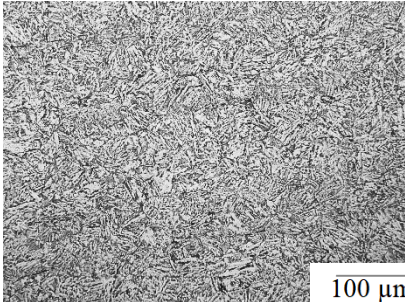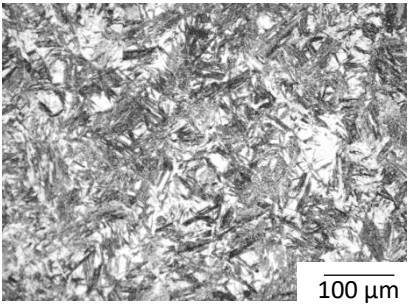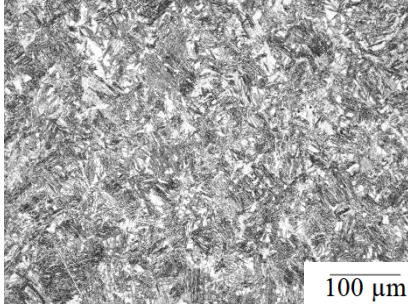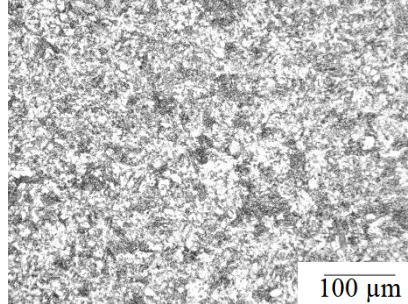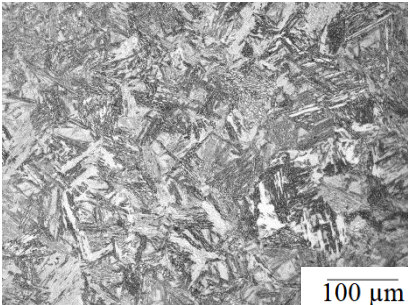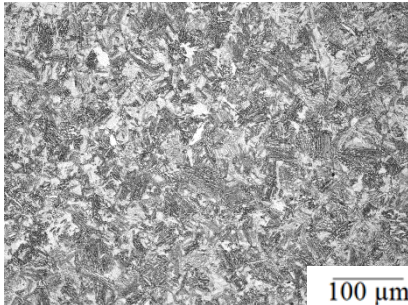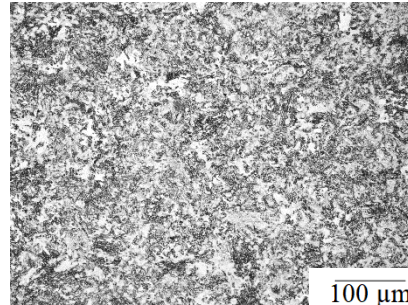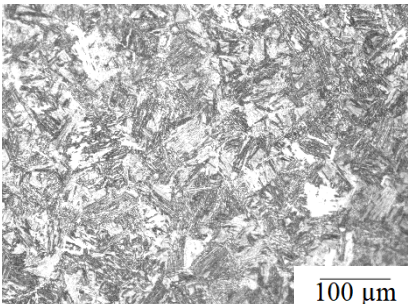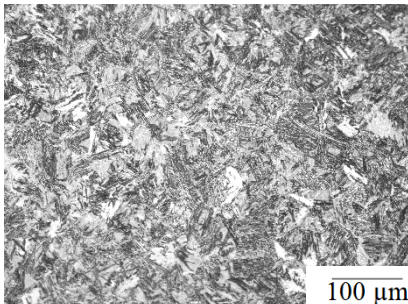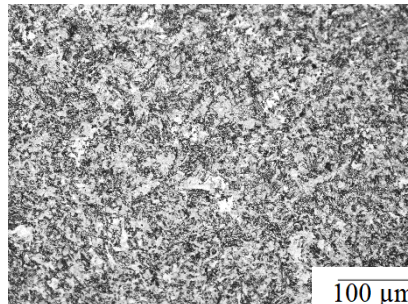
Weld	Critical		Intercritical	Subcritical
3PH				
6PH				
6PH+3PWP				

Table 29. Light micrographs of selected regions of the HAZ, as a function of the number of PH cycles. For welds quenched at 300°C.
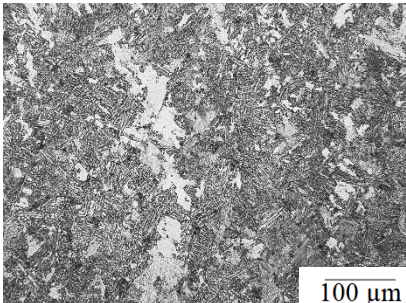
Weld	Critical	Intercritical	Subcritical
4PH			
5PH			
6PH			

5.7. Three-Point bend tests

Three welds and a conventional B360 grade rail were tested at the three-point bending machine in British Steel, Scunthorpe. The three welded rails tested were: 4PH, 5PH and 6PH, quenched at 300°C.

An "as rolled" B360 60E2 rail was also tested on the three-point bend tester. The test was performed until it reached a load of 2113.42 kN, and an examination of the deflection performance was made at 1677.45 kN and 1845.33 kN.

The welded rails analysed were tested until complete breakage, although, usually after production they are tested until they satisfied the minimum deflection of 1500 kN for 60E1 and 60E2 grades, as specified in EN14587-1:2018 [67]. Figure 106 represents the load versus time traces on one of the rails tested (4PH). The other load vs displacement curves can be observed in the appendix.
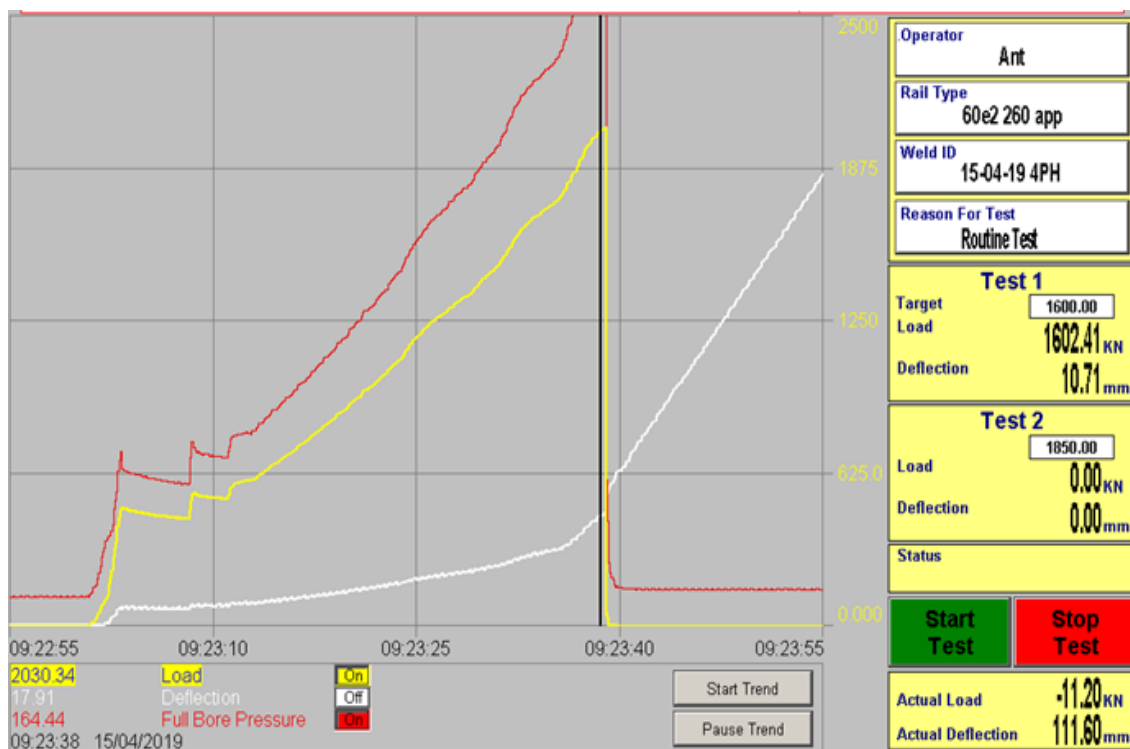
Figure 106. Load versus time trace of three-point bend tests.

Table 30 shows a summary of all the parameters obtained after the three-point bend test in terms of load and deflection. As observed, all the rails tested satisfied the minimum bend load criterion of 1600 MPa for 60E1 and 60E2 rails, as stated in

EN14587-1:2018 [67]; but none of the welded rails achieved the minimum deflection of 20 mm.

Table 30. Load and deflection values obtained after the 3-point bend test, on rails welded with 4PH, 5PH, 6PH and a conventional B360 rail not welded.

Welded B360 rail	Load (kN)	Deflection (mm)
4 PH	2030.34	17.91
5 PH	1608.70	11.12
6 PH	1684.02	11.52
As Rolled rail	**Load (kN)**	**Deflection (mm)**
	1677.45	10.30
B360 60E2	1845.33	12.64
	2113.42	20.15

Table 31, represents the minimum bend test requirements for 60E2 rails. As it is observed, these requirements are specific for pearlitic grades, there is not a specific standard for bainitic steels.

Table 31. Minimum bend tests requirements according to European standard EN14587-1:2018 [67]

Rail Profile	Minimum bend test deflection (mm)		Minimum bend test force (kN) for approval and production	
	R220, R260 and R260Mn grade	R350HT grade	R220 grade	R260, R260Mn and R350HT grade
60E1			1 500	1 600
60E2	20	20		
56E1			1 230	1 330
55E1			1 200	1 300

The minimum deflection of 20 mm was achieved by the "as rolled" B360 60E2 only after reaching a load higher than 2000 kN. However, when testing the load and deflection requirements in conventional rails, the three-point bend test automatically stops at 1600 kN [58],[67], therefore, ideally, the minimum deflection has to be

reached before the minimum required load or lower, which doesn't seem to be produced in the case of bainitic grades. The usual deflection in pearlitic grades at 1600 kN is usually of 26-40 mm [60].

According to the Hall-Petch relationship, pearlite yield strength (YS) is a function of the interlamellar spacing [97], however, bainite microstructure has very fine ferritic laths surrounded by retained austenitic regions in a nano-metric scale, thus will confer even higher YS than the ones achieved in conventional pearlitic rails [98]. Therefore, bainitic grades might not go through the plastic region before failure as pearlitic do; leading to lower deflection rates.

Figure 107, represents the influence of lower deflection rates on the three-point bend tested as rolled B360 grade, after a load of 2113.42 kN was applied.
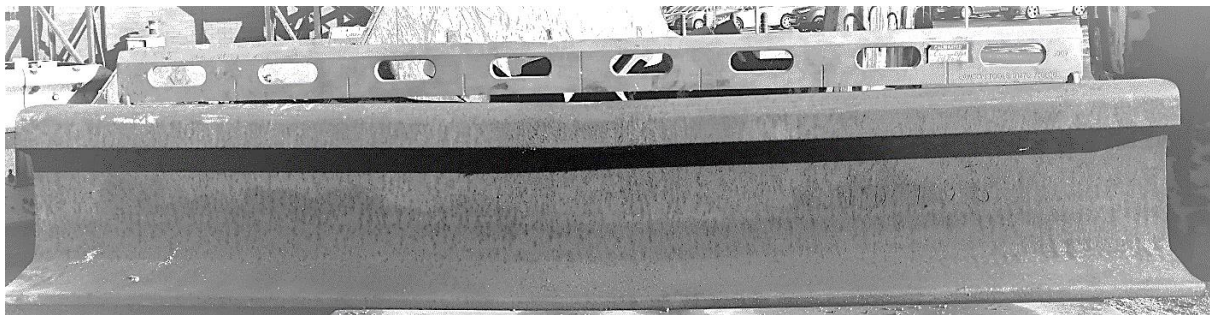
Figure 107. "As rolled" B360 after three-point bend testing.

Similar concerns have also been previously raised within British Steel when studying harder pearlitic rail grades such as 350LHT [99]. The very fine interlamellar spacing of 350HT grades confers higher YS than R260 grades. Whilst doing the examination of welded HT rails, it was found that the deflection achieved after a load of 1600 kN was of 14.7 mm [99].

Nonetheless, according to P.Secordel and H.M.Smith [73] the 20 mm minimum deflection criterion for pearlitic steels was likely to be chosen due to historical data of pearlitic FBWs rather than due to any track criteria, as achieving the minimum test force is more critical. It is also important to consider that the minimum bend load criterions shown in Table 31, are not likely to be experienced in service by rail welds.

I. Fracture surface examination.

Table 32 shows the fracture surface of the three welds after three-point bend testing, showing the path of the fracture surface which seems to run in a vertical orientation towards the weld fusion line in the three cases; which could be produced due to the welds being too cool due to the lower number of PH cycles. Similar behaviour was found in the previous attempts made on CFBs.

Table 32. Fracture surface of the three rails tested after three-point bend tests.
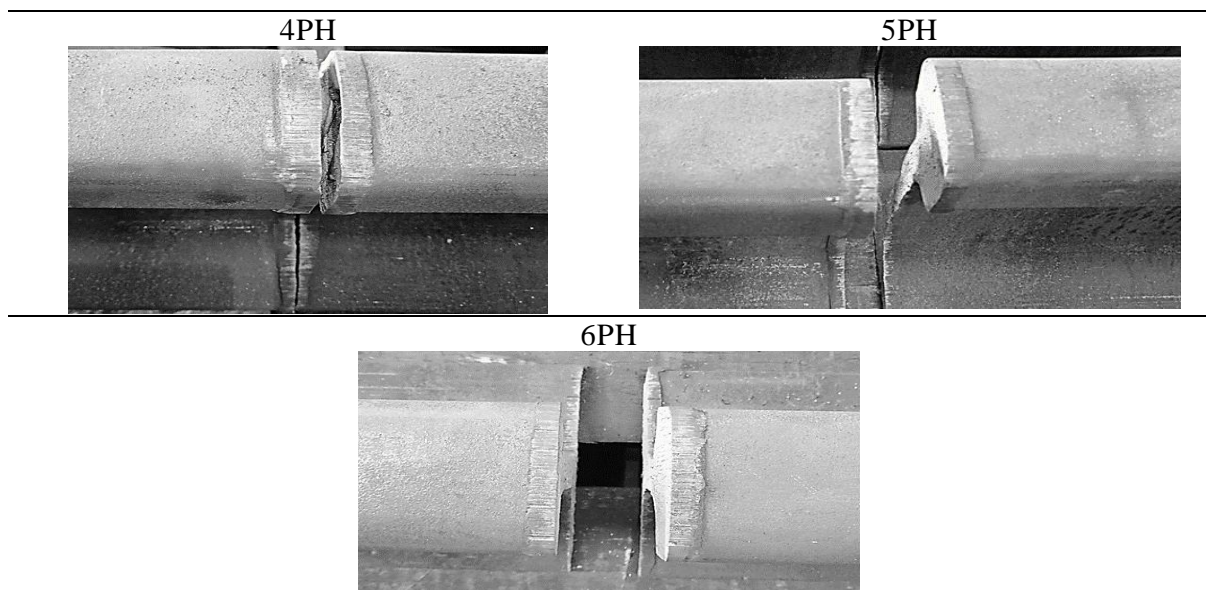
A more in detail examination of the rail welds fracture surface can be observed in Table 33. It can be observed, that the fracture surface of the welds with 5 and 6 PH have a fully brittle microstructure. This could be due to the weld being cooler due the lower number of preheats. In the 4PH sample the only area that looked like it might be slightly less brittle was the feature in the head, observed more in detail in Figure 108. A higher amount of ferrite or RA there might be the cause for the more ductile fracture.

Figure 108. Photograph of the fracture surface after 3-point bend testing of the FBW rail with 4PH.

149

Table 33. Fracture surfaces of the weld joints after three-point bend testing.

Number of PHs	Fracture surfaces
4	
5	
6	

5.8. Measurement of residual stresses after welding

Rail residual stresses will change during FBW procedures in the weld region, when comparing with the ones of the parent rail; thus, will have a direct influence on RCF resistance. In addition, the residual stress distribution in the parent rail will vary from the one of the HAZ.

The residual stresses were measured in three of the rails: 4PH, 5PH and 6PH, by strain measurement after saw cutting as described in the experimental procedure. The obtained strain data was converted into residual stress by multiplying by the steel Young Modulus; 207 GPa [27]. Table 34, represents the longitudinal and transversal residual stresses of the three welds under study.

Table 34. Longitudinal and transversal residual stresses (MPa) of 4PH, 5PH and 6PH welds, measured with strain gauges by sectioning.

Weld	Position	Longitudinal Residual Stress	Transverse Residual Stress
4PH	Head	-70	49
	Foot	-76	114
	Web1	-125	Gauge failed
	Web2	167	46
5PH	Head	-55	71
	Foot	-37	88
	Web1	-82	115
	Web2	-30	156
6PH	Head	-44	34
	Foot	-22	-70
	Web1	-77	100
	Web2	-11	111

A more in detail representation of the vertical and transverse residual stresses measured as a function of the distance from the rail head (mm) can be observed in Table 35

As observed, whilst longitudinal residual stresses seem to be compressive, transversal stresses are more tensile.

Those represent a typical behaviour of FBW procedures, being more compressive in the head and foot and more tensile within the web region.

Longitudinal residual stresses seem to be more compressive with narrower HAZ welds, as represented in Figure 109. When reducing the PHs number, the rail temperatures will be lower, leading to a higher cooling rate which will increase the number of contractions within the material, leading to lower residual stress values. For this analysis, the rail head was selected as it is where the RCF cracks are found on B360 steels when in track
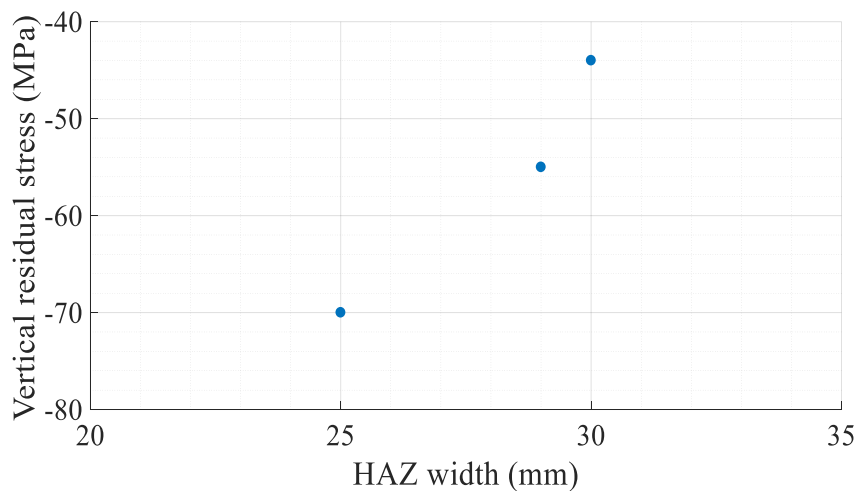
Figure 109. HAZ width versus variation in vertical residual stresses (MPa).

In addition, variations were found in the measurements of the right and left regions of the web. The major imbalance was found in the longitudinal residual stress on the 4-pre-heat weld with one side being compressive and the other highly tensile in the middle of the web; this might be an influence of variations during the rolling straightening procedure.

Table 35. Residual stress measurements; rails 4PH, 5PH and 6PH

Longitudinal residual stress
Left web
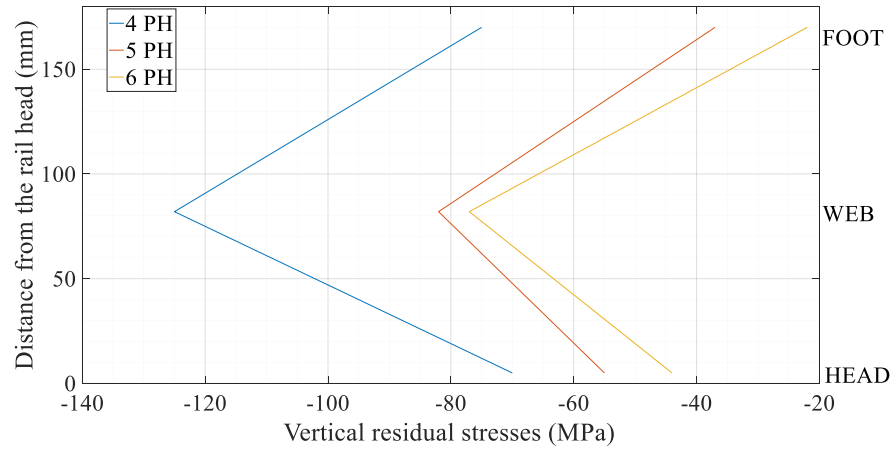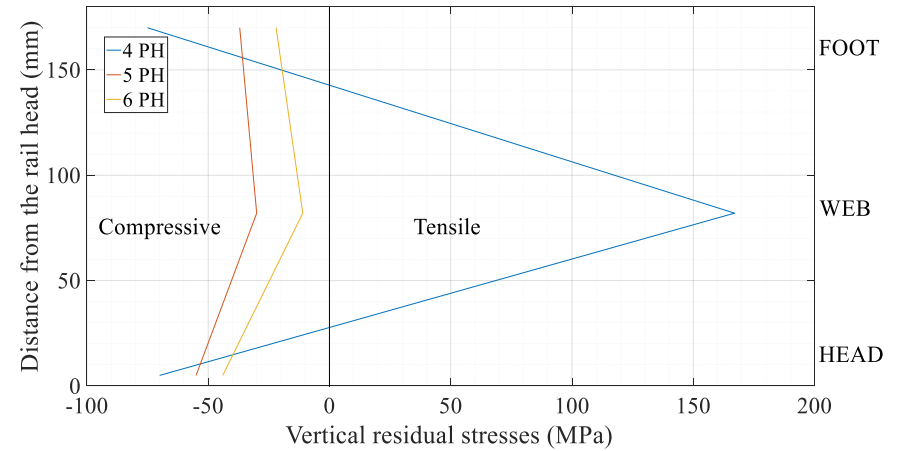
Right web

Transverse residual stress
Left web
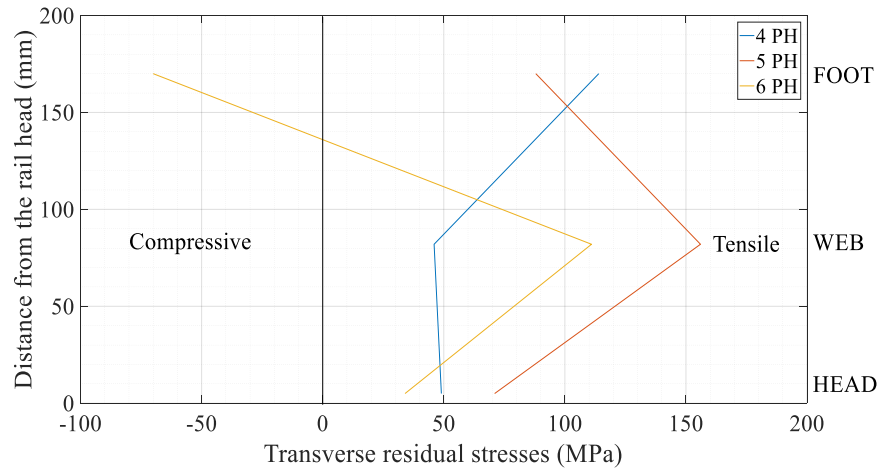
Right web
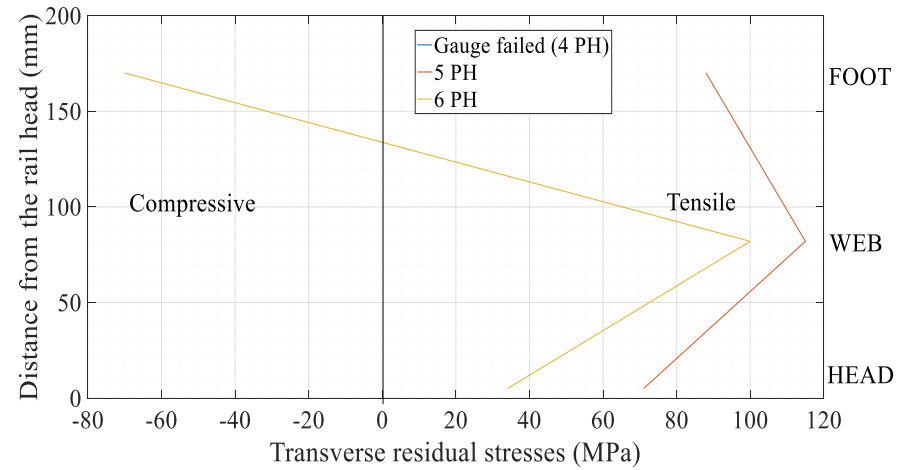
5.9.   Discussion of results

On this chapter, an analysis of the influence of the number of PH cycles and quenching temperature on the mechanical properties of B360 welds was performed. The aim was to reduce the existing wide HAZ of CFB B360, reducing the number of PH cycles in order to produce cooler, and therefore, narrower welds. A comparison between these trials, and the ones previously performed by British Steel, is described below.

I. Narrow HAZ program

Problems were encountered in two of the welds analysed: 3PH and 6PH+3PWP. After the welding procedure, the strippers could not pass by and remove the extruded excess of material filled with oxides and impurities. In the case of 3PH, not enough heat was achieved for a proper consolidation of the weld. Even though the weld with PWP showed issues, it should have no problems with the strippers, therefore, a repetition of this weld is recommended.

As expected, in the aforementioned trials made in the Schlatter welder, lowering the number of PH cycles has led to a narrower HAZ, as represented in Figure 110.
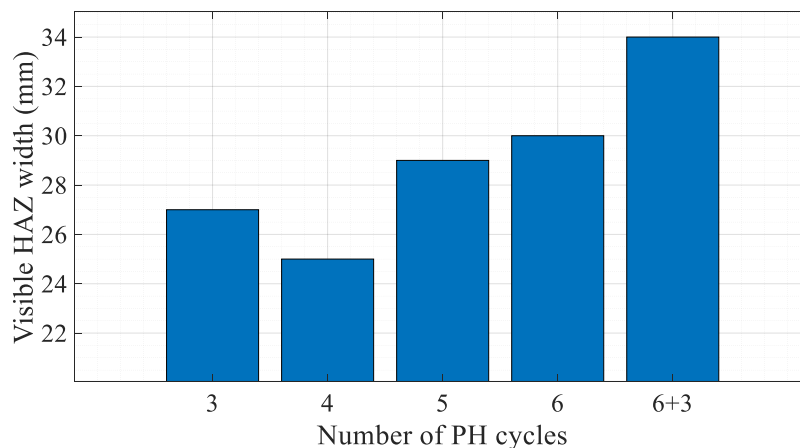
Figure 110. Visible HAZ width versus number of PH cycles.

The same behaviour was observed in previous attempts made on both pearlitic and bainitic steels[16],[86],[68],[53]. An exception was found in the weld in which 3PH cycles were utilised, this variation is believed to be produced due to a combination of

stripper problems and daily machine variations. The narrowest visible HAZ from all the weld trials (4PH) had a width of 25 mm, which is 15 mm narrower than the "standard" B360 FBW analysed in Chapter 4 (8PH cycles). Table 36, represents a summary of the data obtained in comparison with previous attempts by British Steel.

Table 36. Visible HAZ width, as a function of the "ON" time (Time that the rails are in contact per pre-heat) selected and the number of PH cycles; comparison of previous trials with the authors.

Number of PHs	"ON" time (s)	Visible HAZ width (mm)
Author's trials		
3	2.0	27
4	2.0	25
5	2.0	29
6	2.0	30
6+3PWHP	2.0	34
8 (Hayange)	4.6	40
British Steel trials		
3	2.5	27
6	2.0	27.5
6	3.3	31
10 (Hagendorf)	4.6	42
10 (Hagendorf)	5.1	52
10 (Castleton)	4.6	40

As discussed, and observed in Table 36, lowering the number of PHs seems to have a direct influence in the visible HAZ width extension. Also, longer preheating ON times

(s), produce a slight increment in the visible HAZ width. This behaviour is clear when looking at the two welds produced in the Hagendorf plant using 10PH cycles and a preheating time of 4.6 and 5.1; having 10 mm wider HAZ the one with longer ON time. Other aspects to take into consideration will be the equipment used and daily machine variations. As it is observed, by Hagendorf versus Castleton's results, these variables using the same welding program will also have a direct influence on the weld properties.

II.Hardness variations

Table 37 represents a summary of the parameters obtained in comparison with the previous rail welds analysed in Chapter 4; pearlitic R260 and bainitic B320 and previous attempts made by British Steel.

All the welds produced in the Schlatter welder seem to be narrower than the previously analysed 8PH weld in Chapter 4.

As observed, high hardness variations were also evident in previous trials carried out by British Steel in both Hagendorf and Castleton welding plants by H.M.Smith and P.Secordel. Four welds were produced, with 10, 6 and 3 PH cycles [86].

As described in the experimental procedure, a similar welding program was used by the author, with variations only in the number of PH cycles and the ON, OFF times (s). From a first approach it can be noted that the maximum and minimum hardness values obtained seem to be less accentuated in the trials produced at Castleton and Hagendorf than in the Schlatter. For instance, the maximum hardness values obtained in the narrow HAZ program (478HV1); in which 3PH cycles were applied, are lower than the ones obtained in the Schlatter trials with the same welding program (482.7HV1). Also, the minimum hardness value was of 335HV1, in comparison with the 301.3HV1 obtained. In addition, the SCHAZ has the same extension than in the Scatter; which is of 15 mm.

When making a more in detail examination of the SWEP charts and weld program, it is observed that the main differences in the welds will be produced due to:

The shorter ON time (s): As aforementioned, shorter ON times were selected, producing a decrement on the heat input with the main objective of generating a narrower HAZ. However, it could be argued that because of the combination of shorter ON times and low number of PHs, the procedure might be more sensitive to heat input variations. Furthermore, high maximum hardness values in the weld CHAZ are expected to occur.

The first preheat current (kA): The one reached on both Hagendorf and Castleton welding plants was between 65-68 kA, compared to the values obtained in trials of 49-53 kA; this is due to modifications in the phase current. This, will also have a direct influence in the extension of the HAZ, the maximum CHAZ hardness values and the weld integrity.

Machine variations: It should be borne in mind, that every weld is different. Even though the same welding program is used, there can be variations due to the different FBW machines, cleanness of the rail, and copper die and upset force values (kN).

Another aspect to consider will be the differences between the B320 and R260 versus B360 rail welds. The extension of the SCHAZ is similar in the Schlatter B360 4PH and in the B320 FBW, whilst the hardness variation in the B360 ICHAZ seems to be greater. As previously mentioned, the narrower HAZ extension of B320 steels is likely to be a cause of the higher vanadium content, which leads to precipitation hardening [100]. Moreover, the high hardness values obtained in the B360 grade are more likely to be produced due to its higher carbon content.

Table 37. Summary of maximum, minimum hardness and extension of the SCHAZ as a function of the number of Preheats.

Number of PHs	Max hardness (HV1)	Min hardness (HV1)	Variation in the IC zone	Extension of the SC HAZ (mm)
		Authors trials		
3	482.7	301.3	180.4	15
4	478.7	312.7	166	13
5	478.2	292.7	155	15
6	464.7	309.7	186	17
6*	459.3	295.7	163.6	20
6+3PWP	443.3	299.3	144	17
8PH (Hayange)	420	282	138	60
		FBW B320 - R260 (As received welds)		
8PH (Hayange) B320	351	309	42	12
8PH (Hayange) R260	321.5	247.5	74	6
		British Steel trials [86] [80] [68]		
10	450	320	130	55
10	458	315	143	No Data
6	455	310	145	No Data
3	478	335	140	15

When adding PWHP, a slow cooling rate was expected, which led to a steadier hardness variation. As previously mentioned, an increment of the visible HAZ was produced. Nevertheless, this represents only the extension from the weld FZ to the end of the ICHAZ. When looking at the extension of the SCHAZ, this was narrower than expected. Therefore, the extension of the SCHAZ seems to be only influenced by the number of PHs, having the weld with PWHP only an influence in the extension of the visible HAZ. The author could not find information related to the use of Post Weld Pulses (PWP) after FBW procedures.

III. Web region of the HAZ

In the analysed welds, the HAZ width was found to be narrower within the railhead and foot than the web, which is a typical behaviour of FBW procedures, due to the "skin effect"; similar behaviour has been previously observed in both bainitic and pearlitic rail steels.

If looking at the variation of the rail hardness in the web, low hardness values are produced at a distance of even 80 mm from the weld FZ, coinciding with the wider visible HAZ. The author has not found data up to date of an analysis of the weld B360 web and foot. Taking into account examinations produced by H. M. Smith on the B360 parent web hardness (~520HV) on a rail welded with 10PH cycles, it is possible that the tempered HAZ region will be even more extended within the web than in the head and foot; however, further micrographic examination would be necessary to support this.

IV. Metallographic examination

From the metallographic point of view, a standard micrographic examination of FBW procedures can be observed [86],[68], with higher amount of martensite and lower bainite present in narrow HAZ welds. Very similar microstructures were found when comparing with the standard wide HAZ weld analysed in Chapter 4.

The main differences when comparing the metallographic examination of the welds with the ones produced in British Steel, will be the mentioned presence of a dark

etching 'carbide-aggregate' within the PAGBs at the ICHAZ, believed to be clusters of pearlite.

V. Three-point bend test performance

When analysing rail integrity of the FBW trials, the three welds tested achieved the minimum load of 1500-1600 kN, however, none of the welds reached the minimum deflection of 20 mm, according to the standard EN 14587-1:2018 [67].

Table 38, represents a summary of the results obtained in three-point bend test for the 4PH, 5PH and 6PH welds; showcasing the maximum load and deflection rate. Together with data obtained from three welded rails by H. M. Smith in the Castleton plant, with 6, 10 [86] and 3PH [68].

The number of PHs and welding program seems to not have any significant influence in the weld integrity.

The fracture surface of the rails under consideration was observed to be typical of previously analysed B360 grades, being brittle. A cause for this brittleness could be the low heat input generated during the FBW. The most ductile fracture was observed in the rail with 4PH, which could be a cause of higher amount of RA or ferrite.

As represented in Table 38, none of the welds satisfy the minimum deflection of 20 mm, this was only achieved by the as-rolled rail at a load of more than 2000 kN. However, as previously mentioned, this is only a standard for pearlitic steels, having lower YS than bainitic. Therefore, a new standard for bainitic steels seems necessary.

Table 38. Comparison of three-point bend test data for grade B360 rail FBW, and as-rolled B360 rail

PHs	HAZ width (mm)	'ON' (s)	'OFF' (s)	PH current (kA)	Maximum load (kN)	Deflection (mm)
Authors trials						
4	25	2.0	0.5	50.7	2030.34	17.9
5	29	2.0	0.5	50.4	1608.70	11.1
6	30	2.0	0.5	50.9	1684.02	11.5
As rolled B360 (Not broken)					2113.42	20.15
British Steel trials [86],[80],[68]						
10	42	4.6	1.1	No Data	1706.4 ± 218.1	16.9 ± 4.4
6	27.35 ± 0.21	2.0	0.5	65.9 ± 0.1	1966.5 ± 15.6	19.3 ± 1.7
6	30.23 ± 0.45	3.3	0.5	66.8 ± 1.2	1932.7 ± 58.2	18.4 ± 2.3
3	24	2.0	0.5	No Data	1777.3 ± 92.2	16.8 ± 2.2

5.10. Summary

A series of FBWs were performed in the Schlatter welding machine, Scunthorpe, UK; in order to develop a narrow HAZ weld, retaining weld integrity. The main highlights of this chapter are:

Reducing the number of PH cycles and ON-OFF times (s) was found to reduce both, the visible HAZ width and the extension of the SCHAZ. However, there is a trade-off between the hardness variation of the ICHAZ and the extension of the HAZ; having an increment on both the maximum and minimum hardness on the narrowest HAZ welds.

Adding PWHP seems to have a direct influence in both the extension of the tempered SCHAZ and the hardness variation of the ICHAZ; having a steadier hardness variation and a narrowing of the SCHAZ.

The microstructural features developed through the rail running surface HAZ, were consistent in both wide and narrow HAZ welds.

No influence in the recorded properties was observed when changing the quenching temperature from 200 to 300 °C. This points out to a potential reduction of production costs as less time is necessary for the rail to cool down, which could result in significant monetary gains.

Differences were found when using the same welding program in both the author and British Steel trials; the main difference of the welds could be focused on modifications on the phase current. Even though the same welding program was utilised, using dissimilar FBW machines could have a direct influence in the weld properties. Therefore, the phase current should be adjusted to obtain the desired first PH current.

During three-point bend testing, all the welds satisfied the minimum bend load of 1500-1600 kN, according to the standard [67]. However, problems are encountered when trying to reach the minimum deflection of 20 mm. The as rolled B360 rail, only reached this deflection at a load of more than 2000 kN. This, is only based on pearlitic rail steels behaviour; and could be a result of bainitics higher YS.

A decrement of the HAZ widths has seen to increase the compressive longitudinal residual stresses. The HAZ width seem to not have any influence in tensile residual stresses.

Modifications of the standards for bainitic steels seem necessary, as standards used for pearlitic steels are not appropriate.

Chapter 6

Summary and future work

I. Summary

This work has had two main approaches. Understanding the microstructural evolution of CFB more specifically B360 FBW and producing a new welding program for CFB B360 in order to develop a narrower HAZ.

a. Understanding conventional B360 FBWs.

It has been demonstrated that CFB steel welds have more complex microstructural evolution than conventional pearlitic steels used in the railway industry, being more influenced by the dissimilar phases present than the grain size itself.

The main factor to consider when comparing the HAZ of CFB with the one of pearlitic steels, is the much wider HAZ present; with an extension of the B360 8 PH weld SCHAZ of 58 mm in comparison with the 7 mm extension of the pearlitic R260. Therefore, B360 steels show low resistance to tempering. This, could result in preferential wear and plastic deformation when in track applications.

When comparing B360 with B320 welds, there is also a reduction of 51 mm of the softened SCHAZ; having the B320 a behaviour that resembles more the one of pearlitic steels.

It has been demonstrated with TEM examination that the higher tempering resistance of B320 is directly related with precipitation hardening of Vanadium. The amount of Vanadium is also believed to influence the size and quantity of carbides present in the SCHAZ, slowing down austenite decomposition into carbides.

b. Producing a narrow HAZ FBW.

A reduction in the SCHAZ extension of B360 welds might improve the final properties of the weld. In order to achieve a narrower HAZ during FBW procedures, a limitation on the number of PHs, the pre contact (ON) and separation diffusion (OFF) times (s) was applied, with the main objective of generate a smaller HAZ extension whilst retaining weld integrity.

Reducing the HAZ width has shown to have a detrimental effect in terms of variation of the ICHAZ hardness levels, as none of the welds produced satisfy the minimum or maximum HAZ hardness variation according to the European standard (P+60, P-30). However, it is important to bear in mind, that the standard utilised is for pearlitic steels and there is not actual standard for bainitic rail steels. Therefore, a re-evaluation of the bainitic rail steels standards seems necessary.

When tested in the three-point bend tester, all the rails achieved the minimum load of 1600kN, however not even the "as rolled" B360 rail reached the minimum deflection of 20 mm; this could be a cause of bainitic steels having lower YS than pearlitics. This is, as before, another example of the necessity of new standards for bainitic steels.

II.Future work

Further work should be focussed in three main sections:

a. **Further study of B360 FBW and its in track performance**

The author suggests a study of the in-track behaviour of narrow HAZ B360 FBWs. For this purpose, a repetition of the weld with better performance and further examination in both hardness variation and mechanical properties with a three-point bend test should be performed (4PH weld). Further trials, could also be made by adding modifications in the phase current, in order to obtain a larger preheat current (kA), and therefore, improving weld integrity.

Later on, an examination of its in-track behaviour could be produced in a twin disc tester to study the wear performance of these rails. If results continue to be promising, trials should be focussed in leaving the welded rail in-track in the Scunthorpe line, with periodic examination of its behaviour.

If the results for this steel continue to be promising a new standard for CFB has to be developed.

b. **Study of other welding procedures.**

Although this thesis was only focussed on the stationary FBW concern, similar studies need to be made on mobile FBW machines.

It is important to bear in mind that rails welded with mobile FBW will perform differently that stationary machines. Mobile FBWs produce a continuous flashing instead of the previously mentioned preheating and burn off stages, obtaining a wider HAZ than stationary welding machines. Therefore, modifications in the welding program have to be made.

c. **Modifications on the chemical composition**

Another aspect to consider for further work, will be an analysis of the influence of vanadium on precipitation hardening on both B320 and B360 steels in order to reduce the softening of the SCHAZ. Further work on this topic is currently being carried out by British Steel.

References

[1]   R. A. Smith, "Rolling Contact Fatigue of Rails: What Remains to be Done?," China Railw. Serv., vol. 3, p. 001, 2002.

[2]   U. Zerbst, R. Lundén, K.-O. Edel, and R. A. Smith, "Introduction to the damage tolerance behaviour of railway rails – a review," Eng. Fract. Mech., vol. 76, no. 17, pp. 2563–2601, Nov. 2009

[3]   R. Sawley, K. & REIFF, "Rail failure assessment for the office of the rail regulator. An assessment of rail track's methods for managing broken and defective rails. Report of the transportation Technology centre, Colorado, USA," 2020.

[4]   H. Smith, "Bainitic rail steels- By private comunication- British Steel," 2008.

[5]   V. A. Profidillis, Railway engineering. Brookfield, USA: Avebury Technical, 1995.

[6]   C. E. Volos, "Interaction between superstructure and substructure in railways," Concrete, no. 5, pp. 2–9, 2010.

[7]   Chandra Satish and Agarwal M.M., "Railway Engineering (2nd Edition)," Oxford Univ. Press, vol. 20, pp. 1–2, 2015

[8]   T. C. Abadi, "Effect of sleeper and ballast interventions on rail track

performance," University of Southampton, 2015.

[9] S. Iwnicki, "Future trends in railway engineering," Proc. Inst. Mech. Eng. Part C J. Mech. Eng. Sci., vol. 223, pp. 2743–2750, 2009

[10] D. Bilow and G. Randich, "Slab track for the next 100 years," Am. Railw. Eng. Maintenance-of-w. Assoc. - Proc. 2000 Annu. Conf., no. 1, pp. 1–20, 2000.

[11] Y. Bezin, D. Farrington, C. Penny, B. Temple, and S. Iwnicki, "The dynamic response of slab track constructions and their benefit with respect to conventional ballasted track," Veh. Syst. Dyn., vol. 48, no. SUPPL. 1, pp. 175–193, 2010

[12] D. Campbell, J. Brougham, and R. Caldwell, "Uncovering and Understanding Australia's First Railway," Aust. J. Multi-Disciplinary Eng., vol. 7, no. 2, pp. 147–156, 2017

[13] J. Fernández, L. Museo, and D. Ferrocarril De Asturias, "Del Hierro Al Acero: La Producción De Duro Para La Compañía Del Noroeste Los Primeros Carriles Fabricados En España," pp. 1–12,

[14] R. I. Carroll, "Surface Metallurgy and Rolling Contact Fatigue of Rail," University of Sheffield, 2005.

[15] J. Locke, "The advent of the steel rail 1857-1914," J. Transp. Hist., pp. 18–31, 1914.

[16] A. S. J. A. Z. Jilabi, "Welding of Rail Steels," University of Manchester, 2015.

[17] P. Connor, "Track basics," Railway Technical Website, no. 2, pp. 1–13.

[18] EN13674-1 European standard UIC60/60E1 900A railway steel rail. .

[19] U. Olofsson and T. Telliskivi, "Wear, plastic deformation and friction of two rail steels - A full-scale test and a laboratory study," Wear, vol. 254, no. 1–2, pp. 80–93, 2003

[20] E. Sheinman, "Wear of rails. A review of the American press," J. Frict.

Wear, vol. 33, no. 4, pp. 308–314, 2012

[21] K. M. Lee and A. A. Polycarpou, "Wear of conventional pearlitic and improved bainitic rail steels," Wear, vol. 259, no. 1–6, pp. 391–399, Jul. 2005

[22] S. Fretwell-smith, R. Steel, and D. Driver, "Rail Degradation Mechanisms - British Steel- By private communication," 2012.

[23] E. Magel, P. Sroba, K. Sawley, and J. Kalousek, "Control of rolling contact fatigue of rails," Cent. Surf. Transp. Technol., pp. 1–29, 2005

[24] J. E. Garnham, D. I. Fletcher, C. L. Davis, and F. J. Franklin, "Visualization and modelling to understand rail rolling contact fatigue cracks in three dimensions," Proc. Inst. Mech. Eng. Part F J. Rail Rapid Transit, vol. 225, no. 2, pp. 165–178, 2011

[25] H. M. Smith, "Bainitic presentation February 2011- British Steel- By private communication." 2011 .

[26] T. Mount and H. Street, "Squats and squat-type defects in rails : the understanding to date," Proc. Inst. Mech. Eng. Part F J. Rail Rapid Transit, vol. 226, pp. 235–242, 2011

[27] L. J. Drewett, "The Measurement of Residual Stresses - British Steel- By private communication," 2001.

[28] H. Xiao, Q. Chen, E. Shao, D. Wu, Z. Chen, and Z. Wang, "The effect of shot peening on rolling contact fatigue behaviour and its crack initiation and propagation in carburized steel," Wear, vol. 151, no. 1, pp. 77–86, 1991

[29] H. M. Smith, "The bainitic rail steel - Key property requirements - British Steel- By private communication," 1998.

[30] J. Jaiswal and C. Rail, "CORUS PREMIUM GRADES TO ADRESS WEAR - British Steel - By private communication."

[31] A. C. Athukorala, D. V. De Pellegrin, and K. I. Kourousis, "Characterisation of head-hardened rail steel in terms of cyclic plasticity

response and microstructure for improved material modelling," Wear, vol. 366–367, pp. 416–424, 2016

[32] H. K. D. H. Bhadeshia, "Bainite in Steels," 2001.

[33] J. Kalousek, D. M. Fegredo, and E. E. Laufer, "The wear resistance and worn metallography of pearlite, bainite and tempered martensite rail steel microstructures of high hardness," Wear, vol. 105, pp. 199–222, 1985.

[34] P. Clayton and N. Jin, "Unlubricated sliding and rolling/sliding wear behavior of continuously cooled, low/medium carbon bainitic steels," Wear, vol. 200, no. 1–2, pp. 74–82, Dec. 1996

[35] H. K. D. H. Bhadeshia and D. V. Edmonds, "Bainite in silicon steels: new composition–property approach Part 1," Met. Sci., vol. 17, no. September, pp. 420–425, 1983, doi: 10.1179/030634583790420646.

[36] H. K. D. H. Bhadeshia, "Some phase transformations in steels," Mater. Sci. Technol., vol. 0836, no. 1999, 2013

[37] Y. T. Chi, Y. T. Tsai, B. M. Huang, and J. R. Yang, "Investigation of idiomorphic ferrite and allotriomorphic ferrite using electron backscatter diffraction technique," Mater. Sci. Tecnol., vol. 0836, 2017, doi: 10.1080/02670836.2016.1216027.

[38] H. K. D. H. Bhadeshia, "Interpretation of the Microstructure of Steels," https://www.phase-trans.msm.cam.ac.uk/. .

[39] H. K. D. H. Bhadeshia, "Widmanstatten Ferrite," https://www.phase-trans.msm.cam.ac.uk/. .

[40] H. K. D. H. Bhadeshia and R. Honeycombe, "Related to carbide-free bainitic steels and method of producing such steels, US5879474A," 2017.

[41] G. I. Rees and H. K. D. H. Bhadeshia, "Bainite transformation kinetics Part 1 Modified model," Mater. Sci. Technol., vol. 0836, 2013, doi: 10.1179/mst.1992.8.11.985.

[42] S. B. Singh and H. K. D. H. Bhadeshia, "Estimation of bainite plate-

thickness in low alloy steels," Mater. Sci. Eng., 1997.

[43] W. M. Johnson, "Reaction kinetics in processes of nucleation and growth," Trans. Am. Inst. Min. Metall. Eng., vol. 135, pp. 419–442, 1939.

[44] F. G. Caballero, H. K. D. H. Bhadeshia, K. J. a. Mawella, D. G. Jones, and P. Brown, "Design of novel high strength bainitic steels: Part 2," Mater. Sci. Technol., vol. 17, no. 5, pp. 517–522, 2001, doi: 10.1179/026708301101510357.

[45] D. V. Pereloma, E., & Edmonds, "Phase transformations in steels: Diffusionless transformations, high strength steels, modelling and advanced analytical techniques," Elsevier, 2012.

[46] H. K. D. H. Bhadeshia and V. Jerath, "Related to carbide-free bainitic steels and method of producing such steels," 1996.

[47] V. C. Igwemezie and P. C. Agu, "Development of Bainitic Steels for Engineering," Int. J. Eng. Res. Tech, vol. 3, no. 2, pp. 2698–2711, 2014.

[48] H. K. D. H. Bhadeshia., "Novel Steels for Rails," in Encyclopedia of Materials Science: Science and Technology, 2002, pp. 1–7.

[49] F. Fau et al., "Short note Subject : Stress corrosion testing of B360 bainitic and R260Mn pearlitic rails for Prorail," no. 02280000, pp. 1–10, 2014.

[50] H. M. Smith, "The characterization of 'Carbide-Free' bainitic rail steels in terms of their tempering, cold-working and rolling contact wear behaviour - British Steel- By private communication. no. S2286," 1997.

[51] H. M. Smith, L. J. Drewett, G. Thomson, V. Jerath, J. Jaiswal, and By private communication, "Bainitic Rail Steel Developments: A technical status report," 2000.

[52] L. Drewett, "Welding issues on Tata Steel bainitic rail steels. By private communication.," 2014.

[53] P. Secordel, "Review of B360 and B320- British Steel- By private communication," 2019.

[54] "Private communication by British Steel." .

[55] D. Tawfik, P. J. Mutton, and W. K. Chiu, "Experimental and numerical investigations: Alleviating tensile residual stresses in flash-butt welds by localised rapid post-weld heat treatment," J. Mater. Process. Technol., vol. 196, no. 1–3, pp. 279–291, Jan. 2008, doi: 10.1016/J.JMATPROTEC.2007.05.055.

[56] W. Li, G. Xiao, Z. Wen, X. Xiao, and X. Jin, "Plastic deformation of curved rail at rail weld caused by train – track dynamic interaction," Wear, vol. 271, no. 1–2, pp. 311–318, 2011, doi: 10.1016/j.wear.2010.10.002.

[57] G. Demofonti, S. Budano, and C. Viglialoro, "Role of residual stresses and microstructure on fatigue initiation and crack growth in welded rails. Office f. Official Publ. of the Europ. Communities.," 1998.

[58] "Flash butt welding technology for rails-a review . British Steel - By private communication," 2008.

[59] H. Farhangi and M. Engineering, "HORIZONTAL SPLIT-WEB FRACTURES OF FLASH BUTT," no. November, pp. 509–517, 2007.

[60] S. Gleeson, "Knowledge transfer session- British Steel - By private communication." 2019.

[61] P. R. VISHNU, Solid state transformations in weldments. 1993.

[62] R. Lewis, Wheel-Rail Interface Handbook. 2009.

[63] M. Pástor, "Introducción a la metalurgia de la soldadura.," p. 350, 2005.

[64] A. SAARNA, M; LAANSOM, "Rail and rail weld testing," Proc. 4th Int. DAAAM Conf. Ind. Eng. as Compet. Edge SME, pp. 217–219, 2004.

[65] "The influence of the working procedures on the formation and shape of the HAZ of flash butt and aluminothermic welds in rails . INNOTRACK. Project no. TIP5-CT-2006-031415," 2008.

[66] H. M. Smith, "Narrow HAZ B360 - Power Point presentation - British Steel - By private communication," 2008.

[67] BS EN 14587-1:2018. Railway applications. Infrastructure. Flash butt welding of new rails. R220, R260, R260Mn, R320Cr, R350HT, R350LHT, R370CrHT and R400HT grade rails in a fixed plant.

[68] S. H. M. Boulanger D., Rouquie P., "Narrow HAZ B360 flash butt B360 welds - British Steel- By private communication," 2006.

[69] O. Engler and V. Randle, Introduction to texture analysis. 2010.

[70] et al. CARTER, BARRY AUTOR, "Transmission Electron Microscopy: A Textbook for Materials Science," Springer Sci. Bus. Media, vol. 1, 1996.

[71] E1558-09, "Standard guide for eletrolytic polishing of metallographic specimens"ASTM Int. vol 09. 2019.

[72] P. Secordel and H. Smith, "The development of a revised procedure for the flash butt welding of the B360 grade," 2011.

[73] H. M. Smith, "Development of a revised procedure for the FBW of a bainitic B360 rail - British Steel - By private communication," 2011.

[74] S. I. Kuchuk-Yatsenko, "Flash-butt welding of high-strength rails," Mining–Informatics, Autom. Electr. Eng. 54, 2016.

[75] X. Luo, X. Chen, T. Wang, S. Pan, and Z. Wang, "Effect of morphologies of martensite–austenite constituents on impact toughness in intercritically reheated coarse-grained heat-affected zone of HSLA steel," Mater. Sci. Eng. A, vol. 710, no. October 2017, pp. 192–199, 2018

[76] M. T. Morito, S., Nishikawa, J., "Dislocation density within lath martenstie in Fe-C and Fe-Ni alloys," vol. 43, no. 9, pp. 1475–1477, 2003.

[77] M. Saarna and A. Laansoo, "Rail and rail weld testing," no. April, 2004.

[78] C. B. Huppi, G.S.; Damkroger, B.K.;Dallam, "Metallography and microstructures of weldments," in ASM Handbook, Volume 9: Metallography and microstructures, 2004, pp. 1047–1056.

[79] H. M. Smith, "A metallurgical examination of SBB Thermit welded grade 360 grooved Ri60 bainitic rails - British Steel - By private

communication," 2003.

[80] H. M. Smith, "A metallurgical examination of an SBB flash butt welded 60E1 grade 360 bainitic rail - British Steel - By Private communication - n. 110586," 2004.

[81] S. H. Talebi, M. Jahazi, and H. Melkonyan, "Retained austenite decomposition and carbide precipitation during isothermal tempering of a medium-carbon low-alloy bainitic steel," Materials (Basel)., vol. 11, no. 8, 2018

[82] Y. Ju, A. Goodall, M. Strangwood, and C. Davis, "Characterisation of precipitation and carbide coarsening in low carbon low alloy Q&T steels during the early stages of tempering," Mater. Sci. Eng. A, vol. 738, no. August, pp. 174–189, 2018

[83] L. RYDE, "Application of EBSD to analysis of microstructures in commercial steels," vol. 11, p. 1297,1306, 2006.

[84] J. K. BOWLES, J.S.; MACKENZIE, "The crystallography of martensite transformations III. Face-centred cubic to bodu centred tretragonal transformations," Acta Metall., vol. 2, no. 2, pp. 224–234.

[85] P. Secordel, "Influence du Vanadium sur la resistance au revenu du B320 - British Steel, Hayange," 2019.

[86] H. M. Smith, "A metallurgical examination of a flash butt welded grade B360 60E1 rail for SBB - British Steel- By private communication. Project number: 1064719," 2009.

[87] H. A. Aglan, S. Ahmed, K. R. Prayakarao, and M. Fateh, "Effect of Preheating Temperature on the Mechanical and Fracture Properties of Welded Pearlitic Rail Steels," Engineering, vol. 05, no. 11, pp. 837–843, 2013, doi: 10.4236/eng.2013.511101.

[88] D. Tawfik, O. Kirstein, P. J. Mutton, and W. K. Chiu, "Verification of residual stresses in flash-butt-weld rails using neutron diffraction," Phys. B Condens. Matter, vol. 385–386, pp. 894–896, 2006

[89] C. W. Ziemian, M. M. Sharma, and D. E. Whaley, "Effects of flashing and upset sequences on microstructure, hardness, and tensile properties of welded structural steel joints," Mater. Des., vol. 33, no. 1, pp. 175–184, 2012

[90] H. M. Smith, "Development of bainitic rails for commercial track applications - British Steel- By private communication," 2002.

[91] Z. P. B. D. Popovic and H. P. Neff, "Introductory Electromagnetics," Prentice Hall, no. April, pp. 1–581, 2000

[92] H. Mansouri and A. Monshi, "Microstructure and residual stress variations in weld zone of flash-butt welded railroads," Sci. Technol. Weld. Join., vol. 9, no. 3, pp. 237–245, 2004

[93] D. C. Kim, W. J. So, and M. J. Kang, "Effect of flash butt welding parameters on weld quality of mooring chain," Arch. Mater. Sci. Eng., vol. 38, no. 2, pp. 112–117, 2009.

[94] W. Leonhard, K. Jörg, and E. Norbert, "Temperature Field Evolution During Flash Butt Welding of Railway Rails," no. January, 2017

[95] Z. Xiong, S. Liu, X. Wang, C. Shang, X. Li, and R. D. K. Misra, "The contribution of intragranular acicular ferrite microstructural constituent on impact toughness and impeding crack initiation and propagation in the heat-affected zone (HAZ) of low-carbon steels," Mater. Sci. Eng. A, vol. 636, pp. 117–123, 2015

[96] E. Mazancova, A. Jonsta, and E. Al, "Physical Metallurgy of Acicular Ferrite Formation," Acta Metall. Slovaca, vol. 3, pp. 1–6, 2003.

[97] O. P. Modi, N. Deshmukh, D. P. Mondal, A. K. Jha, A. H. Yegneswaran, and H. K. Khaira, "Effect of interlamellar spacing on the mechanical properties of 0.65% C steel," Mater. Charact., vol. 46, no. 5, pp. 347–352, 2001

[98] H. A. Aglan, Z. Y. Liu, M. F. Hassan, and M. Fateh, "Mechanical and fracture behavior of bainitic rail steel," J. Mater. Process. Technol., vol. 151, no. 1-3 SPEC. ISS., pp. 268–274, 2004

[99] S. Fretwell-smith, S. Danks, R. Lambert, R. Walker, and D. Benton, "Examination of a Mobile Flashbutt Weld produced at Crossrail - British Steel - By private communication. B700-20 R058," 2016.

[100] P. Secordel, "Bainitic rail presentation. Rail Annual Technical Forum 2019 - British Steel- By private communication," 2020.

Appendix

a. Weld programs, Schlatter GAAS 80/580 Flash Butt Weld machine, Scunthorpe, UK

    i.   3 PH cycles

20.1   Form B-595 FORM_A   **schlatter**

Workpiece: _____   Date: _____

Welder Type: _ GAAS 80 / 580 _____   Series Number: AS1.2653.02949

Order number: _____

Operator: _____

Welding Task: _____

_____

Material: _____   Cross section: [mm2]: _____

Machine setup data

Hydraulic system pressure	[bar]:	_____
Upsetting valve pressure	[bar]:	_____
Clamping force left	[kN]:	_____
Clamping force right	[kN]:	_____
Reference electrode gap	[mm]:	_____
Electrode-gap Start	[mm]:	_____
Electrode-gap End	[mm]:	_____
Transformer tap: _____	U20 [V]:	_____
Diagram No. _____		

Setup Schlatter - Recorder REC 01: →

Remarks:

20.2 **Form B-595 FORM_B** AS1.2653.02949 **schlatter**

SWEP06 Editor PGM # 006
Description:
est Bainitic

BASIC STEP | 01 PGM#

| 02.0 | 03.0 | 08.0 | 100 | 200 | 49.1 | 01 STEP |
| 400 | 0.00 | 0.00 | 0.00 | | | 01 CODE |

schlatter SWEP 06

*** FLASHING *** ▾ | 01 PGM#

| 02.0 | 900 | 060 | 180 | 000 | | 02 STEP |
| 05.0 | 700 | 080 | 200 | | 000 | 02 CODE |

schlatter SWEP 06

>*<PREHEATING>*< ▾ | 01 PGM#

| 1.00 | 2.00 | 130 | 500 | | 006 | 03 STEP |
| 02.5 | 0.50 | 0.25 | 105 | 01.0 | 222 | 04 CODE |

schlatter SWEP 06

*** FLASHING *** ▾ | 01 PGM#

| 10.0 | 850 | 050 | 120 | 000 | | 04 STEP |
| --- | --- | --- | --- | | 033 | 02 CODE |

schlatter SWEP 06

*** FLASHING *** ▾ | 01 PGM#

| 11.0 | 850 | 999 | 065 | 000 | | 05 STEP |
| 14.5 | 800 | 999 | 110 | | 033 | 02 CODE |

schlatter SWEP 06

180

SWEP06 Editor PGM # 006

						01	PGM#

*** FLASHING *** ▼

15.0	800	999	130	000		06	STEP
18.0	800	999	150		033	02	CODE

schlatter SWEP 06

>>>UPSETTING<<< ▼   01 PGM#

0.50	29.0	000	170	001		07	STEP
0.20	680	450	38.0		044	06	CODE

schlatter SWEP 06

∧∧∧∧HEATING∧∧∧∧ ▼   01 PGM#

0.75	408	000	000	001	38.0	08	STEP
0.75	408	000	000		045	05	CODE

schlatter SWEP 06

∧∧∧∧HEATING∧∧∧∧ ▼   01 PGM#

3.00	100	500	000	003	38.0	09	STEP
1.50	100	000	000		045	05	CODE

schlatter SWEP 06

EMPTY STEP ▼   01 PGM#

						10	STEP
						00	CODE

schlatter SWEP 06

181

schlatter

SYSTEM PARAMETER	20 PGM#

0	0.01	0.02	0.03	789	500
49.1	101	0.80	950	850	0

schlatter SWEP 06

SYSTEM PARAMETER	21 PGM#

0.30	0.20	2.38	0.00	0.00	000

schlatter SWEP 06

SYSTEM PARAMETER	40 PGM#

1.0	2	7	960	002	006
003	006	021			

schlatter SWEP 06

Force Controller Network Board NH

S1   6

C28   330 nF
R54   1'000 kΩ
R52   270 kΩ
R53   0 kΩ
R51   820 kΩ

IC 21 Board NM Current Calibration

R2   18 kΩ
R1   27 kΩ

Front Panel Board VC

ON
S1
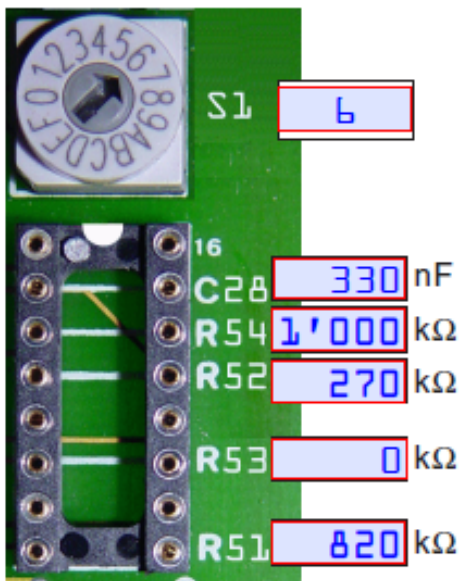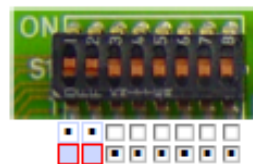
SWEP 06   (A) (D) (A) (0) (0)

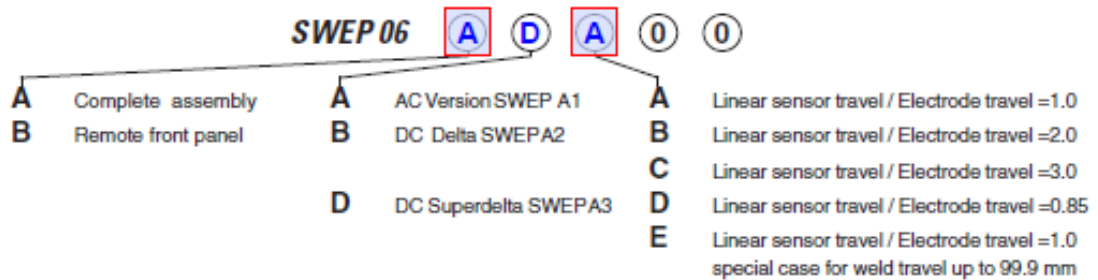## SWEP06 Customer Related Information

Purchaser: **Corus Rail Scunthorpe**   Enduser: **Corus Rail Scunthorpe**   Date: **Feb.01.07**

Welder Type: **GAAS 80 / 580**   Welder Serial Number: **AS1.2653.02949**

Target Date: **November 25, 2005**   Administrator: **Ernst Iberg**

[Reset FORM_E]

Welder Engineering Data

☐ AC Current   ☐ DC Delta Current   ☑ DC Superdelta Current

1.	Maximum carriage travel (theoretical)		50.00	[mm]
2.	Maximum carriage travel (measured at electrodes)	s_{max}	49.10	[mm]
3.	Effective piston area forward side	A_{ADV}	628.32	[cm²]
4.	Effective piston area backward side	A_{BACK}	500.00	[cm²]
5.	Piston areas ratio	A_{BACK}/A_{ADV}	0.80	[1]
6.	Mechanical ratio Piston travel / Electrode travel		1.00	[1]
7.	Nominal upsetting force of the welder	F_N	600	[kN]
8.	Hydraulic pressure required for F_N	p_{FN}	127.32	[bar]
9.	Nominal clamping force of the welder	F_{CLAMP}	1900	[kN]
10.	Hydraulic pressure required for F_{CLAMP}	p_{FCLAMP}	140.00	[bar]
11.	Operating pressure of the hydraulic aggregate	p_{PUMP}	140.00	[bar]
12.	Operating pressure of the hydraulic bladder accumulator	p_0	65.00	[bar]
13.	Ratio clamp-force / upsetting-force	F_{CLAMP}/F_N	2.38	[1]

14. Proportional Valve used for upsetting ☑ no   ☐ yes →   - - -   [bar/V]
15. Proportional valve used for clamping ☑ no   ☐ left side   ☐ right side   - - -   [bar/V]
16. Proportional valve type upsetting: Catridge Block
17. Proportional valve type clamping: Setup Logic T without Stop open 3/4 Turn
18. Upsetting valve installed   ☐ no   ☑ yes →   nominal size   25   [1]
19. Control valve type: BOSCH 4WRPH 6 C3B40L −2X/G24Z4 /M 0811 404 036   40   [l/min]
20. Line voltage phase to phase   ☑ 50 Hz   ☐ 60 Hz U_N 415   [Volt]
21. Transformer open loop secondary voltage U_{20} 6.85   [Volt]
22. Maximum short-circuit weld current I_{2CC} 215   [kA]
23. Welding transformer winding ratio   ü   35   [1]
24. Pressure sensor type: BOSCH 0 811 405 532   250 bar System ▼ Pressure System: 250   [bar]
25. Current sensor type: LEM LT 2000S   Shunt resistor: 5.6   [Ω]
26. Linear position transducer type: Honeywell SLF076R2M4500B8A 75 mm
27. Linear position transducer mounting: ☐ Carriage   ☑ Piston
28. Calibrating workpiece: Material: CEN 60   Cross section: 7686   [mm²]

SWEP 06 (A) (D) (A) (0) (0)

A	Complete assembly	A	AC Version SWEP A1	A	Linear sensor travel / Electrode travel =1.0
B	Remote front panel	B	DC Delta SWEP A2	B	Linear sensor travel / Electrode travel =2.0
				C	Linear sensor travel / Electrode travel =3.0
		D	DC Superdelta SWEP A3	D	Linear sensor travel / Electrode travel =0.85
				E	Linear sensor travel / Electrode travel =1.0 special case for weld travel up to 99.9 mm

ii.   6PH +3PWP

20.1   Form   B-595 FORM_A

schlatter

Workpiece: _____   Date: _____

Welder Type: __GAAS 80 / 580_____   Series Number: AS1.2653.02949

Order number: _____

Operator: _____

Welding Task: _____

_____

Material: _____   Cross section: [mm2]: _____

Machine setup data

Hydraulic system pressure	[bar]: _____	
Upsetting valve pressure	[bar]: _____	
Clamping force left	[kN]: _____	
Clamping force right	[kN]: _____	
Reference electrode gap	[mm]: _____	
Electrode-gap Start	[mm]: _____	
Electrode-gap End	[mm]: _____	
Transformer tap:_____	U20 [V]: _____	
Diagram No._____		

Setup Schlatter - Recorder REC 01: →

Remarks:

160 kN/Volt	24.6 kA/Volt	10 mm/Volt
160 kN/cm	24.6 kA/cm	10 mm/cm

EXT. SPEED CONTROL mm/s

START   1   2.5   5   10   25   50   100

Reset FORM_B and FORM_C

BASIC STEP						**01** PGM#
02.0	03.0	08.0	100	200	49.1	**01** STEP
400	0.00	0.00	0.00			**01** CODE

schlatter SWEP 06

SWEP06 Editor PGM # 006
Description:
est Bainitic

*** FLASHING *** ▼						**01** PGM#
02.0	900	060	180	000		**02** STEP
05.0	700	080	200		000	**02** CODE

schlatter SWEP 06

>*<PREHEATING>*< ▼						**01** PGM#
1.00	2.00	130	500		006	**03** STEP
02.5	0.50	0.25	105	01.0	222	**04** CODE

schlatter SWEP 06

*** FLASHING *** ▼						**01** PGM#
10.0	850	050	120	000		**04** STEP
---	---	---	---		033	**02** CODE

schlatter SWEP 06

*** FLASHING *** ▼						**01** PGM#
11.0	850	999	065	000		**05** STEP
14.5	800	999	110		033	**02** CODE

schlatter SWEP 06

SWEP06 Editor PGM # 006

*** FLASHING *** ▼						01 PGM#
15.0	800	999	130	000		06 STEP
18.0	800	999	150		033	02 CODE

schlatter SWEP 06

>>>UPSETTING<<< ▼						01 PGM#
0.50	29.0	000	170	001		07 STEP
0.20	680	450	38.0		044	06 CODE

schlatter SWEP 06

^^^^HEATING^^^^ ▼						01 PGM#
0.75	408	000	000	001	38.0	08 STEP
0.75	408	000	000		045	05 CODE

schlatter SWEP 06

^^^^HEATING^^^^ ▼						01 PGM#
3.00	100	500	000	003	38.0	09 STEP
1.50	100	000	000		045	05 CODE

schlatter SWEP 06

EMPTY STEP ▼						01 PGM#
						10 STEP
						00 CODE

schlatter SWEP 06

SYSTEM PARAMETER   20 PGM#   RDY   7 8 9 *
                                            4 5 6 ▲
| 0 | 0.01 | 0.02 | 0.03 | 789 | 500 | STEP   1 2 3 ▼
| 49.1 | 101 | 0.80 | 950 | 850 | 0 | CODE   EXT   0 STO RCL PGM

schlatter SWEP 06

SYSTEM PARAMETER   21 PGM#   RDY   7 8 9 *
                                            4 5 6 ▲
| 0.30 | 0.20 | 2.38 | 0.00 | 0.00 | 000 | STEP   1 2 3 ▼
| | | | | | | CODE   EXT   0 STO RCL PGM

schlatter SWEP 06

SYSTEM PARAMETER   40 PGM#   RDY   7 8 9 *
                                            4 5 6 ▲
| 1.0 | 2 | 7 | 960 | 002 | 006 | STEP   1 2 3 ▼
| 003 | 006 | 021 | | | | CODE   EXT   0 STO RCL PGM

schlatter SWEP 06

Force Controller Network Board NH

S1   6

C28   330 nF
R54   1'000 kΩ
R52   270 kΩ

R53   0 kΩ

R51   820 kΩ

IC 21 Board NM Current Calibration

R2   18 kΩ
R1   27 kΩ

Front Panel Board VC

ON
S1

SWEP 06   (A) (D) (A) (0) (0)

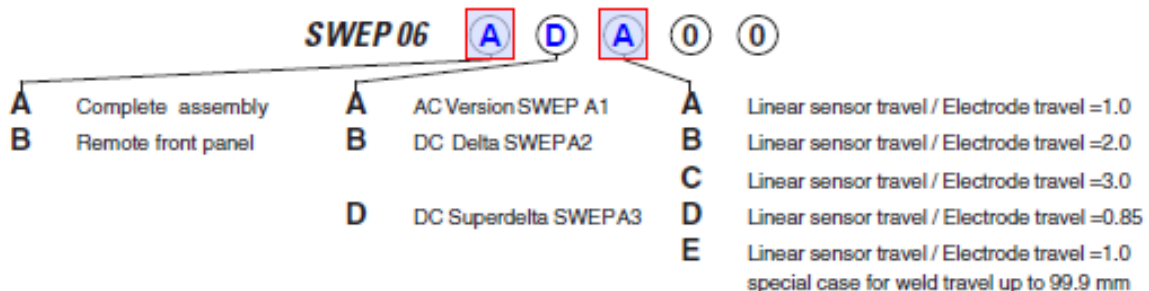187

SWEP06 Customer Related Information

Purchaser: **Corus Rail Scunthorpe** Enduser: **Corus Rail Scunthorpe** Date: **Feb.01.07**

Welder Type: **GAAS 80 / 580** Welder Serial Number: **AS1.2653.02949**

Target Date: **November 25, 2005** Administrator: **Ernst Iberg**

[Reset FORM_E]

Welder Engineering Data

☐ AC Current   ☐ DC Delta Current   ☑ DC Superdelta Current

1.	Maximum carriage travel (theoretical)		50.00	[mm]
2.	Maximum carriage travel (measured at electrodes)	S_{max}	49.10	[mm]
3.	Effective piston area forward side	A_{ADV}	628.32	[cm²]
4.	Effective piston area backward side	A_{BACK}	500.00	[cm²]
5.	Piston areas ratio	A_{BACK} / A_{ADV}	0.80	[1]
6.	Mechanical ratio Piston travel / Electrode travel		1.00	[1]
7.	Nominal upsetting force of the welder	F_N	800	[kN]
8.	Hydraulic pressure required for F_N	p_{FN}	127.32	[bar]
9.	Nominal clamping force of the welder	F_{CLAMP}	1900	[kN]
10.	Hydraulic pressure required for F_{CLAMP}	p_{FCLAMP}	140.00	[bar]
11.	Operating pressure of the hydraulic aggregate	p_{PUMP}	140.00	[bar]
12.	Operating pressure of the hydraulic bladder accumulator	p_0	65.00	[bar]
13.	Ratio clamp-force / upsetting-force	F_{CLAMP} / F_N	2.38	[1]

14. Proportional Valve used for upsetting ☑ no   ☐ yes → ` - - - ` [bar/V]
15. Proportional valve used for clamping ☑ no   ☐ left side ☐ right side ` - - - ` [bar/V]
16. Proportional valve type upsetting: **Catridge Block**
17. Proportional valve type clamping: **Setup Logic T without Stop open 3/4 Turn**
18. Upsetting valve installed ☐ no ☑ yes → nominal size 25 [1]
19. Control valve type: **BOSCH 4WRPH 6 C3B40L –2X/G24Z4 /M 0811 404 036** 40 [l/min]
20. Line voltage phase to phase ☑ 50 Hz ☐ 60 Hz U_N 415 [Volt]
21. Transformer open loop secondary voltage U_{20} 6.85 [Volt]
22. Maximum short-circuit weld current I_{2CC} 215 [kA]
23. Welding transformer winding ratio ü 35 [1]
24. Pressure sensor type: **BOSCH 0 811 405 532   250 bar System ▾** Pressure System: 250 [bar]
25. Current sensor type: **LEM LT 2000S** Shunt resistor: 5.6 [Ω]
26. Linear position transducer type: **Honeywell SLF076R2M4500B8A 75 mm**
27. Linear position transducer mounting: ☐ Carriage ☑ Piston
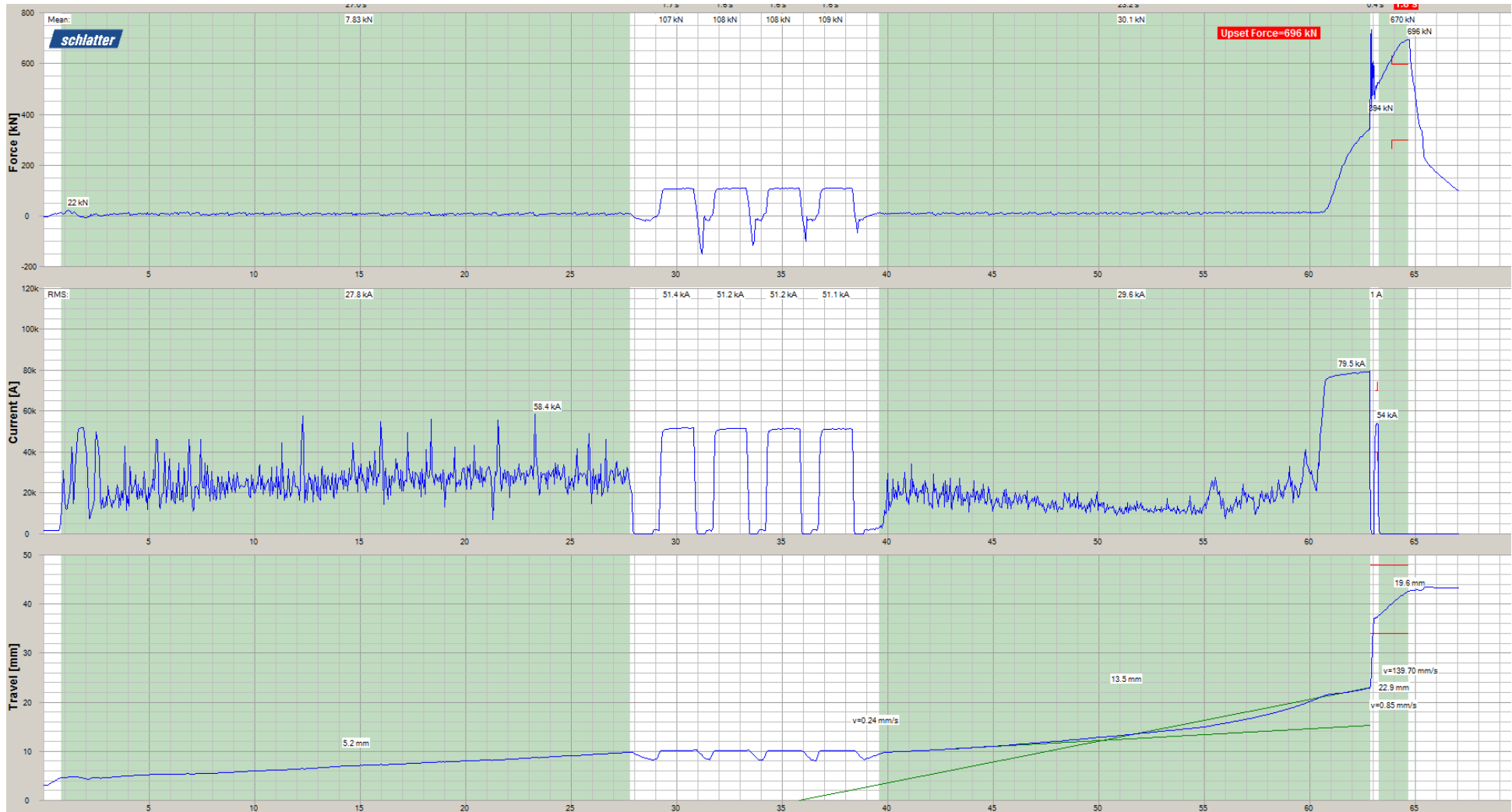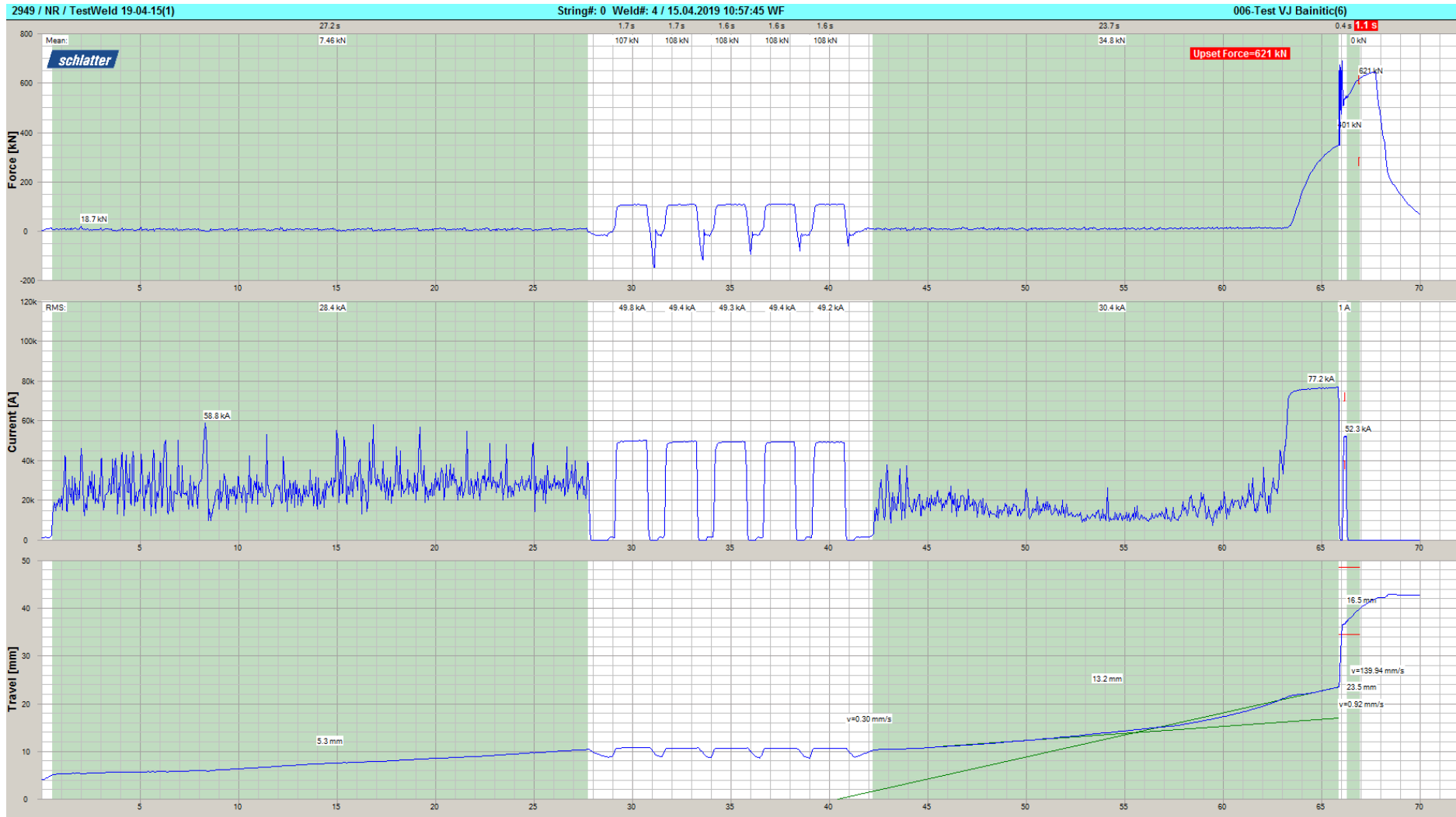28. Calibrating workpiece: Material: **CEN 60** Cross section: 7686 [mm²]

SWEP 06 Ⓐ Ⓓ Ⓐ ⓪ ⓪

A	Complete assembly	**A**	AC Version SWEP A1	**A**	Linear sensor travel / Electrode travel =1.0
B	Remote front panel	**B**	DC Delta SWEP A2	**B**	Linear sensor travel / Electrode travel =2.0
				C	Linear sensor travel / Electrode travel =3.0
		D	DC Superdelta SWEP A3	**D**	Linear sensor travel / Electrode travel =0.85
				E	Linear sensor travel / Electrode travel =1.0 special case for weld travel up to 99.9 mm

---

b. Weld charts

i. 3 PH cycles

iii. 5 PH cycles

iv.   6 PH cycles

v. 6 PH + 3PWP

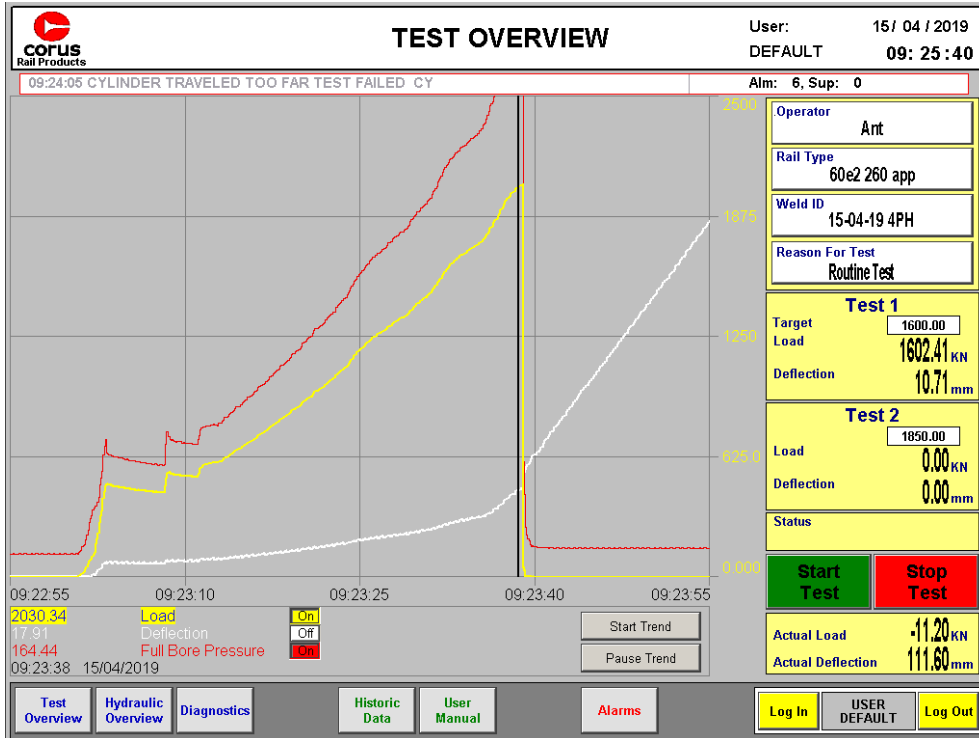### c. Three-point bend test trials

i. 4 PH weld

ii. 5 PH weld

iii.   6 PH weld

195